AD-A090 235 FLORIDA UNIV GAINESVILLE DEPT OF MATERIALS SCIENCE --ETC F/G 11/6
ROLE OF MICROSTRUCTURE IN HIGH TEMPERATURE OXIDATION.(U)
MAY 80 F N RHINES, R G CONNELL, M S CHOI DAAG29-77-G-0056
UNCLASSIFIED ARO-13968.2-MS NL

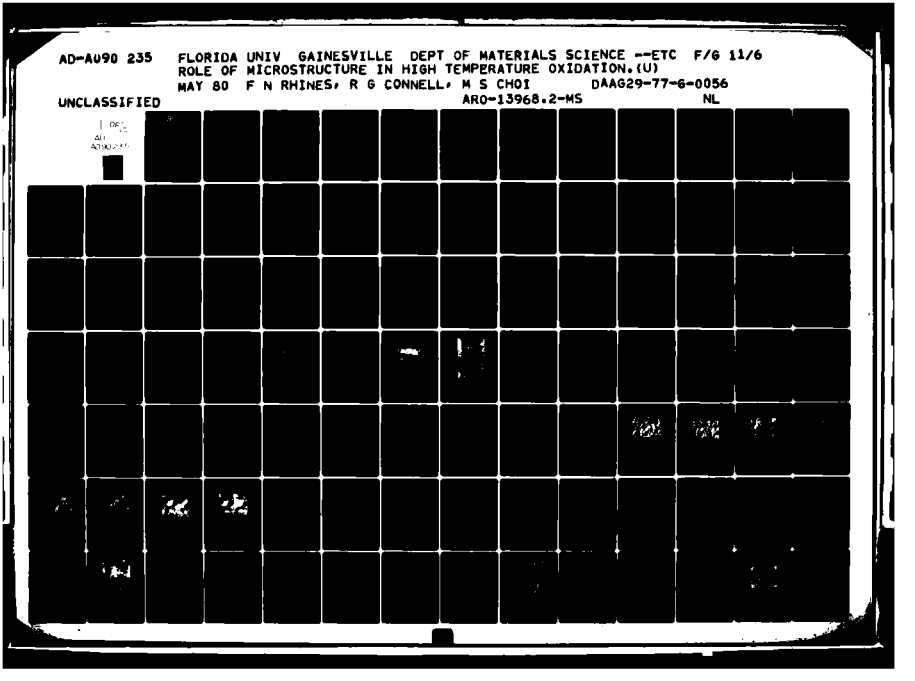

# ROLE OF MICROSTRUCTURE IN HIGH TEMPERATURE OXIDATION

FINAL REPORT

JANUARY 1, 1977 - JANUARY 31, 1980

F. N. RHINES*, R. G. CONNELL, JR.*, and M. S. CHOI**

MAY 1980



U. S. ARMY RESEARCH OFFICE

GRANTS DAAG 29-77-G-0056 and 79-G-0051

DEPARTMENT OF MATERIALS SCIENCE AND ENGINEERING
UNIVERSITY OF FLORIDA
GAINESVILLE, FLORIDA 32611

* Co-principal Investigators
** Graduate Research Assistant

SECURITY CLASSIFICATION OF THIS PAGE (When Data Entered)

# REPORT DOCUMENTATION PAGE

READ INSTRUCTIONS BEFORE COMPLETING FORM

| | |
|---|---|
| 1. REPORT NUMBER: 19 139 C-4, 1-MS | 2. GOVT ACCESSION NO.: AD-A090235 |
| 3. RECIPIENT'S CATALOG NUMBER: | |
| 4. TITLE (and Subtitle): ROLE OF MICROSTRUCTURE IN HIGH TEMPERATURE OXIDATION | 5. TYPE OF REPORT & PERIOD COVERED: FINAL REPORT 1/1/77 - 1/31/80 |
| | 6. PERFORMING ORG. REPORT NUMBER: |
| 7. AUTHOR(s): 10 F. N. Rhines, R. G. Connell, Jr. and M. S. Choi | 8. CONTRACT OR GRANT NUMBER(s): 15 DAAG 29-77-G-0056, DAAG 29-79-G-0051 |
| 9. PERFORMING ORGANIZATION NAME AND ADDRESS: Department of Materials Science and Engineering, University of Florida, Gainesville, Florida | 10. PROGRAM ELEMENT, PROJECT, TASK AREA & WORK UNIT NUMBERS: |
| 11. CONTROLLING OFFICE NAME AND ADDRESS: U. S. Army Research Office, Post Office Box 12211, Research Triangle Park, NC 27709 (12) 168 (11) | 12. REPORT DATE: May 1980 |
| | 13. NUMBER OF PAGES: 176 |
| 14. MONITORING AGENCY NAME & ADDRESS(if different from Controlling Office): 9) Final rept. 1 Jan 77-31 Jan 80 | 15. SECURITY CLASS. (of this report): Unclassified |
| | 15a. DECLASSIFICATION/DOWNGRADING SCHEDULE: |

16. DISTRIBUTION STATEMENT (of this Report)

Approved for public release; distribution unlimited.

17. DISTRIBUTION STATEMENT (of the abstract entered in Block 20, if different from Report)

NA

18. SUPPLEMENTARY NOTES

The view, opinions, and/or findings contained in this report are those of the author(s) and should not be construed as an official department of the Army position, policy, or decision unless so designated by other documentation.

19. KEY WORDS (Continue on reverse side if necessary and identify by block number)

High-temperature oxidation of nickel
Microstructure of NiO
Mechanism of NiO scale growth
Influence of impurities upon the oxidation of nickel

20. ABSTRACT (Continue on reverse side if necessary and identify by block number)

See the following page for Abstract.

DD FORM 1 JAN 73 1473 EDITION OF 1 NOV 65 IS OBSOLETE

4-1-77 dk

SECURITY CLASSIFICATION OF THIS PAGE (When Data Entered)

## ABSTRACT

The major objective of this research work was to study the influence of minor impurity elements present in nickel upon its oxidation behavior, specifically as regards the correlation between scale thickening and its concurrent microstructural evolution. Materials chosen for this work were Nickel 270 and a nickel of lower purity, Nickel 200. The Nickel 270 served as a standard of comparison for the oxidation behavior of Nickel 200. Initially the research activity was concentrated on a study of the microstructural evolution of the inner scale layer and the metal-oxide interface of Nickel 270. The results of this work combined with those of a previous research dealing with the outer scale layer formed a basis of comparison for the work on Nickel 200.

The oxidation of Nickel 200 proceeds in three distinct stages as does that of Nickel 270. There are, however, notable differences, mainly attributed to the higher impurity level of Nickel 200, which can be seen as affecting both the microstructure of the scale and the rate of scale thickening. Impurities in the Nickel 200 result in mo-e sub-scale formation in the form of gas blown porosity and inert oxide particles. As the metal containing the sub-scale is erroded away by the advancing oxide front, the inert particles and gas pores become embedded in the scale. The role of the vapor phase pores in the scale growth of Nickel 200 may be associated with the following gross differences in its oxidation behavior as compared to Nickel 270: 1) a doubling of the rate of scale thickening; 2) a relative thickening of the inner layer with respect to the outer layer; 3) a refinement of the grains at the inner layer especially near the metal-oxide interface; 4) the presence of porosity in the inner layer and extending into the metal and 5) the presence of fine idiomorphic grains of NiO lining the pores. All of these can be ascribed to the presence of carbon, if it is supposed that carbon can react with oxygen to form a sub-scale of pores containing NiCO and, or CO in mixture. Pores containing this gaseous mixture provide for the vapor phase transport of $Ni^{++}$ ions through the inner scale layer. Inert particles in the scale are presumed to retard grain growth in the inner layer thus allowing for the persistence of a wide variation in the grain size from very small at the metal-oxide interface to that approximating the size of the columnar grains at the boundary separating the two scale layers.

A secondary study was made of the oxidation behavior of high purity copper in air at 800°C where the predominent oxide is CuO. The scale thickening and microstructural evolution of CuO formed under these conditions are similar to the oxidation behavior of Nickel 270.


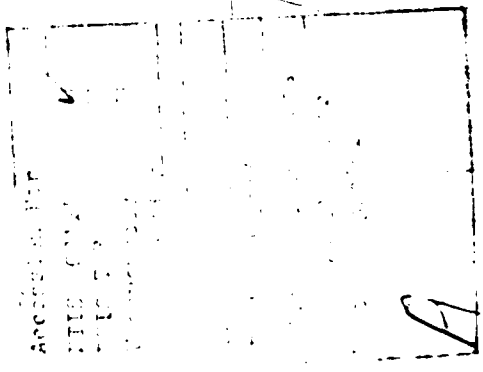

TABLE OF CONTENTS

## LIST OF FIGURES

## LIST OF TABLES

Page

## INTRODUCTION

For over a half century the classical view of the high temperature oxidation of metals has remained relatively unchanged. Observations within the last fifteen years by the current authors and others have shown that the classical view is inadequate to explain such important aspects of the high temperature oxidation process as its rate and the effects of minor elements in the metal. These observations have also indicated that an important key to deeper understanding, and possibly to better control of oxidation lies in a knowledge of the role played by the microstructure of the oxide scale in the mechanism of oxidation.

Through the years, an enormous amount of research has been devoted to various aspects of oxidation, so that we have much factual knowledge of oxidation in many metals and alloys. Yet, at the outset of the research herein reported, it was obvious that a thorough understanding of how the process operates had not been developed in any great detail. It had assumed that, because of growth rate has a roughly parabolic form, it follows that new oxide is formed either at the air-oxide interface or at the metal-oxide interface, but not both at once. Evidence obtained in the few years prior to this research had made it clear , however, that new oxide formation occurs throughout the scale layer and that the oxide scale grows by swelling. Further, it had been found that the grain structure of NiO and its growth rate are closely linked. (1) The oxide grain boundary area in the outer layer of the two layer scale is proportional precisely to the scale thickness. Indications were that both copper and iron behave similarly and that the same may be true for all metals of which nickel may be regarded as the prototype. The implications of these findings suggested, among other things, that control

over scale growth may be achieved through measures known to be applicable to grain growth.

It was apparent that a detailed knowledge of the scale microstructure and of its evolution during the course of oxidation must become essential parts of the control of oxidation. The scarcity of knowledge in this field was readily accounted for by extreme experimental difficulty in applying standard methods of microscopy to the thin, brittle and optically complex bodies that constitute the scale. The progress which had been made upon the basis of metallographic techniques developed in the several years preceeding this research served as a beginning for a continued study to develop further understanding of the interrelations between microstructure of the scale and its growth.

Scope of the Research

The scope of this research was established as follows:

(1) To explore the relations between the microstructure of the scale and its growth using the tools of quantitative microscopy in order to add to the knowledge of the mechanisms involved in high-temperature oxidation of nickel.

(2) To relate the structure and growth of the inner scale layer to present knowledge of the growth of the outer scale layer.

(3) To initiate a study of the influence of minor impurities in the nickel upon its high temperature oxidation behavior through a comparative study of Ni-200 (commercial purity) and Ni-270 (high purity).

(4) To make a brief study of the oxidation behavior of high purity copper as a comparison with Ni-270.

## Summary of Conclusions

The new knowledge obtained during the course of this research has allowed the authors to expand their view of hightemperature oxidation. Highlights of the current view are summarized in the following statements.

(1) The oxidation of nickel is presumed to proceed in three stages:

(a) A fast chemisorption of oxygen followed by the almost instantaneous formation of islands of NiO which spread laterally to impingement. During this stage, nickel ions are in excess so that the rate of oxidation is controlled by the supply of oxygen and is therefore pressure sensitive.

(b) The oxide islands thicken to form columnar grains at a rate controlled by the delivery of nickel ions to the external surface. During this stage, the structure of the inner layer begins to develop through the nucleation of new NiO grains at $NiO^3$-Ni quadruple points upon the metal oxide interface. In the absence of impurities in the nickel this nucleation process is continuously repeated, but its frequency diminishes so rapidly that it practically ceases after two layers of grains are nucleated. Grain boundary sweeping and grain growth commence toward the end of this stage in response to plastic deformation of the scale which relieves stresses induced by new oxide formation along NiO grain boundaries within the scale. As the second stage ends, the mean intercept grain size of the columnar grains becomes established at a constant ratio of 1/3 to the columnar layer thickness and 1/2 to the thickness of the equiaxed layer.

(c) A general swelling of the entire scale, regulated by the rate of grain boundary sweeping. Throughout this stage oxidation proceeds according to a cube-root of time law.

(2) The NiO grain size distribution at the metal-oxide interface is log-normal, except that the smaller size grains are in excess. New grains are thus being nucleated at the metal-oxide interface. The number of new grains is proportional to the number of $NiO^3$-Ni quadruple points upon the metal-oxide interface. Consequently, as the scale grows under grain boundary sweeping (grain growth) control, the nucleation rate of new grains decreases in inverse proportion to the rate of grain growth.

(3) Over the whole range of third stage scale growth, the distribution of grain sizes within the NiO remains log-normal.

(4) Grain growth of NiO is steady state because the relative width of the log-normal distribution does not change during oxidation either upon the metal-oxide interface or within the body of the scale.

(5) Inert foreign particles in the nickel become enveloped in the inner layer of the scale and maintain their relative positions within that layer. Plastic extrusion concurrent with scale growth occasionally sweeps some particles into the outer layer.

(6) In the absence of less noble elements in the nickel, the oxide scale is essentially free of inert particles and porosity in the scale, except for a few gas blown micropores. Occasionally pores develop at the metal-oxide interface. These eventually spheroidize and shrink as the scale thickens. Each such pore is surrounded by a halo of fine grains, the generation of which is associated with the presence of carbon in the metal.

(7) In scales grown upon Ni-200, the scale is composed of a columnar-grained outer layer and a porous inner layer of equiaxed grains. The thicknesses of the two layers is practically equal and constant throughout growth. The entire scale grows faster than its Ni-270 counterpart.

(8) For Ni-270 there is also a quantitative correlation between scale growth and the rate of grain growth for the scale as a whole. The grain size in the inner layer varies from very small at the metal-oxide interface increasing in size to that of the transverse intercept length of the columnar grains at the interboundary of the two scale layers. The grain size at the metal-oxide interface is always the same independent of time.

(9) Ni-200 oxidizes internally; thus, its oxide scales contain more inert foreign particles than do the Ni-270 scales.

(10) Numerous pores (more than 5 volume percent) exist near the metal-oxide interface in Ni-200 scales and extend to, but not beyond the boundary dividing the inner and outer layers. The size and volume fraction of pores both diminish with increasing distance from the metal-oxide interface. Pores are usually nested with halos of fine idomorphic NiO grains.

(11) The faster rate of Ni-200 oxidation, the presence of pores in the inner layer and its grain size refinement can be ascribed to the presence of carbon in the metal which presumably forms pores containing $Ni(CO)_4$ and/or CO in mixture. Nickel carbonyl is postulated to account for nickel transport which is more rapid than solid state diffusion; thus, accounting for faster oxidation. Fine idiomorphis NiO grains

inside the pores are believed to be sublimate particles from the gas phase in the pores.

(12) The oxidation of high purity copper at 800° C, where the majority of the scale is $Cu_2O$, follows the oxidation behavior, similar to the third stage oxidation of Ni-270.

## SCIENTIFIC BACKGROUND FOR THE RESEARCH

### The Classical Theory of Oxidation and Its Deficiencies

The fifty year old classical theory of oxidation leading to parabolic growth of NiO (thickness of NiO is proportional to the square root time) requires the oxidation of nickel to proceed by the diffusion of one of the reactants through the scale to form new oxide upon the growing interface where oxygen and nickel ions meet. Tammann [2], at first, introduced this concept with respect to the formation of iodide layers on silver, copper, and other metals. Subsequently, Pilling and Bedworth [3] , who accepted Tammann's idea, assumed inward diffusion of oxygen in the formation of oxide layers on metals. Later, Wagner [4] argued that the outward diffusion of nickel is the sole transport mechanism. He based his idea on the observation that the NiO scale upon nickel is nickel-deficient, i.e., p-type semi-conductor. This implies the existence of nickel vacancies in the NiO crystal lattice, which would promote the diffusion transport of nickel, but not of oxygen. This mechanism predicts the formation of new NiO upon the external surface where nickel ions encounter oxygen in the atmosphere.

Even though the idea of the sole diffusion of nickel has been widely accpted and supported by many authors [5, 6-18, 19, 20, 21], this model has four major deficiencies:

First, the rate of oxidation diminishes more rapidly than would be expected of parabolic behavior [22, 23, 24].

Second, the polycrystalline oxide scale thickens at a rate greater than is predicted by diffusion of nickel alone through an everthickening scale [23]. The classical oxidation rate computed by Graham, Caplan, and Cohen [24] from their determination of nickel diffusivity through NiO was found to be an order of magnitude smaller than the measured value.

Third, inert markers placed on the nickel surface before the experiment were found after oxidation to be near the middle of the scale. Thus, the new oxide must have formed both above and beneath the inert matter. This result is counter to the classical theory, which predicts that the markers should be located at the interface between Ni and NiO. Pfeil first noticed this fact in his work with iron and others confirmed the same result using nickel [25-28, 29]. These experiments always produced NiO scales with the markers located in the middle part of the NiO layer on the interface between two microscopically discernible layers with different structures.

Fourth, the classical model provides no explanation of the generation of compressive stresses within the scale. It has been [30] pointed out that growth can occur only upon a surface that lies normal to the flux of the reactants [30]. Therefore, the direction of any stress generated by the classical model will be normal to the reaction surface, and this stress can be continuously and fully relieved by the forward motion of the reaction front where there is room to grow. For this reason, the compressive stresses which have been observed by many investigators [30-33] can not be explained by the classical theory.

For these reasons, it is here asserted that a quantitative experimental proof of the classical theory has not been established [34].

## The Non-Classical Model of Oxidation

Numerous investigators have reported non-parabolic growth of NiO [1, 16, 22-23, 35-41], often asserting that the rate is cubic. Two of the present authors [1], who verified that the scale thickness increases in proportion to the cube root of time, proposed an alternative mechanism, the so-called "grain boundary sweeping mechanism" for the oxidation of nickel.

These authors assumed that the oxidation of nickel occurs by the counter diffusion of nickel and oxygen within the scale. Nickel ions diffusing outward through the NiO crystals and oxygen ions diffusing inward along the NiO grain boundaries meet upon grain boundaries, there forming new NiO. The grain boundaries are in motion because grain growth is also in progress and the new NiO is thus deposited everywhere throughout the volume of the scale.

When new oxide is formed within the scale, growth occurs by swelling. A compressive stress is generated thus, parallel with the metal surface, by the lateral "wedging effect" of the new oxide, since the whole scale is attached to the nickel substrate. This stress is locally most intense at grain boundaries. The first plastic response to relieve this stress would be extrusion of oxide outward along the NiO grain boundaries. [This phenomenon has been observed in an early stage of oxidation, by scanning electron microscopy to produce ridges of NiO, outlining the NiO grain boundaries.]

As shear occurs in the vicinity of grain boundaries, in the course of plastic deformation, it must impart local curvature to the NiO grain

boundaries, in response to which the grain boundaries can migrate under the influence of surface tension at high temperature. Such sweeping boundaries, charged with oxygen diffusion inward from the exterior, act as dynamic reaction fronts for the formation of new oxide and distribute it throughout the volume of the scale. The plastic deformation has the additional effect of moving the grain boundaries past pinning points such as those at the metal-oxide interface. Grain boundary sweeping must also result in conventional grain growth which is thus proportional to the formation of new oxide.

## Basic Subjects Underlying This Research

The grain boundary sweeping mechanism proposed the present authors [1] has been put forward to explain the major deficiencies of the classical theory. It provides a satisfactory oxidation mechanism for the formation of the outer layer of NiO grown upon pure nickel. However, the oxidation mechanism of the inner layer of NiO has not yet been clarified. This research, extending the knowledge of the grain boundary sweeping model, has focused upon ascertaining the mechanism of structural evolution of the inner layer of NiO as formed upon pure nickel and upon impure nickel.

In order to carry out this research there was required a background basic knowledge in several areas. These areas include:

(1) Microstructure of NiO.

(2) Mechanism of the double-layered structure formation.

(3) The effect of oxide microstructure upon the oxidation rate.

(4) The transport of reactants in NiO.

(5) Mechanical properties of NiO.

(6) Stresses generated within the scale.

(7) Plastic deformation.

(8) Nucleation of NiO and early stage of oxidation.

(9) Kinetics of oxidation.

(10) The effect of minor elements upon the oxidation rate.

(11) Porosity.

(12) The effect of specimen geometry and surface preparation upon oxidation.

Full knowledge of each of these subjects was essential for this research, since all of those factors provided the scientific background for the grain boundary sweeping model as well as for this research. A review of the prior knowledge follows:

Microstructure of NiO

Most of the investigators who studied the high temperature oxidation of nickel have reported that NiO formed upon flat nickel surfaces, under pure oxygen at one atmosphere, is composed of two layers [1, 22, 23, 29-30, 42-50]. The metallographic cross section reveals that the outer layer of the scale is composed of columnar grains and the inner layer is composed of equiaxed grains. In high purity nickel, the distinction between the two layers is not very clear, while it becomes clearer for the less pure nickel.

The relative scale thickness and the grain size of the two layers is dependent upon the metal purity. This structural dependence of NiO upon the purity is clearly demonstrated [1, 23] using Ni-270 (nominally 99.98 + % nickel) and Ni-200 (nominally 99.4% nickel) flat specimens. They showed that the outer layer of the scale is much thicker than the inner layer for the pure nickel, whereas approximately half of the scale is composed of the inner layer on the less pure nickel. In the latter

case, the grain size of the inner layer is so fine that the grain boundaries become indistinguishable. Similar results are shown in the works of Sartell and Li [5] and Lowell [35] for pure nickel and for impure nickel, respectively.

Mechanism of the Double Layered Structure Formation

Mechanisms for the formation of the bi-layered structure of NiO have been proposed by several investigators [18, 44, 51-52]. Stott et al. [52], working with nickel and cobalt-base alloys at 1000° C, attributed the two-layered structure of oxide scale to the existence of foreign oxide particles [35, 46, 53] which are enveloped and precipitated within the scale as the oxide grows. They suggested that the embedded oxide particles prevent the grain growth of the surrounding NiO, and result in a fine-grained, inner layer of NiO beneath the outer larger columnar-grained layer. They also assumed these particles to act as "sinks" for the vacancies of cations which are presumed to be generated at the metal-oxide interface. This was their explanation for the formation of a questionable porous inner layer. Evans et al. [2] also gave a similar explanation for the formation of the duplex oxide structure upon pure metal.

Gibbs [18] and Hales et al. [51] gave another explanation for the evolution of a fine-grained, equiaxed, and porous inner layer on pure metal. They assumed that the scale, above an interfacial void which is generated by vacancy injection, is thermodynamically unstable, and due to that, oxide grain boundaries can produce micro-channels [44] which gives oxygen gas access to the scale-metal interface. They postulated that new oxide crystals would be nucleated and grow on the exposed metal in a void, as soon as the oxygen penetrates into the oxide along those

channels. By continuing nucleation at a lower level in this way, the porous inner layer can be developed. A similar mechanism, known as the dissociative mechanism, had been proposed by Mrowec [44] for the duplex structure of the oxide.

The Effect of Oxide Microstructure Upon the Oxidation Rate

The influence of oxide microstructure upon the oxidation rate has been reported by several investigators. Pfeil [54] was probably the first to notice that the scale thickening and grain growth are interconnected in the case of oxidation of iron. Grain growth of NiO crystallites with oxidation time was observed by Perrow et al. [55] and Phelps et al. [56] for thin oxide films. Recently, quantitative correlation between grain growth and scale growth of NiO was established by Rhines and Connell [1, 23]. They found that scale thickness and grain size increase in direct proportion to each other. In order to prove that scale growth and grain growth are interrelated, they turned off the oxygen supply during the oxidation experiment, leaving only helium in the furnace. Continued heating did not cause any change in the scale thickness or in the oxide microstructure, indicating that no grain growth occurred where there was no scale growth and vice versa. Arkharvo et al. [29] obtained similar results that oxide thickening does not occur without grain growth.

Caplan and Graham, and Graham et al. [24, 57] showed, through their work with cold worked specimens, that the oxidation rate of polycrystalline NiO is much faster than that of monocrystalline NiO. They also demonstrated that the scale growth rate is dependent upon the NiO grain size, that is, for smaller grain size, a higher growth rate was observed, and vice versa.

Transport of Reactants in NiO

There have been several studies of the diffusion of nickel and oxygen through the oxide scale. Some experimental values of lattice diffusivity for nickel in NiO are as follows:

$$D_{Ni} = 1.83 \times 10^{-3} \exp(-45.6 \text{ Kcal/RT}) \quad [58]$$

$$D_{Ni} = 4.4 \times 10^{-4} \exp(-44.2 \text{ Kcal/RT}) \quad [59]$$

$$D_{Ni} = (1.5 \pm 0.8) \times 10^{-2} \exp(-58.1 \pm 1 \text{ Kcal/RT}) \quad [60]$$

$$D_{Ni} = 1.7 \times 10^{-2} \exp(-56.0 \text{ Kcal/RT}) \quad [61]$$

Shim and Moore [59] found that the diffusion coefficients for nickel in polycrystalline and monocrystalline NiO were identical so that we can conclude that nickel moves only via lattice diffusion of nickel through NiO, not preferentially along the grain boundaries.

Bulk diffusion of oxygen was found to play a negligible role in the oxidation reaction [62, 63]. O'Keefe and Moore [62] reported that the diffusion of oxygen in monocrystalline NiO occurs in small amounts,

$$D_o = 1.0 \times 10^{-5} \exp(-54.0 \text{ Kcal/RT})$$

However, oxygen diffusion experiments conducted by some investigators [64, 65] have shown that oxygen is being delivered from the external surface of polycrystalline NiO all the way to the oxide-metal interface during oxidation process. Holbrook [64], for example, oxidized nickel first in a pure $O^{16}$ atmosphere and then in an $O^{16}$ plus $O^{18}$ atmosphere. By the tracer analysis, he found that $O^{18}$ was present all the way to the metal-oxide interface.

High diffusion rates of oxygen along the oxide grain boundaries have been also found among other oxides. Kuise and Angew [66] and Oshi and Kingery [67] reported preferential diffusion of oxygen along $Al_2O_3$ grain boundaries. Similar results were reported for $Cu_2O$ by Wilkins and

Rideal [68], and for MgO by Hashimoto and Hama [69]. Caplan and Sproule [70] proposed that a polycrystalline growth of $Cr_2O_3$ would develop through the two way transport of cations diffusing outward through the oxide and anions diffusion inward along the oxide grain boundaries.

In conclusion, it may be said that:

(1) $Ni^{++}$ diffuses outward through the NiO grains.

(2) $O^{--}$ diffuses inward along the grain boundaries.

Mechanical Properties of NiO

Mechanical properties of NiO are among the important factors that determine the mechanism of oxidation and the resulting oxidation resistance. Tylecote [71] found the values of the thermal-expansion coefficients of nickel and nickel oxide to be nearly the same, i.e., $17.6 \times 10^{-6}$ for nickel and $17.1 \times 10^{-6}$ for nickel oxide. Steady-state creep rates of nickel and nickel oxide at 1000° C were determined by Rhines and Wolf [30]. They found that the rate of deformation of these two materials is in the same order of magnitude. Bruce and Hancock [72,73], who studied the mechanical properties of NiO, found that the Young's modulus of growing NiO scale decreased with increasing temperature. Values of $46\text{-}60 \times 10^6$ and $37 \times 10^6$ psi have been found at 800° C and 1000° C, respectively. From cooling experiemnts, they demonstrated that nickel oxide can deform plastically above 70° C in agreement with the result of Evans et al. [21] and Menzies et al. [74]. Other authors [5, 44, 75, 76] also have found NiO to be ductile at high temperature.

Stresses Generated Within the Scale

The generation of stresses during scale formation has been a well known fact. Pilling and Bedworth [3] were probably the first investigators who recognized that stresses arise as a result of the volume dila-

tion that occurs on the formation of new oxide. Since then, Evans [32] showed that a thin oxide film, when stripped off the substrate, tended to curl indicating the presence of both a stress and a stress gradient. Dankov and Churaev [33] also observed the bending effect when a thin metal foil was oxidized on one side only. Ueno [31] formed two different types of bi-layers of NiO on both sides of a thin nickel specimen; this resulted in a flexure of the specimen. By removing the scales electrochemically from the substrate, it was shown that the bending occurred due to the difference in the magnitude of the compressive stresses on the two bi-layers.

Several investigators have observed dimension changes in the substrate during oxidation, which they attributed to creep due to the growth stresses [30, 77-79]. Moore [77], who oxidized a copper tube on the outside only at 1000° C, found that the internal diameter of the tube diminished slightly. Stringer [78] obtained a similar result with oxidized tubes of Ta. It was shown that oxidation of nickel near 1000° C is accompanied by lateral stresses in the scale with a magnitude of about 1500 psi, which is sufficient to increase the surface area of the sheet specimen and to elongate a nickel rod [30]. The determination of this value was based on the creep data for Ni and NiO. A similar increase in surface area of a thin film of nickel and of a nickel alloy was observed by Denisenki and Skorokhod [79] and by Norin [80], respectively.

The generation of stresses in the scale is not limited to the nickel. A large increase in the lateral dimensions of uranium specimens was observed by Cathcart et al. [81]. Niobium [81], tantalum [78, 83], and copper [84-85] also showed generation of stresses within the scale during oxidation.

Plastic Deformation

There are numerous papers which show that plastic deformation occurs during the oxidation of nickel. It is easily understood that oxide-metal adhesion during the oxidation of nickel can only be maintained by plastic flow. One of the most direct evidences that plastic deformation is occurring during the oxidation is the extrusion of NiO outward from the grain boundaries.

Hales [86] formed a thin scale of NiO on the nickel substrate at 1000° C. Electron microscopic examination of this scale revealed a well-developed dislocation structure indicating that plastic deformation has occurred by dislocation creep. Evans et al. [21], through their work upon the mechanical properties of NiO, also concluded that plastic deformation of NiO below 1200° C must occur by dislocation glide. Cathcart et al. [87] observed a mosaic structure composed of low angle grain boundaries, which he thought to be formed as a result of relaxation of the strain which exists in the NiO film. A similar subgrain network was observed by Phelps et al. [56] who associated it with recovery from a plastically strained state. Vernon and Spooner [75] confirmed that plastic deformation of NiO occurred above 640° C by observing slip lines and dislocations on the grown crystal.

Direct observation of the creep of NiO scale have made [30, 88]. It has been suggested that if the nickel substrate is thin enough, the stress developed in the scale is sufficient to cause it to bend or to elongate in creep [30]. When the nickel is too massive to yield, the plastic response to the oxidation stress must occur mainly in the scale.

The plastic deformation of oxides other than nickel at high temperature has also been frequently reported. The case of copper was discussed

by Sartell et al. [9]. This property has been exhibited also in CoO [89], in Fe-Cr-Ni alloys [80], in $Cr_2O_3$ [70], in uranium oxide [90], and in iron oxide [91].

Nucleation of NiO and Early Stage of Oxidation

Holloway and Hudson [92] explained the initial stage of oxidation on a Ni(1) surface in three steps, based on their works with LEED and AES: (1) A fast chemisorption of oxygen leading to a surface coverage of approximately 0.4 monolayers; (2) nucleation of clustered NiO islands which undergo sidewise growth by addition of oxygen ions at their edges until two layers thick; and (3) final thickening of the NiO. A similar result was obtained for the initial oxidation of the Ni(110) surface by Mitchell et al. [93]. When the substrate is polycrystalline nickel, Robin [94], Martins [95], Flower and Wilcox [36], and Wood et al. [96] found that the first nuclei of NiO tend to form preferentially along the grain boundaries of nickel. After that, nucleation occurs upon the nickel grains as long as the grain size of the metal is much larger than that of oxide grains [22,97].

An epitaxial relationship between nickel and nickel oxide has been reported by several investigators: (111)Ni//(111)NiO was found by Newkirk and Martin [98]; and by Caplan et al. [57], (110)Ni//(001)Ni [93], (011)Ni//(011)NiO [14], (100)Ni//(100)NiO [99] were also observed.

Different crystal orientation of nickel sometimes led to an anisotropy of the oxidation rate, as reported by various workers [37, 100-102]. Carlson [101] pointed out that if there exists epitaxy, the activation energy for metal atomic jump, strains, vacancies, and dislocations formed in the oxide layer near metal will be influenced by crystal orientation and bring about the different oxidation rates. However,

polycrystalline oxide formed above 1000° C upon nickel generally shows uniform and thick scales, as observed by many investigators [1, 22-23, 57].

Gulbransen [103] speculated that the nucleation and growth of oxide crystal might be related to the defects and inclusions in the metal grain. He found that the density of oxide growth centers in the metal grain was of the same order as the density of dislocations. Flower and Wilcox [36] reported a similar observation concerning the nucleation of oxide on a nickel alloy. Caplan et al. [57] observed that a cold worked specimen of nickel formed an oxide of finer grain size than that upon annealed nickel, indicating that the nucleation rate was enchanced by cold work.

Kinetics of Oxidation

The study of thin film kinetics (less than 500° A) has yielded three kinds of rate laws. A logarithmic rate law was observed by Graham and Cohen [17], Hauffe et al. [140], Mitchell and Sewell [93], Ritchie [105], and by Uhlig et al. [106]. A cubic law and an exponential rate law were also reported by Gulbransen [107] and by Tammann and his collaborators [2, 108], respectively. As the oxide thickens, it has been found that the rate law changes into parabolic and subsequently into cubic [1, 22].

The Effect of Minor Elements Upon the Oxidation Rate

Many investigators have observed that if the amount of impurities or alloying elements in the metal is increased, the oxidation rate of nickel is greatly enhanced [8, 15, 23, 35, 42, 46, 103, 109-112]. One theory to explain the effect of impurities upon the growth kinetics was first developed by Wagner [4, 112] and Hauffe and his collaborators

[113] applying the law of mass action to ionic and electronic defects in solid solutions. If the ions of the alloying element are of lower valency than those of nickel, the oxidation rate will be reduced through reduction of the Ni ion vacancy concentration [111]. However, the oxidation rate will be increased if the addition has ions with higher valency than nickel ion, by increasing the concentration of nickel vacancies [52, 112].

Stott et al. [52] found that the oxidation rate of nickel increased with the addition of chromium up to 1%. Above a 1% chromium addition, the oxidation rate rapidly decreased. The markedly enhanced oxidation rate of Ni-200 compared to that of Ni-270, which was observed by the present authors [1] and Lowell et al. [35], is not satisfactorily explained by the above theory, since this theory is based on the classical model which has been found to be incorrect.

Porosity

Porosity within the inner layer has been reported by most investigators who studied the NiO microstructure [12, 18, 21, 25, 43, 51, 114-115]. Hales et al. [18, 51] and Evans et al. [21] insisted that macroscopic pores can be formed by the precipitation of large number of vacancies in the scale near the metal-oxide interface. This was based on the idea that, when an oxide scale grows on a metal by the outward diffusion of cations, the metal ions should create a reverse flow of vacancies that are injected into the metal substrate. Also, they concluded that the scale should eventually lose its contact with metal after a long time of oxidation, due to the buildup of these pores.

The idea of "vacancy injection" at the metal-oxide interface when the oxide grows upon pure nickel has turned out to be wrong. This is

because the scales formed upon pure nickel are found to be essentially pore-free as will be shown in this research.

It has been observed that porosity in the nickel metal result from the oxidation of nickel that contains carbon. This might be the cause of the porosity as argued by Hales et al. [51] and by Evans [12].

It has been suggested that such cavities can also arise as a consequence of grain boundary shearing in high temperature creep [30]. Metallographic artifacts caused by polishing are sometimes confused with real porosity in the case of pure metal. This was also pointed out by Hussey et al. [116]. These arguments do not exclude the possibility of blistering, spalling, and other discontinuities in the scale, which are often found as real, but such factors do not alter the basic mechanism of oxidation of nickel.

It has been reported that temperature and metal purity affect the porosity. Wood and Wright [14] reported, in their review article, that the porosity of the inner layer of oxide scale decreases as the temperature increases [46] or the metal purity goes up [45].

The Effect of Specimen Geometry and the Surface Preparation Upon Oxidation

That the curvature of the metal surface and the surface treatment can affect oxidation has been shown by several workers [6, 22, 35, 100, 117-118]. Electropolishing, etching [1], grinding [35] of nickel prior to oxidation or magnitude of surface area of nickel [117, 118] have been reported to result in different oxidation kinetics. For the specimen curvature effect, Healey [22] showed that both the thickness and grain size of NiO grown upon convex surfaces are smaller than those on concave surface. Romansky [118] demonstrated a similar effect of metal surface

curvature upon the oxidation of iron and showed that specimen size and shape influenced the kinetics of oxidation of both nickel and copper.

## EXPERIMENTAL METHODS

Some of the experimental procedures used for this research had been developed* and described in former research [1]. The processes and experimental techniques that have been newly developed are described in the following paragraphs.

### Specimen Preparation

In order to study the microstructural evolution of NiO scale and its effects upon the high temperature oxidation of nickel, two grades of nickel were used. Specimens of Ni-270 (nominally 99.98 + % nickel) and Nickel 200 (nominally 99.4 % nickel) were prepared from sheet 1.5 mm in thickness, obtained from the International Nickel Company. These sheet specimens were cut into coupons 20.5 mm x 11 mm x 1.5 mm. Prior to oxidation, these nickel specimens were preoxidized and surface treated according to the method outlined in Table I, which provided the most reproducible experimental results. After the cleaning, oxidation was started within one hour.

Copper specimens (99.999% Cu) were prepared in a like manner, but the preoxidation step was omitted.

### Oxidation

Oxidation treatments were conducted in a furnace system consisting of an all-nickel reaction tube and stainless steel (AISI Type 316) gas

---

* "Control of Environmental Surface Reactions," Final Report, June 15, 1972, to September 15, 1973, F. N. Rhines, E. D. Verink , Jr., L. L. Hench, and Associates, Department of Materials Science and Engineering, University of Florida. Prepared for NSF under Grant No. GH-3455.

piping. This system is drawn schematically in Figure 1. As shown in this figure, the oxidation was carried out in an all nickel environment (chamber) to minimize possible contamination from other materials. The enclosing furnace was of the split-tube type, that could be heated to the desired temperature (1000° C) prior to placing it around the reaction tube. The heating element of the furnace was Kanthal-A wire, permitting the use of reaction temperatures up to 1200° C. A chromel-alumel thermocouple was placed at the hot zone of the reaction tube to insure that the oxidation temperature was being maintained with ±5° C. Both ends of the reaction tube were water cooled for ease of handling.

The oxidation step began with the cleaned nickel coupons which were prepared according to the procedures shown in Table I. These cleaned specimens were suspended upon a specimen hanger made of Ni-270 wire inside the reaction tube. After closing the system, the cold reaction tube was purged with high purity helium (AIRCO GRADE 5) for 20 minutes. Then, the hot split-tube furnace was placed around the nickel reaction tube, heating the specimens to 1000° C, still in the helium atmosphere. Upon reaching 1000° C, the helium supply was turned off and high purity oxygen (AIRCO GRADE 5) was fed into the nickel chamber at about one atmosphere of pressure for the planned duration of oxidation (1, 4, 9, 16, 36, 64, 81, 225 hours). Following oxidation, the split-tube furnace was removed so that the reaction tube was exposed to air. The cooling of the specimens to 400° C was performed in the oxygen atmosphere, whereupon air was introduced into the reaction tube for about 15 minutes.

Copper specimens were oxidized in a refractory lined furnace with air supplying the oxygen. They were placed in the preheated furnace, the time of oxidation being taken from the time at which the specimens

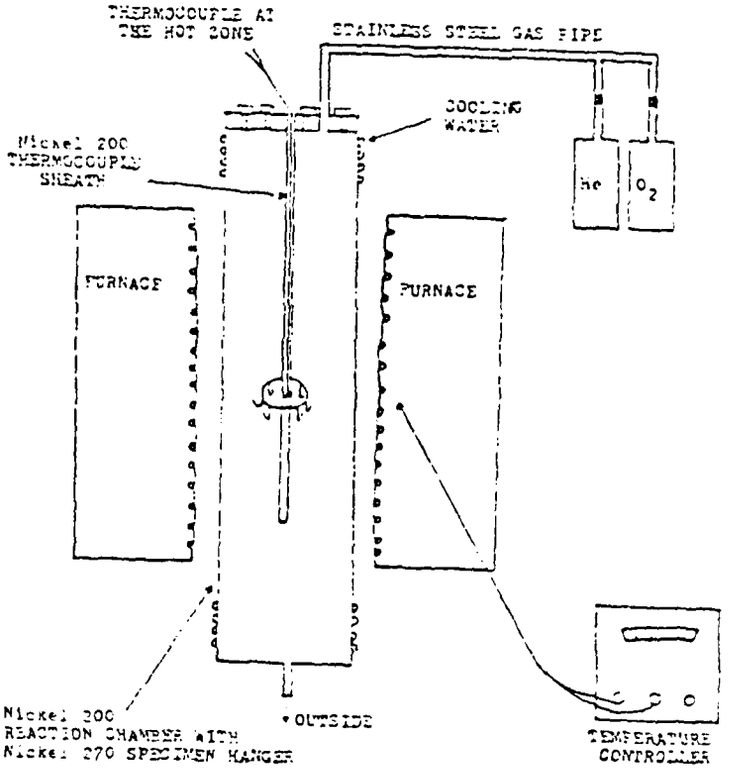


Figure 1. Schematic diagram of the furnace system used for the oxidation of Ni 270 and Ni 200 specimens.

Table I

Standardized Surface Treatment of Ni 270 and Ni 200 Specimens Before Oxidation

1. Preoxidize at 1100°C for 1 hour in air.

2. Remove oxide by grinding on 180, 320, and 600 grit SiC papers using water as a lubricant.

3. Surface clean with following sequence:
   (a) Rinse in acetone--5 minutes (ultrasonic).
   (b) Rinse in boiling distilled water--5 minutes.
   (c) Rinse in ethanol--5 minutes (ultrasonic).
   (d) Rinse in distilled water--5 minutes (ultrasonic).
   (e) Rinse in ethanol--5 minutes (ultrasonic).
   (f) Dry in air.

were placed in the furnace. At the end of the predetermined oxidation period, the specimens were slowly cooled in the furnace to retard the tendency of the scale to spall.

Metallographic Preparation

Two kinds of mounting techniques were used for the metallographic examination of the NiO surface. The conventional normal sectioning method, wherein the specimen is cut at 90° to the place of the oxidized surface, was utilized to measure the scale thickness and mean intercept length of the NiO grains. Although normal sections provided a good measure of the relative thickness of the outer and inner layer of the scale, or structural distinction between the two layers, they do neither reveal the grain size clearly with respect to position in the scale layer, nor show how the foreign matter and pores, if any, are disposed within it. In order to observe these features in more detail, another metallographic study was undertaken in which the scales were taper sectioned, at an angle of 3° - 5° from the plane of the metal-oxide interface, Figure 2. This small angle section method allowed for the available thickness of the oxide, revealed in the plane of polish, to be extended by a factor of as much as 2 times the perpendicular thickness of the scale. With this extension of the scale thickness, it was possible to observe the microstructural character of the scale in more detail throughout the scale thickness.

Mounting and Polishing

The oxidized nickel specimens were mounted with epoxy resin* and epoxy hardener (mixing ratio of resin to hardener is 5:1 by weight) in

*Product of Buehler Co. Ltd.

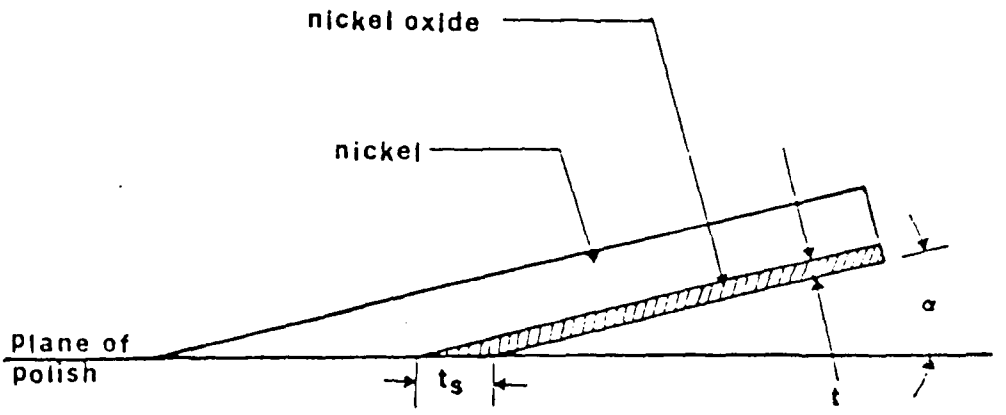


$t_s$ — apparent thickness of scale in plane of polish

t — normal thickness of scale

α — taper section angle

$$t_s = t/\sin\alpha$$

Figure 2. Schematic representation of the small angle sectioning method.

an aluminum ring on a glass plate with vaseline grease rubbed on it. After the epoxy hardened, the mounted samples were sectioned on a lathe and consecutively ground on a series of metallographic papers. Table II outlines the metallographic procedures that were used to produce a high quality of polished and etched surface.

Copper specimens were mounted in Buehler Epoxide and polished by standard metallographic techniques using diamond abrasives. Only sections normal to the metal-oxide interface were prepared. The microstructure of the scale was revealed by etching in as solution containing 55 $^{v}$/o $HNO_3$, 25 $^{v}$/o $CH_3$ COOH (glacial) and 20 $^{v}$/o $H_3$ $PO_4$.

Scale Thickness Measurements

The measurements of scale thickness were under a Bausch and Lomb Research II Metallograph using a reticle scale calibrated with a standard micrometer at 600X or 1000X. For each of the specified oxidation times (1, 4, 16, 36, 64, 81, 225 hours), both normal section and taper section specimens were prepared for the thickness measurements. For normal section specimens, the total scale thickness ($X_{TOT}$) was measured upon the polished surface, at a minimum of 2 positions for each specimen. Specimens which developed a non-uniform scale thickness were measured at many more positions than those which developed a relatively uniform scale thickness.

The columnar layer thickness ($X_{COL}$) was measured on the etched surface and the equiaxed layer thickness ($X_{EQ}$) was obtained by taking the difference between the total scale thickness and columnar layer thickness. The mean value of the measurements as well as the 95% confidence interval was determined for each time of oxidation. For taper sectioned specimens, the total thickness, which was usually longer than

Table II

Polishing Procedure

Grinding: 120 grit SiC with water

180 grit SiC with water

320 grit SiC with water

600 grit SiC with water

Polishing: 6μ diamond, AB* Texmet Cloth

1μ diamond, AB Texmet Cloth

Electrolytic etching to reveal the NiO microstructure

Solution: 1 vol. HF (48%)

1 vol. $CH_3COOH$ (glacial)

4 vol. $H_2O$ (distilled)

Anode: Specimen

Potential: 10 to 15 volts (open circuit)

Time: about 1 minute for Ni 270 specimens

about 5 minutes for Ni 200 specimens

Temperature: 25°C

---

*Product of Buehler Co., Ltd.

250 μm, was measured upon the etched surface only three or four times for each specimen and the average value was taken. From this value and the normal (perpendicular) thickness data, the taper angle was calculated. The ratios of the inner layer thickness and outer layer thickness to the total thickness were determined to evaluate the relative growth rate of each layer.

Measurement of the Mean Grain Intercepts

The mean intercept grain sizes of the columnar layer and inner layer were also determined using the Bausch and Lomb Research II Metallograph furnished with a calibrated test line of 0.1475 mm or 0.07375 mm in length. The test line was superimposed upon the image of the scale parallel to the metal-oxide interface, or perpendicular to it corresponding to Figure 3. The number of NiO grain boundary intercepts made with this test line was counted at various positions in the scale. The magnification used was 600X or 1000X.

Upon normal sections, readings of the mean intercepts of columnar grains were taken at a position roughly halfway between the external surface and the columnar-equiaxed interface. The equiaxed readings were taken by applying the test line roughly within 3% of the total thickness from the metaloxide interface. Enough areas of the scale were measured on each specimen so that 400 or more NiO grain boundary intercepts were counted to permit only a 5% of statistical sampling error. For taper sections, the intercept counting was carried out as a function of the distance from the metal-oxide interface to the outer surface with the test line placed parallel. Mean intercept counts were also made perpendicular to the metal surface.

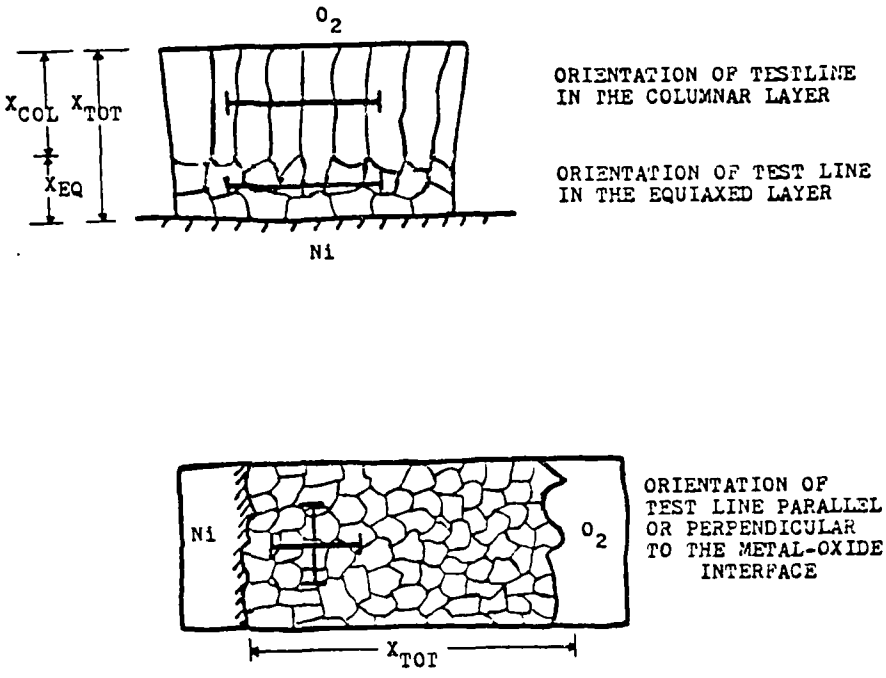


Figure 3. Application of the test line upon the image of NiO scale to determine the number of the NiO grain boundary intercepts in the columnar and equiaxed layers.

The mean number of NiO grain boundary intercepts per unit length of test line ($\bar{N}_L$) was computed by dividing the mean values of the number of grain boundary intercepts with the calibrated length of test line (0.07375 mm or 0.1475 mm) for all the measurements. Mean intercept grain size ($\lambda_{COL}$, $\lambda_{EQ}$, or $\lambda_{Taper}$) were obtained by taking the reciprocal of the corresponding $\bar{N}_L$ values. The ratios of these mean intercept lengths to the total thickness, or to the thickness of either layer, were determined for the further evaluation of the relationship between scale growth and grain growth.

Measurement of Porosity

Another global property that was utilized in this research was the measurement of volume fraction of pores, as viewed upon the taper section of Ni-200 specimens. Rectangular grid points (4 x 4 or 6 x 6) were applied upon the photographic image of the NiO scale and the number of grid points which were touching the pores was counted, Figure 4. Following the computation of the mean value of the number of pore-touching grid points per single application, as well as the 95% confidence interval, this value was divided by the total number of grid points (16 or 36) to yield the volume fraction of pores. Repeating this process from the metal-oxide interface to the outer surface, the change of porosity in volume fraction was obtained with the depth of the scale from the metal surface.

Microstructure at the Metal-Oxide Interface

For reasons of clarity, this topic will be treated under a subsequent section.

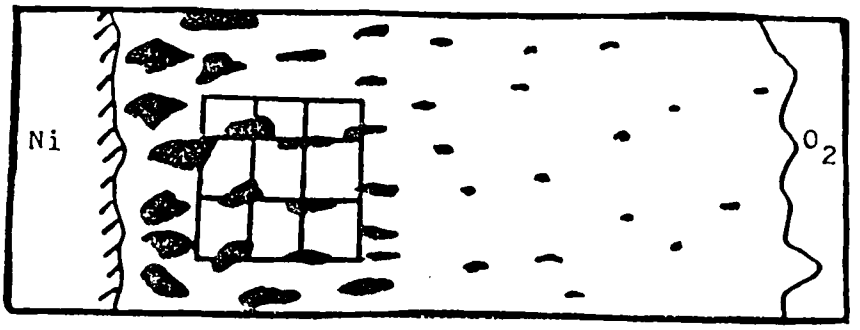


Figure 4. Application of rectangular grid points for measurement of porosity upon small angle section.

## EXPERIMENTAL RESULTS AND DISCUSSION

### Oxide Scales on Nickel 270

The oxide scales grown at high temperature upon Ni-270 invariably two layered [1, 23] as shown in the normal section photomirograph of Figure 5. Equiaxed grains form the inner layer, while the outer layer is composed of columnar grains. Metallographic sections made at small grazing angles (about 5°) through the scale ("taper sections") show little or no difference either in the grain size or grain shape between the two layers Figure 6. In fact, in taper section, it is difficult to locate the boundary between the two layers without prior knowledge from observations made upon corresponding normal sections. The constancy of grain size and shape, from the metal-oxide interface to the external surface, as seen in taper section, established that grain growth occurs throughout the scale at more or less a constant rate

### Measurements Made Upon Normal Sections

Measured values of total scale "thickness ($X_{TOT}$) and columnar layer thickness ($X_{COL}$) of scales grown upon Ni-270 are given in Table III. It also contains the inner layer thickness, taken as ($X_{TOT}$) - ($X_{COL}$), the mean intercept grain sizes of columnar grains ($\bar{\lambda}_{COL}$) and equiaxed grains ($\bar{\lambda}_{EQ}$). One-third of the outer layer thickness, given in parentheses in column 5 of Table III, is approximately equal to both the mean intercept grain sizes of the columnar and equiaxed grains. Thus, columnar grains remain have a height to breadth ratio of about three to one during scale growth. Further, the equiaxed grains have about the same dimensions as the breadth of columnar grains. These results are in agreement with Healey [22].

Figure 5. Normal section of the NiO scale upon Ni-270, oxidized for 16 hours at 1000°C in pure oxygen at one atmospheric pressure, 1000X.

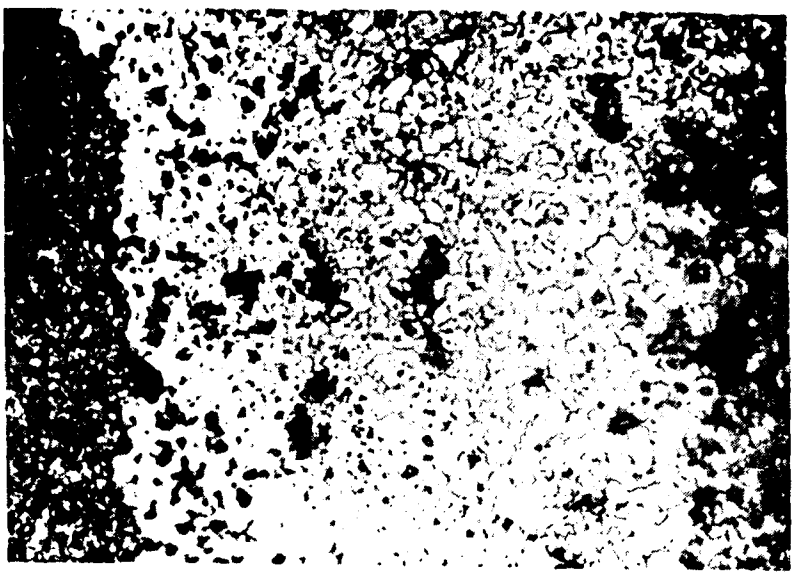

(a) Specimen oxidized for 4 hours, 360X.

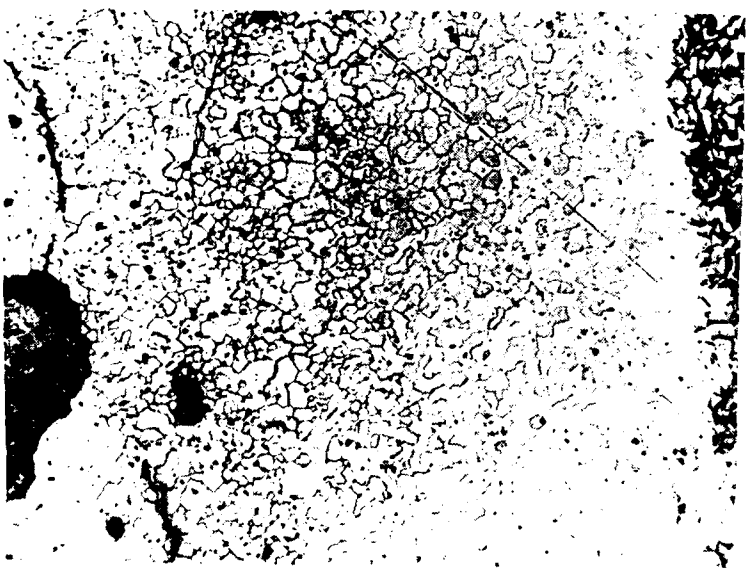

(b) Specimen oxidized for 81 hours, 200X.

Figure 6. Taper sections of NiO scale upon Ni-270, oxidized at 1000°C in pure oxygen at one atmospheric pressure.

Table III

Measurements Made on Normal Sections

| (1) Oxidation Time in hours at 1000°C | (2) Total Scale Thickness ($X_{TOT}$, μm) | (3) Columnar Layer Thickness ($X_{COL}$, μm) | (4) Equiaxed Layer Thickness by Diff. ($X_{EQ}$, μm) | (5) Mean Intercept Length of Columnar Grains ($\bar{\lambda}_{COL}$, μm) | (6) Mean Intercept Length of Equiaxed GRains ($\bar{\lambda}_{EQ}$, μm) |
|---|---|---|---|---|---|
| 4 | 10.62 ± 0.60 | 6.56 ± 0.41 | 4.06 | 2.67 (2.19) | 3.20 |
| 9 | 14.70 ± 0.92 | 8.60 ± 0.32 | 6.10 | (2.87) | -- |
| 16 | 20.54 ± 0.98 | 12.34 ± 0.49 | 8.20 | 3.86 (4.11) | 4.21 |
| 36 | 29.18 ± 1.30 | 18.40 ± 0.76 | 10.48 | 5.59 (6.23) | 5.05 |
| 49 | 30.63 ± 0.91 | 19.82 ± 0.72 | 10.81 | (6.6) | -- |
| 64 | 39.69 ± 2.02 | 23.00 | 16.69 | 6.4 (7.66) | 5.90 |
| 81 | 41.21 ± 1.49 | 23.90 ± 0.72 | 17.31 | 7.45 (7.97) | 6.76 |
| 225 | 57.73 ± 1.13 | 33.48 | 24.25 | (11.16) | -- |

Measurements Made Upon Taper Sections

Given in Table IV are measurements made upon taper sections through entire scales. The thickness of the equiaxed (inner) layer as seen in taper section was obtained by multiplying the corresponding thickness measured in the normal section by the cosecant of the grazing angle. Values of average grain size (columns 5 and 6) were obtained from mean number NiO grain boundary intercepts per unit length of test line ($N_L$). To obtain these values, $N_L$ was measured as a function of distance from the metal-oxide interface to the external surface by placing the test line parallel (column 5) or perpendicular (column 6) to the Ni-NiO interface; these values were then averaged throughout the entire layer.

The total average number of grains in the whole scale thickness, as seen in taper section, is given in column 7.

As a measure of grain size, the mean grain intercept length ($\bar{\lambda}$), the reciprocal of $N_L$, was computed. These "grain sizes" are plotted as a function of position in the scale layer for three oxidation times in Figure 7. From the data and by comparing the data of columns 5 and 6 of Table III with columns 5 and 6 of Table IV, it is conclusively demonstrated that grains of the inner layer of Ni-270 scales are three-dimensionally equiaxed and uniform in size, with the exception of some local fluctuations, throughout the layer. These grains also have the same mean intercept size as that of the transverse mean intercept length of the columnar grains in the outer layer.

Interpretation of the Metallographic Measurements

In Table V are given some ratios computed from the data of Tables III and IV. These ratio are helpful in deducing some of the mechanistic features of NiO scale growth. As viewed in normal section, the boundary

Table IV

Measurements Made on Taper Sections

| (1) Oxidation Time in Hours at 1000°C | (2) Angle of Sections, degrees | (3) Total Scale Thickness, as measured on the taper sections, μm | (4) Equiaxed Layer Thickness in Taper Section, calc. from Table III, μm | (5) Mean Intercept Grain Size ($\bar{\lambda}_{Taper}$) parallel to the surface, μm | (6) Mean Intercept Grain Size ($\bar{\lambda}_{Taper}$) perpendicular to the surface, μm | (7) Total Number of Grains in Taper Sections, perpendicular to the surface |
|---|---|---|---|---|---|---|
| 4 | 2.40 | 254 | 97 | 4.19 | 4.45 | 57 |
| 16 | 3.62 | 325 | 130 | 4.44 | 4.95 | 66 |
| 36 | 5.42 | 309 | 111 | 4.55 | 5.08 | 61 |
| 64 | 2.46 | 926 | 388 | 5.91 | 6.79 | 136 |
| 81 | 3.46 | 682 | 287 | 6.53 | 7.39 | 92 |

Figure 7. Average mean intercept grain size ($\overline{\lambda}_{Taper}$) as a function of depth in the scale from the metal-oxide interface (left) to the external surface (right) of the NiO upon Ni 270, oxidized at 1000°C under one atmosphere of pure oxygen.

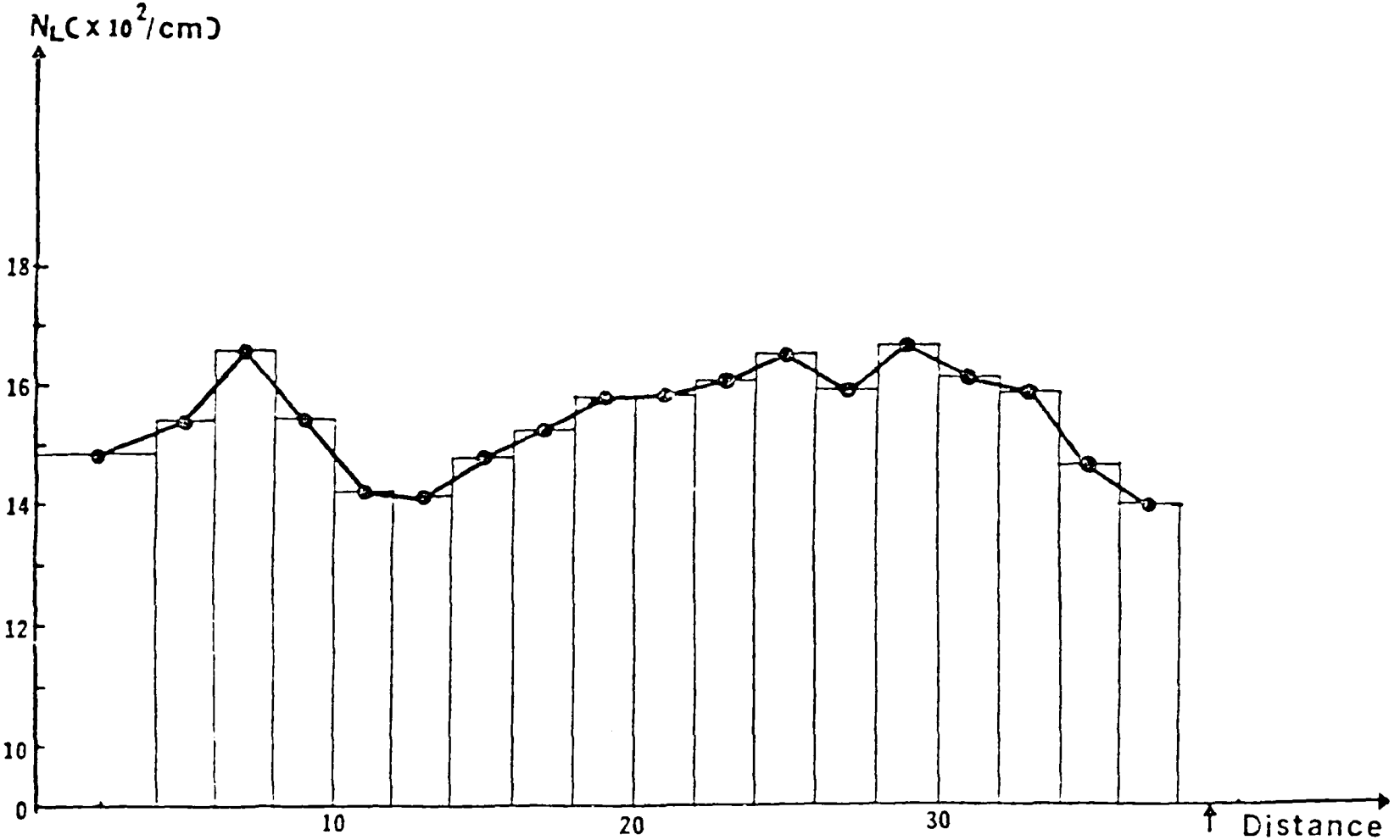


Figure 7(a). Specimen oxidized for 81 hours.

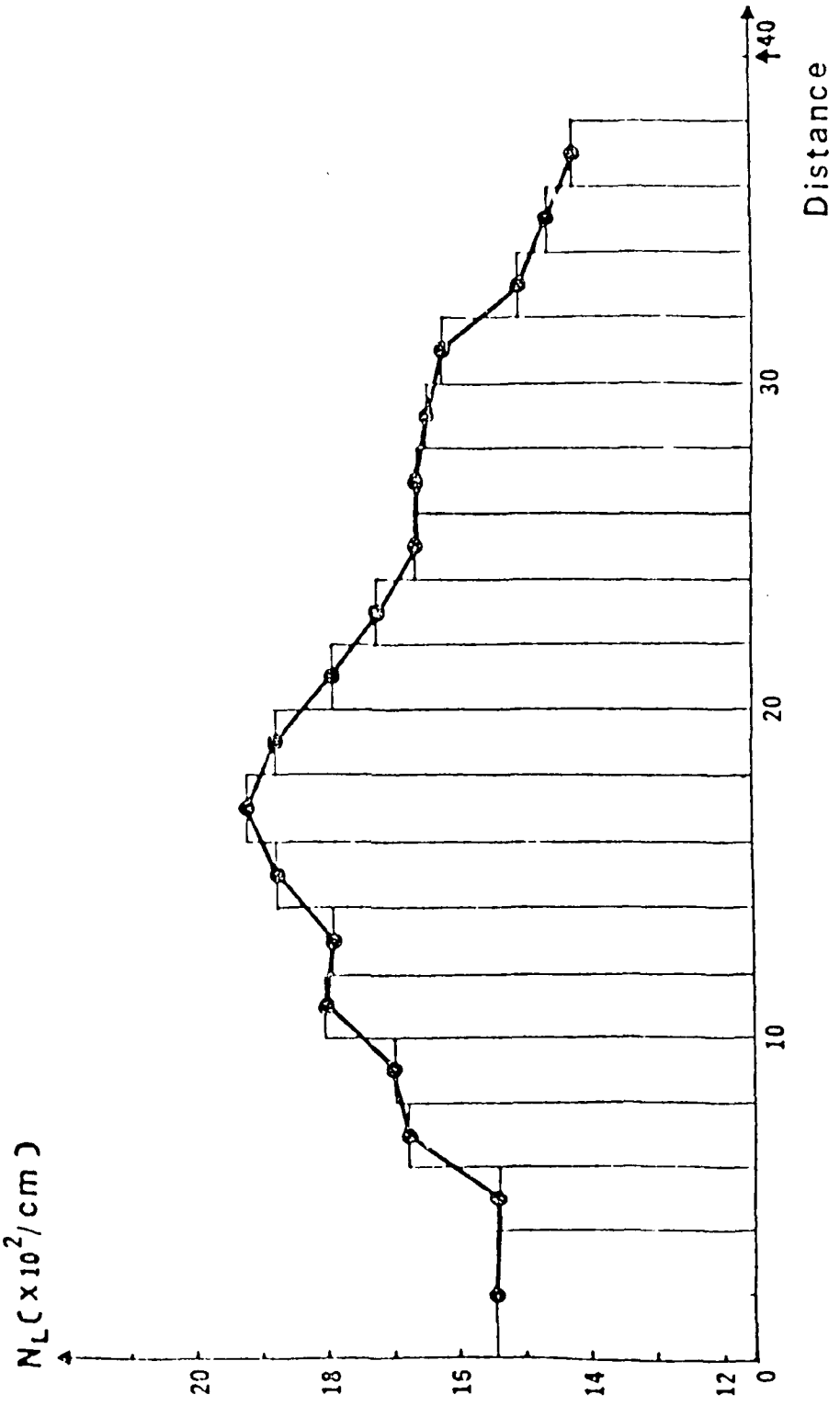


Figure 7(b). Specimen oxidized for 64 hours.

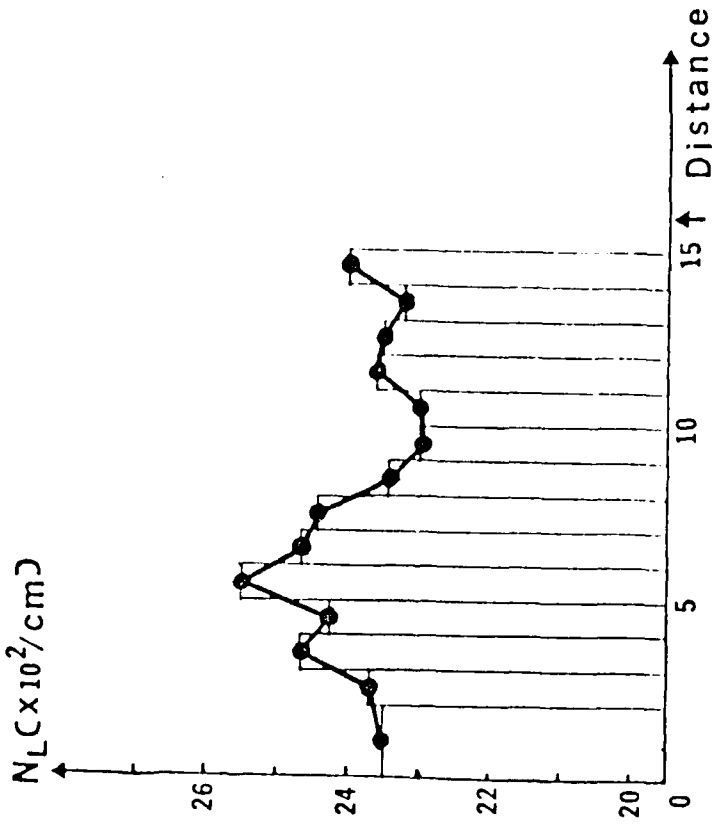


Figure 7(c). Specimen oxidized for 4 hours.

Table V

Ratios from Table III and IV

| (1) Oxidation Time in Hours at 1000°C | (2) $\frac{\text{Column. Thick.}}{\text{Equiax. Thick.}}$ | (3) $\frac{\text{Total Thick.}}{\bar{\lambda}_{COL}}$ | (4) $\frac{\text{Column. Thick.}}{\bar{\lambda}_{COL}}$ | (5) $\frac{\text{Equiax. Thick.}}{\bar{\lambda}_{EQ}}$ | (6) $\frac{\text{Equiax. Thick.}}{\bar{\lambda}_{COL}}$ | (7) 40% of the Number of Grains in the Total Thickness of Taper Sections |
|---|---|---|---|---|---|---|
| 4 | 1.6 | 3.98 | 2.5 | 1.27 | 1.12 | 0.95 |
| 9 | 1.4 | 5.12 | (3.0) | -- | 2.13 | -- |
| 16 | 1.5 | 5.32 | 3.2 | 1.95 | 2.12 | 1.67 |
| 36 | 1.7 | 5.22 | 3.10 | -- | 1.87 | 2.30 |
| 49 | 1.8 | 4.64 | (3.0) | -- | (1.64) | -- |
| 64 | 1.4 | 6.20 | 3.6 | 2.02 | 2.61 | 2.32 |
| 81 | 1.4 | 5.53 | 3.20 | 2.56 | 2.32 | 2.22 |
| Average | 1.5 | 5.14 | 3.09 | 2.15 | 2.03 | 1.89 |

separating the two scale layers is observable by the difference in grain shape, i.e. columnar versus equiaxed. No obvious difference in grain size or shape marks the boundary as seen in taper section, except that occasionally it is marked by a line of inert residues from the original unoxidized surface [5, 119].

Measurements upon normal sections show that the interlayer boundary lies at about two-fifths of the distance between the metaloxide interface and the external surface (column 2, Table V). Other important features observed from the ratios which are constant with oxidation time are, namely:

(1) The mean breadth of the columnar grains is one-fifth of the total scale thickness (column 3), or one-third of the columnar layer thickness (column 4).

(2) The inner layer of the scale is always about two grains in thickness; thus, the thickness of the columnar layer is about three times greater than the grain dimension of the inner layer (columns 4, 5 and 6). This relationship connects grain growth with scale growth and holds throughout the twolayered growth of scales on Ni-270 2%. That this feature of the grain structure of the inner layer is real is also confirmed by measurements on taper sections wherein a significant variation in inner layer thickness with oxidation time is detectable due to small differences in grazing angle. There, the total number of grains traversed in the whole scale as seen in taper section (column 7, Table IV), divided by the cosecant of the grazing angle equals the equivalent number of mean intercept lengths in the total thickness of the scale. Forty percent (two-fifths of the scale thickness) of this number is taken as the average number of grains in the thickness of the inner

layer (column 7, Table V). These values compare favorably with estimates if the number of grains in the inner layer obtained from normal section measurements (columns 5 and 6).

At short oxidation times, the thickness of the inner layer is too small to accomodate even one layer of the first equiaxed grains. This is understood to mean that the first grains of the inner layer are flattened with respect to the metal surface. Non-equiaxedness vanishes with longer oxidation time as the aforementioned ratios become established.

Kinetics of Scale Growth and Grain Growth

The oxide scales on Ni-270 thicken according to the cube root of time law not according to parabolic kinetics. This is true of the whole scale as well as both its inner and outer layers, Figure 8 (a through c). It is to be noted that extrapolation of the three cube root of time curves intersect the oxidation time axis at positive value. Discussion of this latter point is reserved for a later section of this report.

Similarly, the increase in the mean intercept length of the columnar grains ($\bar{\lambda}_{COL}$) measured parallel to the metal-oxide interface obeys cube root of time behavior, Figure 9. Thus, as expected, direct proportionality so that the total scale thickness is five times larger than $\bar{\lambda}_{COL}$, independent of oxidation time over the time range of one to 225 hours of oxidation time, Figure 10. Thus, it is established that scale growth and grain growth are interrelated. It had previously been found that grain growth in NiO did not occur in the absence of scale growth [64].

Microstructure of NiO at the Metal-Oxide Interface

Knowledge of the microstructural evolution at the metaloxide interface was of particular interest because of the information that it

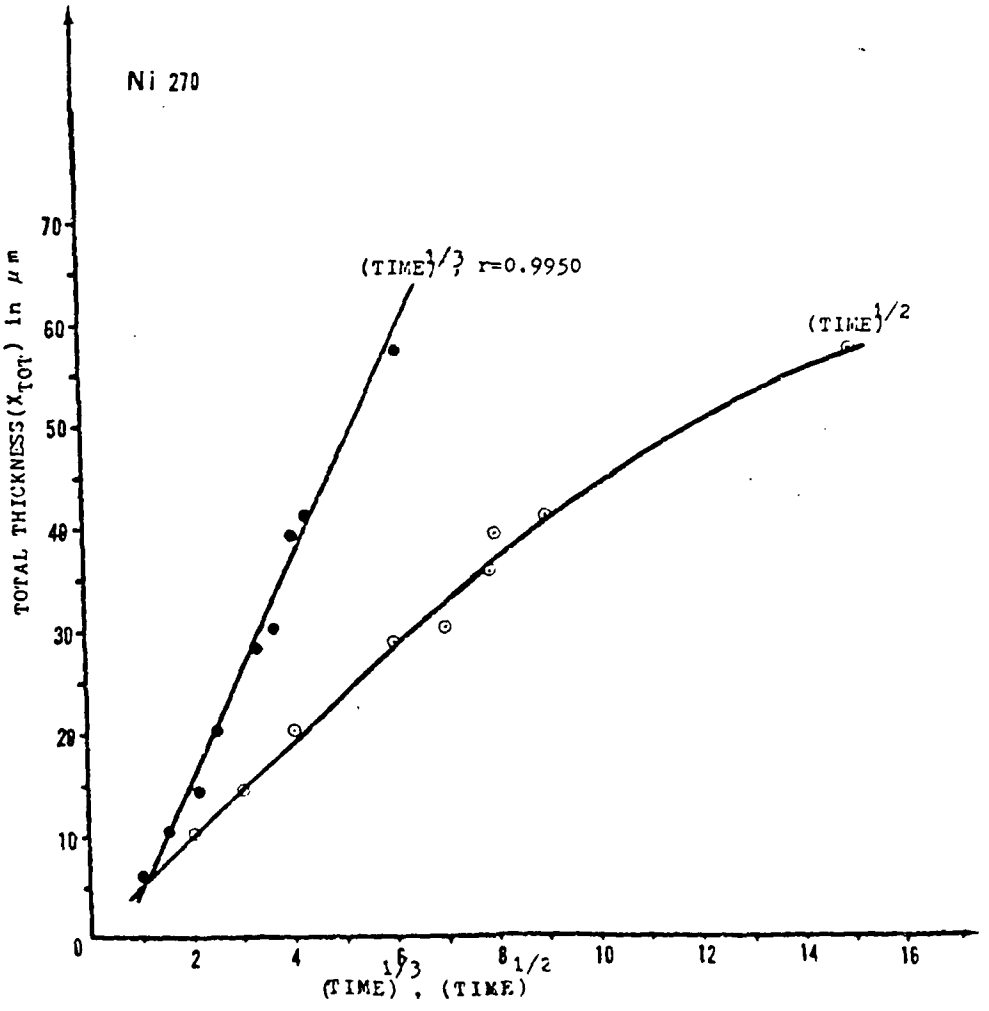


Figure 8(a). Total thickness ($X_{TOT}$) versus $(time)^{1/3}$ or $(time)^{1/2}$.

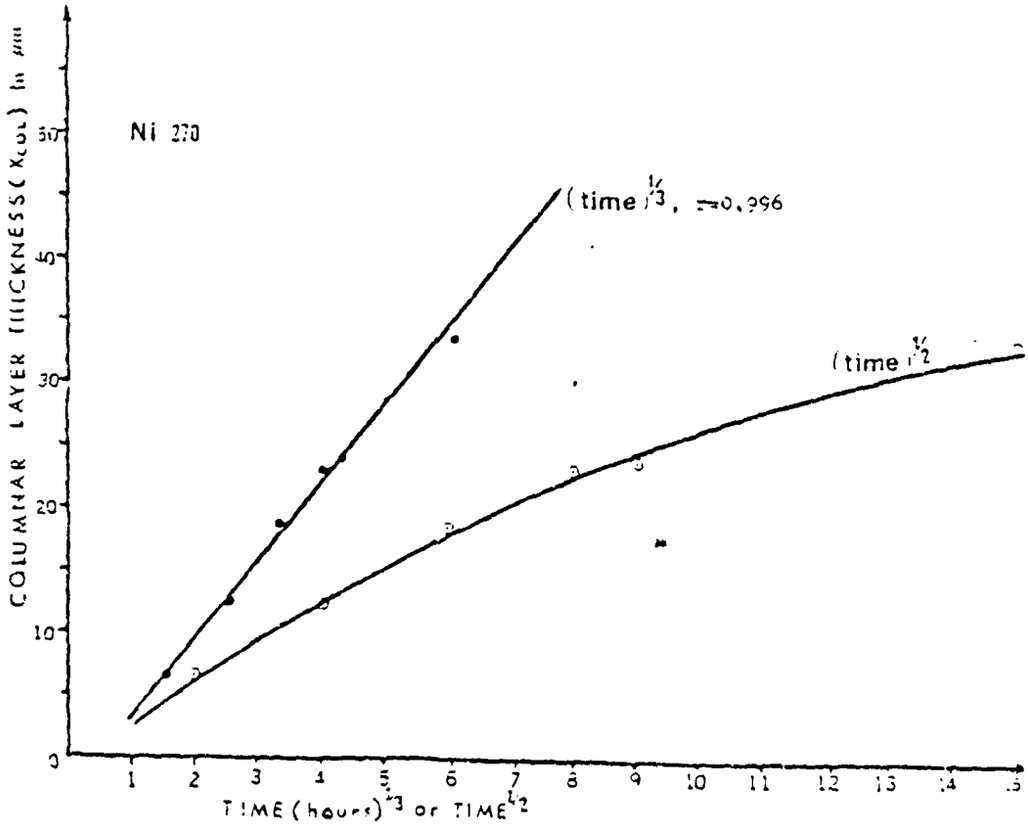


Figure 8(b). Columnar layer thickness ($X_{COL}$) versus $(time)^{1/3}$ or $(time)^{1/2}$.

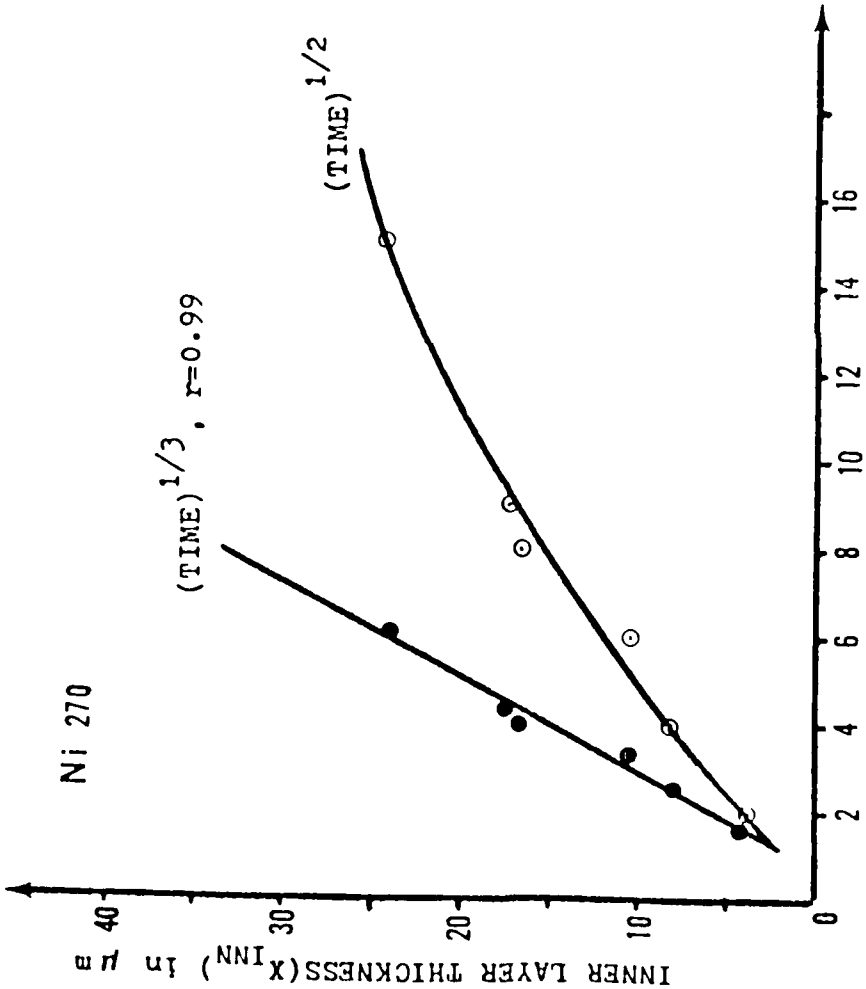


Figure 8(c). Inner layer thickness ($X_{INN}$) versus $(time)^{1/3}$ or $(time)^{1/2}$.

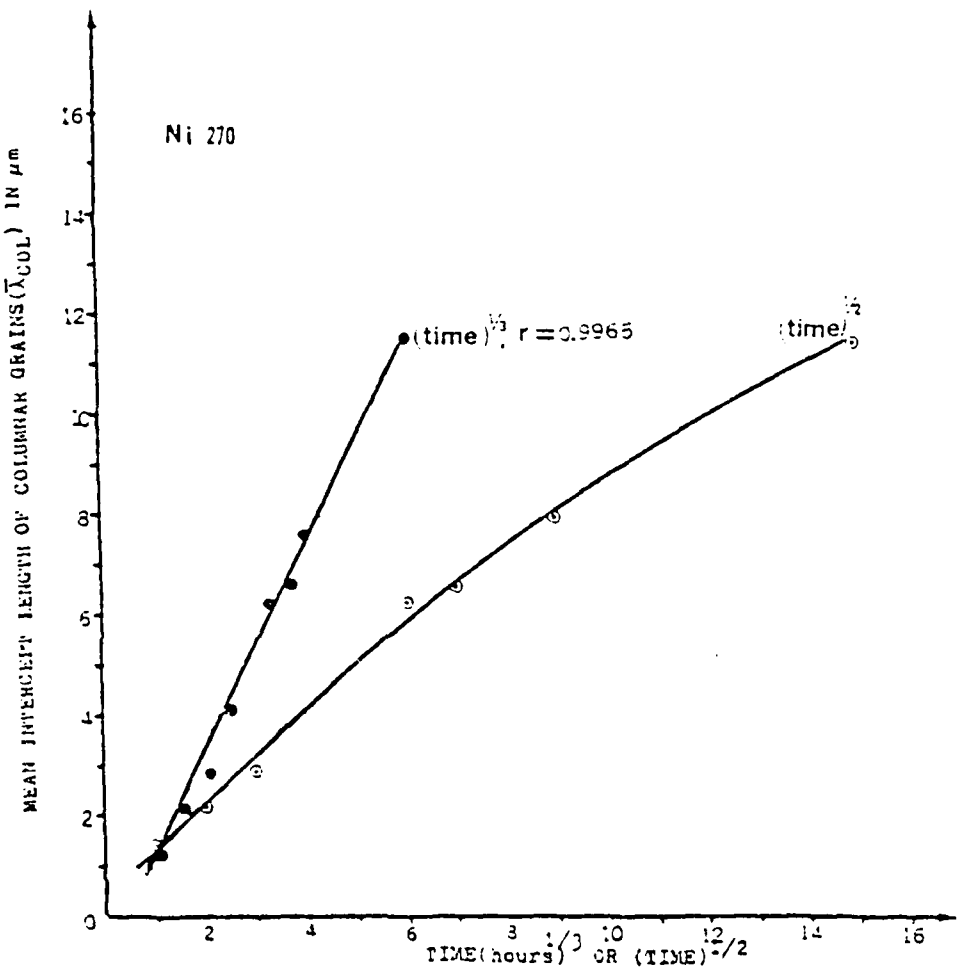


Figure 9. Mean intercept length of the columnar grains ($\bar{\lambda}_{COL}$) versus $(time)^{1/3}$ or $(time)^{1/2}$ for Ni 270 specimens, oxidized at 1000°C in pure oxygen at one atmospheric pressure.

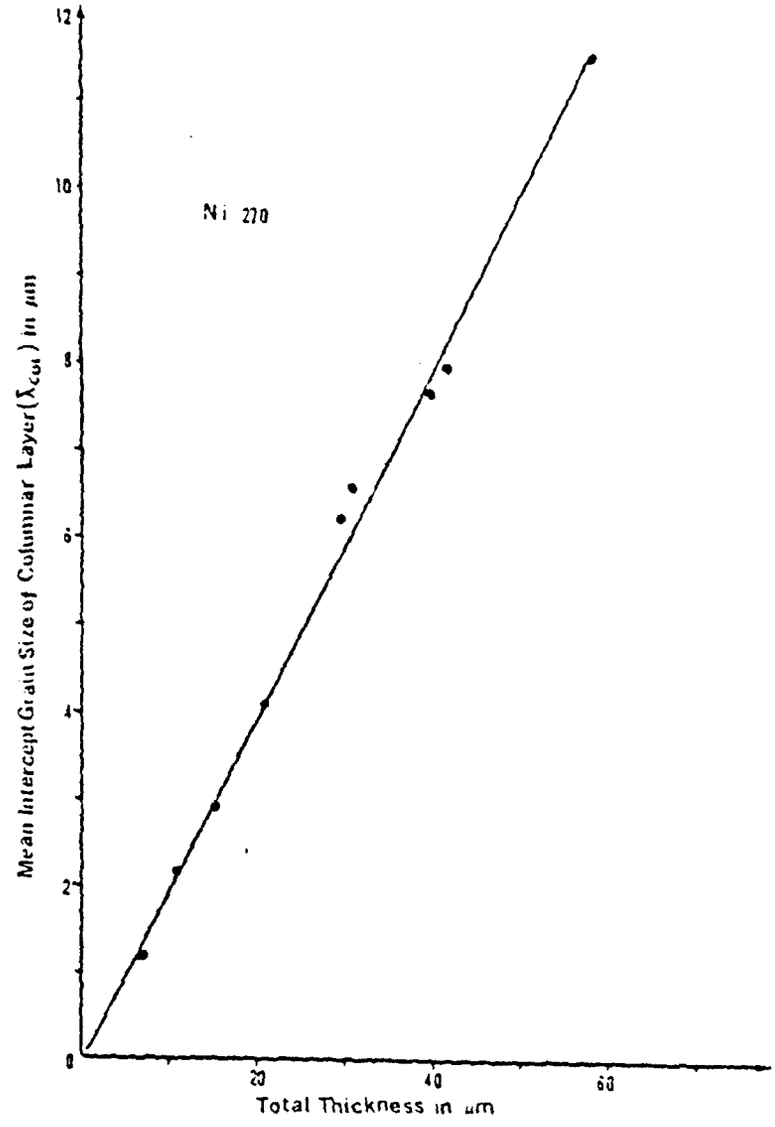


Figure 10. Relationship between scale growth ($X_{TOT}$) versus grain growth ($\bar{X}_{COL}$) for Ni 270 specimens, oxidized at 1000°C in pure oxygen at one atmospheric pressure.

yields regarding the nucleation and growth of new NiO grains and the origin of pore generation in the scale.

To study in detail the oxide grain structure at the interface, NiO scales were detached from the metal substrate by a technique pioneered by Evans [12] a half-century ago for the removal of oxide scales from iron with iodine. In the case of nickel, the substrate was dissolved by immersing an oxidized coupon in a solution of 99.4% bromine and absolute ethyl alcohol mixed in the volume ratio 1:1. The bromine solution attacks only the nickel, thus freeing the oxide scale in tact. Ultrasonic washing of the removed scales in acetone and distilled water removed all traces of the bromine and provided a clean inner scale surface suitable for SEM observations. To provide a electrically conductive surface for proper SEM observation a gold-palladium coating was evaporated onto the surface of the scale which had been in contact with the nickel substrate.

The SEM photomicrographs of Figures 11-14 are representative of the many SEM photomicrographs taken of the inner surfaces of bromine treated scales grown upon Ni-270. The pattern of nickel erosion at the metal-oxide interface, this revealed, is to be associated with the solution of Ni in NiO at various sites over the interfacial surface.

Careful examination of these inner surfaces resulted in the following new and important observations:

(1) At all times of oxidation, the majority of the NiO grains have relatively smooth surfaces, and their contours can be characterized as a variety of dishedness in the middle, surrounded by a relatively high rim

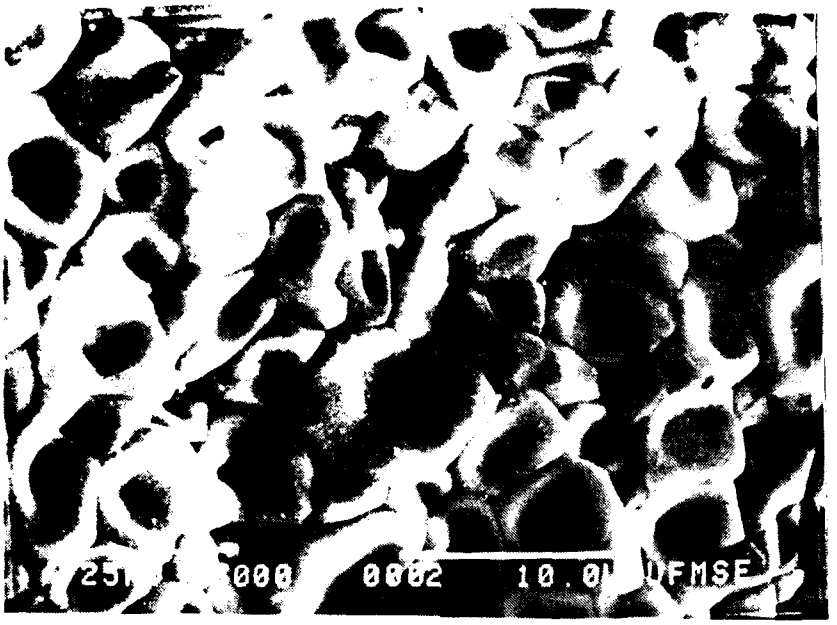

Figure 11. SEM micorgraphs of NiO structure at the metal-oxide interface, taken from the chemically detached scale upon Ni-270, oxidized at 1000°C in one atmosphere pressure of pure oxygen.

Figure 11(a). Specimen oxidized for 4 hours, 3000X.

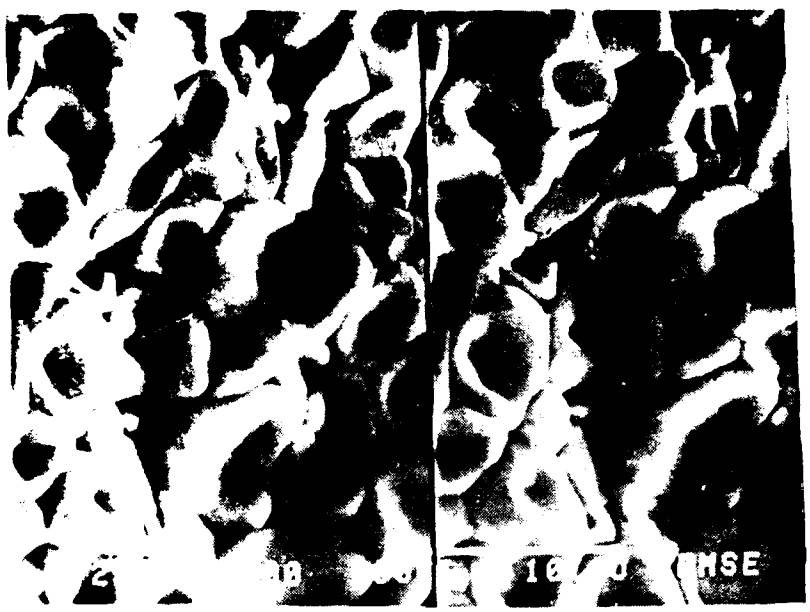

Figure 11(b).SEM stereographic pair of (a).


Figure 12. SEM photomicrographs of NiO structure at the metal-oxide interface, taken from the chemically detached scale upon Ni-270. The randomly scattered small and white materials on the surface of NiO grains are the dirt which remain still after the cleaning.

Figure 12(a). Specimen oxidized for 49 hours, 3000X.

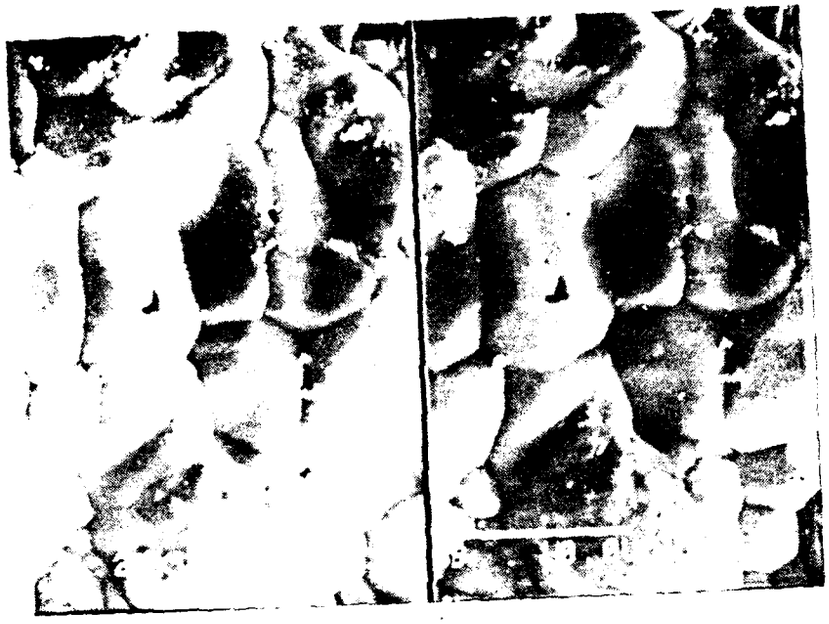

Figure 12(b). SEM stereographic pair of (a).


Figure 13. SEM photomicrographs of NiO structure at the metal-oxide interface, taken from the chemically detached scale upon Ni-270, oxidized at 1000°C in pure oxygen of one atmosphere pressure.

Figure 13(a). Specimen oxidized for 64 hours, 3000X.

Figure 13(b). Microstructure at a different position from (a).

Figure 14. SEM photomicrographs of NiO at the metal-oxide interface, taken from the chemically detached scale upon Ni-270, oxidized at 1000°C in pure oxygen of one atmospheric pressure.
Figure 14(a). Specimen oxidized for 81 hours, 3000X.

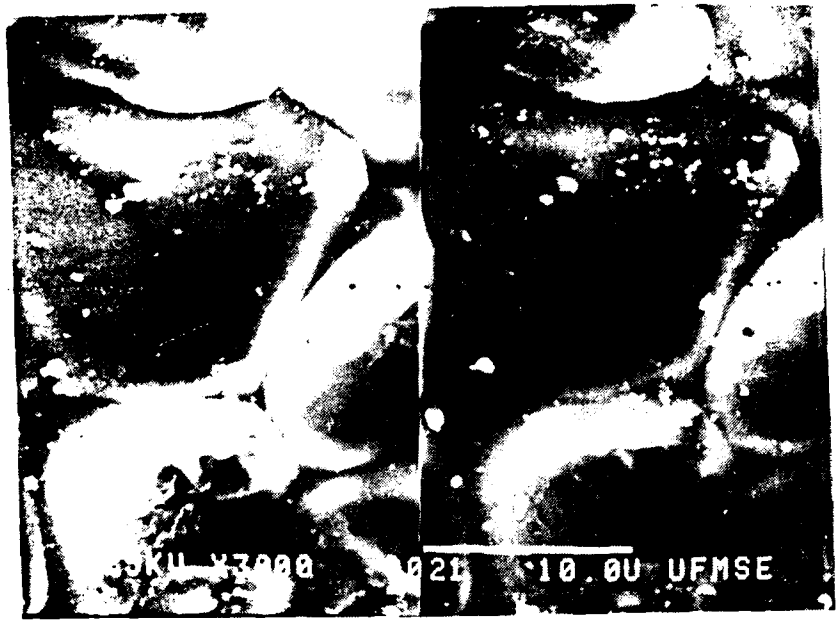


Figure 14(b). SEM stereographic pair of (a).

and rounding off at the edges along grain boundaries.* The shapes of the grain surfaces at the metal-oxide interface presumably results from various rates of $Ni^{++}$ up-take into the NiO from point to point on the metal-oxide interface; the rate of up-take being the slowest at NiO grain centers and the fastest along NiO grain boundaries where the oxygen potential is expected to be the greatest.

(2) The average grain size of the NiO at the metal-oxide interface increases as oxidation proceeds.

(3) Relatively large numbers of very small grains correspond to short oxidation times, Figure 11. There are presumed to be newly nucleated. The frequency of occurrance of small grains diminishes with increasing oxidation times. A feature of note is that small grains consistently seem to appear at the juncture of three large NiO grains, or where the ends of NiO triple lines meet the nickel substrate.

(4) The scales formed upon Ni-270 are essentially pore free except for a very few oddly shaped cavities which are sometimes observed within grains or at oxide grain boundaries. These pores are presumed to be associated with gas evolution at the metal-oxide interface.

(5) Foreign oxide particles that might have existed as subscale particles* in the metal have not clearly been identified. Such particles

---

*It was found that the bromine solution attacks NiO grain boundaries; therefore, the sharpness of grain boundaries could be enchanced by bromine etching without loss of detail in the grains themselves.

*Most impurities in nickel are more easily oxidized than the nickel itself and after oxidation exist in the metal as foreign oxides (subscale) rather than being in solution in the nickel. Because of the relatively high purity of Ni-270, the presence of a subscale was undetectable by the usual techniques of optical or SEM metallography.

have likely been removed by the bromine treatment of the scale. Evidence that they did exist was seen as occasionally observed small faceted spots on the surface where the particles might have resided prior to the bromine removal of the nickel. Figure 13(a and b).

Grain Size Distribution in the NiO Scale Upon Nickel 270

During the growth of a NiO scale, the grains coarsen. If the grains should grow solely by steady-state grain growth, the relative breadth grain size distribution remains essentially unchanged over rather great changes in the average grain volume. However, if nucleation of new grains occurs coincidental with grain growth, the breadth of the grain size distribution is skewed toward the lower class sizes. Thus, studies of the grain size distribution as the microstructure of the scale evolves concurrent with scale growth provide a unique tool by which nucleation of new grains in the scale can be studied.

Grain size distribution measurements in annealed polycrystalline metals [123-129], either by two or three dimensional studies have consistently demonstrated that the distribution is log-normal, i.e. frequency versus the log of the grain size is a Gaussian distribution. From the work of Okazki [127] and Patterson [128] it has been shown that the relative width of the grain size distribution depends upon process history and that the relative spread of this distribution remains unchanged throughout extended periods of grain growth. As a consequence, once the grain size distribution is established, the slope of the linear plot on a logrithmic probability scale does not change during grain growth.

Grain Area Distribution of NiO Upon the Metal-Oxide Interface

The grain size distributions of NiO grains at the metaloxide interface were determined for a series of specimens oxidized for increasing times. This was accomplished by tracing with a planimeter each grain in grain boundary tracings made from SEM photographs taken at a magnification of 300X. Data obtained in this manner is recorded in Tables VI-IX for specimens oxidized for 4, 49, 64 and 81 hours, respectively. These data are plotted as cumulative frequency versus log grain area (= 2 ln $\bar{x}$/ln2) for the four oxidation times in Figure 15. Over much of the range of sizes the distribution is log-normal, but the frequencies of the smallest sizes was always greater than would be expected of log-normal distributions. This is to be associated with small grains which are seen at $NiO^3$ - Ni quadruple points on the metal-oxide interface.

The excess of small grains represents those grains which recently had been nucleated. As oxidation proceeds, the average grain size increases correspondingly reducing the number of $NiO^3$ - Ni quadruple points; thus, the excess number of small grains (newly nucleated ones) would decrease and the deviation from linearity of the plots of Figure 15 would disappear. The deviation from log-normal behavior is greatest at the shortest time of oxidation.

Another measurement, that of the total number of quadruple points contained in a given area (142 $cm^2$ at 3000X) of oxide at the metal-oxide interface was made in order to establish a quantitative relationship between nucleation frequency and the number of quadruple points. By plotting the excess number of small grains, as obtained by the deviation from linearity in the plots of Figure 15, versus the number of quadruple points, Figure 16, it is seen that there exists a direct proportionality

Table VI

Grain Area Distribution of NiO at the Metal-Oxide Interface (4 Hours Oxidation)

| Size Classes | Area Range in $cm^2$ | Mean Area ($\bar{x}$) | Log Grain Size ($2\ell n\ \bar{x}/\ell n2$) | Number of Grains | Frequency (%) | Cumulative Frequency (%) |
|---|---|---|---|---|---|---|
| 1 | 0.03435-0.5716 | 0.303 | -3.445 | 21 | 18.58 | 18.58 |
| 2 | 0.5716-1.109 | 0.840 | -0.502 | 20 | 17.70 | 36.28 |
| 3 | 1.190-1.646 | 1.378 | 0.925 | 17 | 15.04 | 51.33 |
| 4 | 1.646-2.183 | 1.915 | 1.875 | 10 | 8.85 | 60.18 |
| 5 | 2.183-2.721 | 2.452 | 2.588 | 10 | 8.85 | 69.03 |
| 6 | 2.721-3.258 | 2.990 | 3.160 | 7 | 6.19 | 75.22 |
| 7 | 3.258-3.795 | 3.530 | 3.640 | 4 | 3.54 | 78.76 |
| 8 | 3.795-4.333 | 4.064 | 4.050 | 6 | 5.31 | 84.07 |
| 9 | 4.333-4.870 | 4.601 | 4.440 | 0 | -- | 84.07 |
| 10 | 4.870-5.407 | 5.139 | 4.732 | 2 | 1.77 | 85.84 |
| 11 | 5.407-5.944 | 5.680 | 5.010 | 1 | 0.88 | 86.73 |
| 12 | 5.944-6.482 | 6.213 | 5.271 | 6 | 5.31 | 92.04 |
| 13 | 6.482-7.019 | 6.750 | 5.510 | 1 | 0.88 | 92.92 |
| 14 | 7.019-7.556 | 7.290 | 5.730 | 2 | 1.77 | 94.69 |
| 15 | 7.556-8.094 | 7.825 | 5.936 | 0 | -- | 94.69 |
| 16 | 8.094-8.631 | 8.362 | 6.128 | 1 | 0.88 | 95.58 |
| 17 | 8.631-9.168 | 8.90 | 6.308 | 0 | -- | 95.58 |
| 18 | 9.168-9.705 | 9.437 | 6.477 | 2 | 1.77 | 97.35 |
| 19 | 9.705-10.240 | 9.974 | 6.636 | 2 | 1.77 | 99.12 |
| 20 | 10.240-10.780 | 10.511 | 6.790 | 1 | 0.88 | 100 |

Table VII

Grain Area Distribution of NiO at the Metal-Oxide Interface (49 Hours Oxidation)

| Size Classes | Area Range in $cm^2$ | Mean Area ($\bar{x}$) | Log Grain Size ($2\ell n\ \bar{x}/\ell n2$) | Number of Grains | Frequency (%) | Cumulative Frequency (%) |
|---|---|---|---|---|---|---|
| 1 | 0.03435-0.5716 | 0.303 | -3.445 | 21 | 18.58 | 18.58 |
| 2 | 0.5716-1.109 | 0.8403 | -0.502 | 20 | 17.70 | 36.28 |
| 3 | 1.109-1.646 | 1.378 | 0.925 | 17 | 15.04 | 51.33 |
| 4 | 1.646-2.183 | 1.915 | 1.875 | 10 | 8.85 | 60.18 |
| 5 | 2.183-2.721 | 2.452 | 2.588 | 10 | 8.85 | 69.03 |
| 6 | 2.721-3.258 | 2.99 | 3.160 | 7 | 6.19 | 75.22 |
| 7 | 3.258-2.795 | 3.53 | 3.64 | 4 | 3.54 | 78.76 |
| 8 | 3.795-4.333 | 4.064 | 4.05 | 6 | 5.31 | 84.07 |
| 9 | 4.333-4.870 | 4.601 | 4.40 | -- | -- | 84.07 |
| 10 | 4.870-5.407 | 5.139 | 4.723 | 2 | 1.77 | 85.84 |
| 11 | 5.407-5.944 | 5.68 | 5.01 | 1 | 0.88 | 86.73 |
| 12 | 5.944-6.482 | 6.213 | 5.271 | 6 | 5.31 | 92.04 |
| 13 | 6.482-7.019 | 6.750 | 5.51 | 1 | 0.88 | 92.92 |
| 14 | 7.019-7.556 | 7.29 | 5.73 | 2 | 1.77 | 94.69 |
| 15 | 7.556-8.094 | 7.825 | 5.936 | -- | -- | 94.69 |
| 16 | 8.094-8.631 | 8.362 | 6.128 | 1 | 0.88 | 95.58 |
| 17 | 8.631-9.168 | 8.90 | 6.308 | -- | -- | 95.58 |
| 18 | 9.168-9.705 | 9.437 | 6.477 | 2 | 1.77 | 97.35 |
| 19 | 9.705-10.24 | 9.974 | 6.636 | 2 | 1.77 | 99.12 |
| 20 | 10.24-10.78 | 10.511 | 6.79 | 1 | 0.88 | 100 |

Table VIII

Grain Area Distribution of NiO at the Metal-Oxide Interface (64 Hours Oxidation)

| Size Classes | Area Range in $cm^2$ | Mean Area ($\bar{x}$) | Log Grain Size ($2\ell n\ \bar{x}/\ell n2$) | Number of Grains | Frequency (%) | Cumulative Frequency (%) |
|---|---|---|---|---|---|---|
| 1 | 0.1802-1.204 | 0.6921 | -1.06 | 17 | 26.56 | 26.56 |
| 2 | 1.204-2.228 | 1.72 | 1.56 | 17 | 26.56 | 13.13 |
| 3 | 2.228-3.252 | 2.74 | 2.91 | 8 | 12.5 | 65.63 |
| 4 | 3.252-4.276 | 3.76 | 3.82 | 8 | 12.5 | 78.13 |
| 5 | 4.276-5.300 | 4.79 | 4.52 | 5 | 7.81 | 85.94 |
| 6 | 5.300-6.324 | 5.81 | 5.08 | 2 | 3.13 | 89.06 |
| 7 | 6.324-7.348 | 6.84 | 5.55 | 3 | 4.69 | 93.75 |
| 8 | 7.348-8.372 | 7.86 | 5.95 | 1 | 1.56 | 95.31 |
| 9 | 8.372-9.396 | 8.88 | 6.30 | -- | -- | 95.31 |
| 10 | 9.396-10.42 | 9.91 | 6.62 | -- | -- | 95.31 |
| 11 | 10.42-11.44 | 10.93 | 6.90 | 1 | 1.56 | 96.88 |
| 12 | 11.44-12.47 | 11.96 | 7.16 | -- | 1.56 | 98.44 |
| 13 | 12.47-13.49 | 12.98 | 7.40 | -- | -- | 98.44 |
| 14 | 13.49-14.52 | 14.00 | 7.61 | -- | -- | 98.44 |
| 15 | 14.52-15.54 | 15.03 | 7.82 | -- | -- | 98.44 |
| 16 | 15.54-16.56 | 16.05 | 8.01 | -- | -- | 98.44 |
| 17 | 16.56-17.59 | 17.08 | 8.19 | -- | -- | 98.44 |
| 18 | 17.59-18.61 | 18.10 | 8.36 | -- | -- | 98.44 |
| 19 | 18.61-19.64 | 19.12 | 8.51 | -- | -- | 98.44 |
| 20 | 19.64-20.66 | 20.15 | 8.67 | 1 | 1.56 | 100 |

Table IX

Grain Area Distribution of NiO at the Metal-Oxide Interface (81 Hours Oxidation)

| Size Classes | Area Range in $cm^2$ | Mean Area ($\bar{x}$) | Log Grain Size ($2\ell n\ \bar{x}/\ell n2$) | Number of Grains | Frequency (%) | Cumulative Frequency (%) |
|---|---|---|---|---|---|---|
| 1 | 0.762-1.360 | 1.061 | 0.171 | 17 | 23.94 | 23.94 |
| 2 | 1.360-2.344 | 2.054 | 2.08 | 11 | 15.49 | 39.44 |
| 3 | 2.344-3.327 | 2.99 | 3.16 | 14 | 19.72 | 59.15 |
| 4 | 3.327-4.311 | 3.95 | 3.96 | 7 | 9.86 | 69.01 |
| 5 | 4.311-5.295 | 4.92 | 4.60 | 4 | 5.63 | 74.65 |
| 6 | 5.295-6.278 | 5.88 | 5.11 | 4 | 5.63 | 80.28 |
| 7 | 6.278-7.262 | 6.85 | 5.55 | 4 | 5.63 | 85.92 |
| 8 | 7.262-8.246 | 7.81 | 5.93 | 2 | 2.82 | 88.73 |
| 9 | 8.246-9.229 | 8.78 | 6.27 | -- | -- | 88.73 |
| 10 | 9.229-10.21 | 9.74 | 6.57 | 2 | 4.23 | 91.55 |
| 11 | 10.21-11.20 | 10.71 | 6.84 | 3 | 1.41 | 95.77 |
| 12 | 11.20-12.18 | 11.67 | 7.09 | 1 | 1.41 | 97.18 |
| 13 | 12.18-13.16 | 12.63 | 7.32 | 1 | -- | 98.59 |
| 14 | 13.16-14.15 | 13.60 | 7.53 | -- | -- | 98.59 |
| 15 | 14.15-15.13 | 14.56 | 7.73 | -- | -- | 98.59 |
| 16 | 15.13-16.12 | 15.53 | 7.91 | -- | -- | 98.59 |
| 17 | 16.12-17.10 | 16.49 | 8.09 | -- | -- | 98.59 |
| 18 | 17.10-18.08 | 17.46 | 8.25 | -- | -- | 98.59 |
| 19 | 18.08-19.07 | 18.42 | 8.41 | -- | -- | 98.59 |
| 20 | 19.07-20.05 | 19.38 | 8.55 | 1 | 1.41 | 100 |

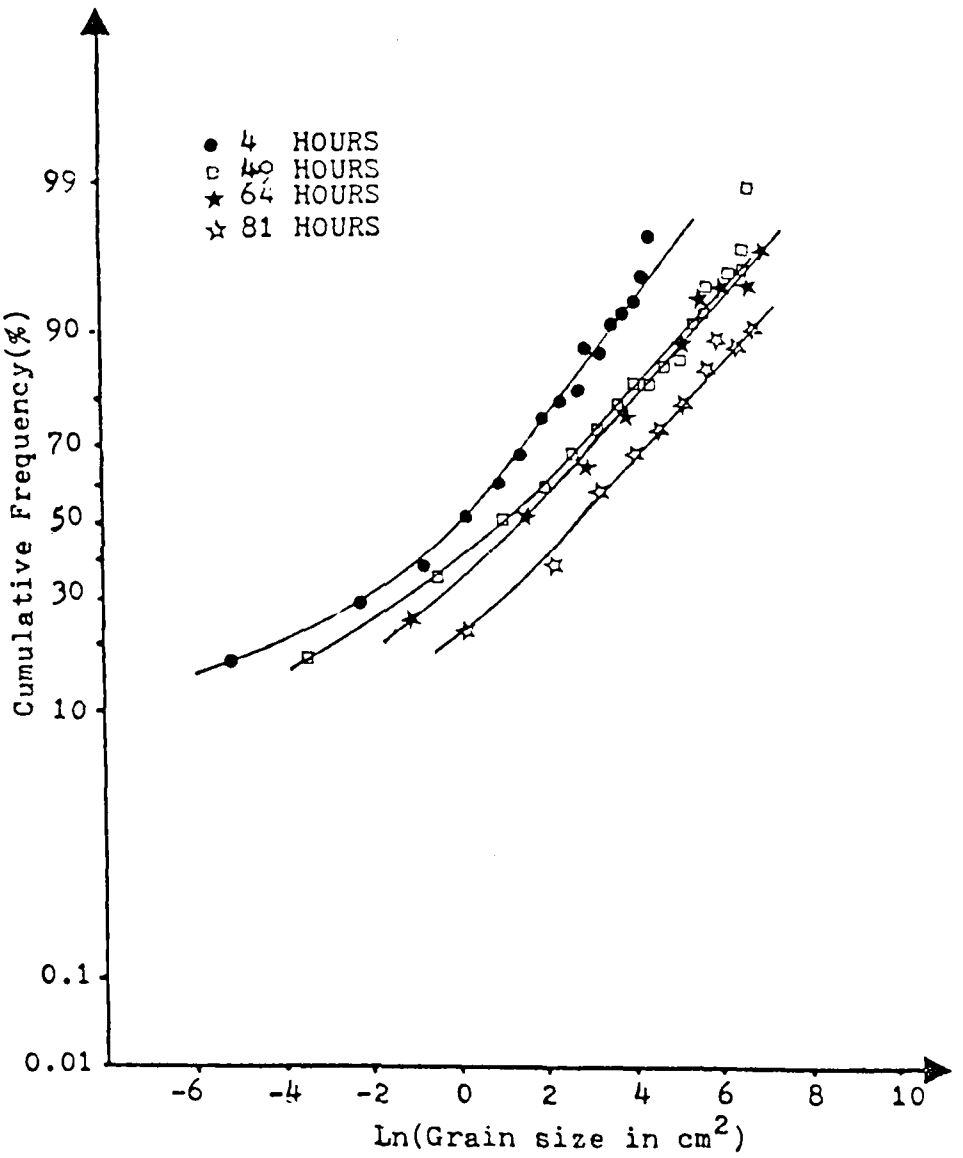


Figure 15. Log-normal probability plot of the grain area distribution upon the metal-oxide interface of Ni 270 specimens.

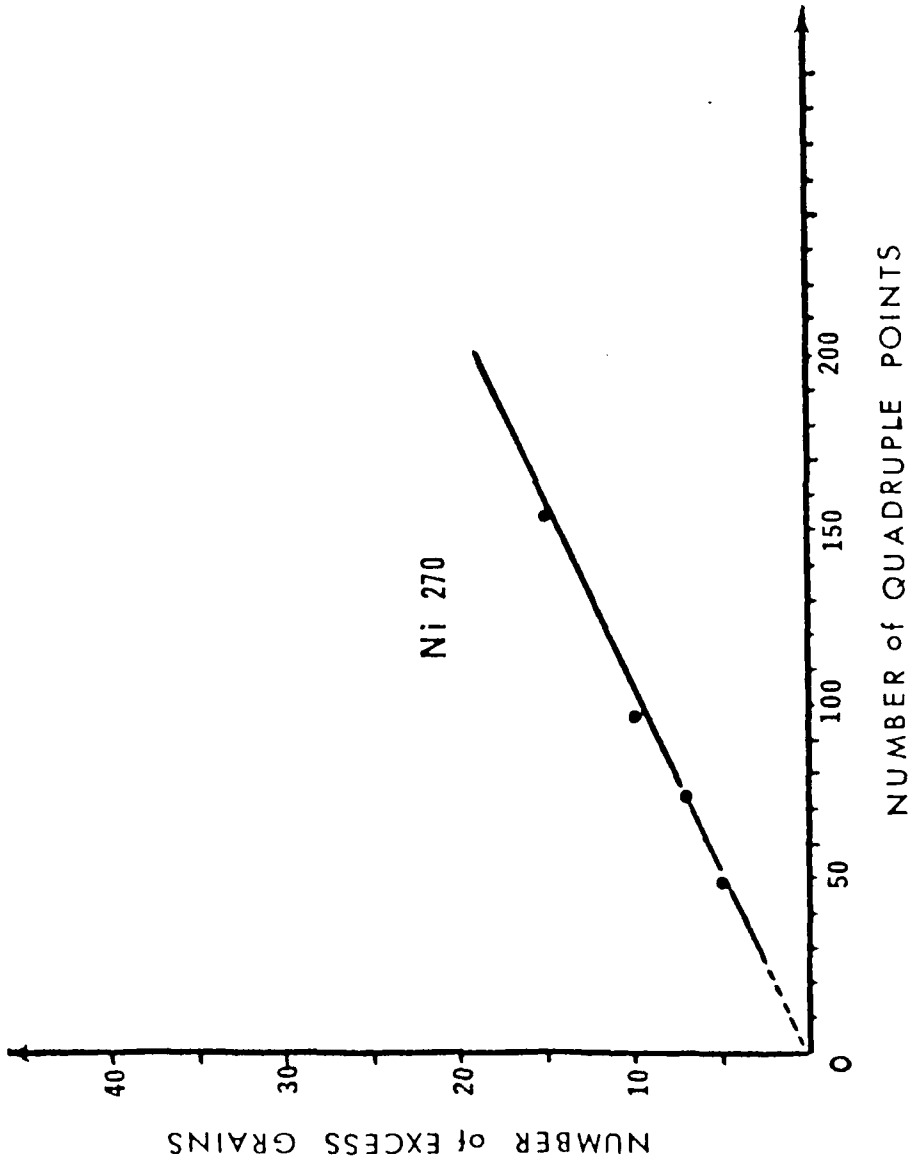


Figure 16. Number of excess small grains (nucleation frequency) versus number of quadruple points.

between the two. Hence, as the grain size increases the rate of nucleation of new grains decreases, because the number of quadruple points decreases.

It is important to note that the slope of the log-normal plots, Figure 15, does not vary a great deal, except for the smallest grains, even though the average grain size monotonically increases with time. Because the standard deviation of the normal distribution of the log arithmics of the grain areas ($\ln\sigma_A$) is inversely proportional to the slope of the log-normal plot, $\ln\sigma_A$ values were calculated from the equation for the standard deviation of the log-normal distribution:

$$\ln \sigma = \left[\frac{\sum_{i=1}^{n} (\ln \sigma_{Ai} - \overline{\ln \sigma_A})}{n-1}\right]^{\frac{1}{2}}$$

Given in Table X are the values of $\ln\sigma_A$ corresponding to the plots of Figure 15 along with the mean grain areas. From these values, it is seen that the relative width of the grain size distribution is practically constant with time, although the NiO grains at the metal-oxide interface are undergoing conventional grain growth concurrent with oxidation.

Grain Area Distribution Within the NiO Scale on Nickel 270

Grain area distributions for the cross-sections of the grains within the equiaxed and columnar layers were obtained by a manner similar to that which was used to obtain the grain area distribution at the metal-oxide interface. Instead of measuring bromine treated scales, measurements were made upon photomicrographs of taper sections taken at levels about midway of the columnar and equiaxed layers. Figure 17 shows photomicrographs of a specimen oxidized for 4 hours. These photomicrographs are representative of those used for this part of the work.

Table X

Parameters of the Grain Area Distribution Upon the Metal-Oxide Interface of Ni 270 Specimens

| Oxidation Time in Hours | Slope ($\ell n\ \sigma_A$) | Mean Grain Area in $cm^2$ at 3000X |
|---|---|---|
| 4 | 1.138 | 1.446 |
| 49 | 1.310 | 2.474 |
| 64 | 1.077 | 3.118 |
| 81 | 1.002 | 3.980 |

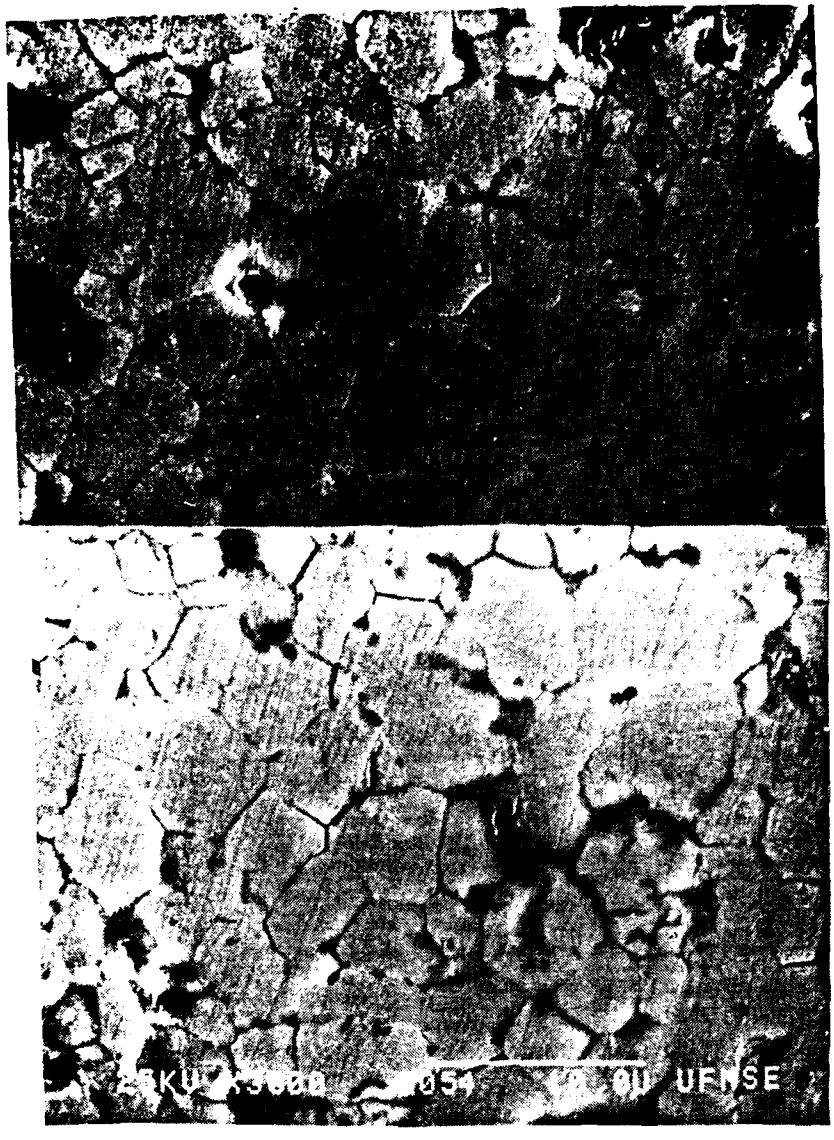

Figure 17. SEM view of the NiO grain structure inside the scale, taken from the etched small angle section.

Figure 17(a). Inner layer region, specimen oxidized for 4 hours, 3000X.

Figure 17(b). Outer layer region, specimen oxidized for 4 hours, 3000X.

The data obtained are given in Tables XI and XII and are shown plotted on a logarithmic probability scale as compared to the data taken at the metal-oxide interface, Figure 18. Both distributions were found to be log normal, and both contained smaller fractions of the finer grains. Thus, it was concluded that the nucleation of new grains occured at the metal-oxide interface rather than in the body of the scale.

The slope and the mean grain size represented by the three curves, Figure 18, are essentially the same, indicating that throughout the whole scale, scale growth and grain growth occurs both homogeneously and according to the same mechanism. This is demonstrated in Table XIII, where the values of mean grain areas and ln $\sigma_A$ are recorded.

The small deviations from log-normal behior apparent at the smallest grain sizes, Figure 18, might be attributed to the inhomogeneous nature of plastic deformation during the course of oxidation. During the deformation of a polycrystalline aggregate, large grains surrounded by smaller ones tend to deform first [130]. It is believed that this circumstance could bring about localized grain growth, resulting in clustering of the smaller grains, photomicrograph of Figure 19(a), and thus explain the departure of log-normal behavior.

An often observed feature of NiO scales as viewed in normal section is that where the grain size is large, (the most grain growth having occurred) the scale is thicker than the average thickness. Because plastic deformation promotes grain growth and in its turn scale growth, regions of the scale which have experienced the most grain growth (large grains) always show a greater scale thickness. One example of local deviations in grain size is seen in the SEM photomicrograph of the exterior surface of an NiO scale, Figure 19(b).

Table XI

Grain Area Distribution of NiO Within the Inner Layer (4 Hours Oxidation)

| Size Classes | Area Range in $cm^2$ | Mean Area ($\bar{x}$) | Log Grain Size ($2\ell n\ \bar{x}/\ell n2$) | Number of Grains | Frequency (%) | Cumulative Frequency (%) |
|---|---|---|---|---|---|---|
| 1 | 0.1613-0.2970 | 0.279 | -3.68 | 12 | 11.11 | 11.1 |
| 2 | 0.3970-0.6328 | 0.515 | -1.92 | 11 | 10.19 | 21.3 |
| 3 | 0.6328-0.8685 | 0.751 | -0.826 | 20 | 18.52 | 39.81 |
| 4 | 0.8685-1.104 | 0.986 | -0.04 | 10 | 9.26 | 49.07 |
| 5 | 1.104-1.340 | 1.222 | 0.58 | 10 | 9.26 | 58.33 |
| 6 | 1.340-1.576 | 1.458 | 1.09 | 12 | 11.11 | 69.44 |
| 7 | 1.576-1.811 | 1.694 | 1.52 | 6 | 5.56 | 75 |
| 8 | 1.811-2.047 | 1.929 | 1.90 | 6 | 5.56 | 80.56 |
| 9 | 2.047-2.283 | 2.165 | 2.23 | 5 | 4.63 | 85.19 |
| 10 | 2.283-2.519 | 2.401 | 2.53 | 4 | 3.70 | 88.89 |
| 11 | 2.519-2.754 | 2.637 | 2.80 | 2 | 1.85 | 90.74 |
| 12 | 2.754-2.990 | 2.872 | 3.04 | 2 | 1.85 | 92.59 |
| 13 | 2.990-3.226 | 2.108 | 3.27 | 1 | 0.93 | 93.52 |
| 14 | 3.226-3.462 | 3.344 | 3.48 | 3 | 2.78 | 96.30 |
| 15 | 3.462-3.699 | 3.579 | 3.68 | 1 | 0.93 | 97.22 |
| 16 | 3.697-3.933 | 3.815 | 3.86 | -- | -- | 97.22 |
| 17 | 3.933-4.169 | 4.051 | 4.04 | -- | -- | 97.22 |
| 18 | 4.169-4.405 | 4.187 | 4.20 | -- | -- | 97.22 |
| 19 | 4.405-4.640 | 4.522 | 4.35 | 1 | 0.93 | 98.15 |
| 20 | 4.640-4.876 | 4.758 | 4.50 | 2 | 1.85 | 100 |

Table XII

Grain Area Distribution of NiO Within the Outer Layer (4 Hours Oxidation)

| Size Classes | Area Range in $cm^2$ | Mean Area ($\bar{x}$) | Log Grain Size ($2\ell n\ \bar{x}/\ell n2$) | Number of Grains | Frequency (%) | Cumulative Frequency (%) |
|---|---|---|---|---|---|---|
| 1 | 0.1437-0.6051 | 0.3744 | -2.83 | 13 | 17.11 | 17.11 |
| 2 | 0.6051-1.066 | 0.8358 | -0.52 | 15 | 19.74 | 36.84 |
| 3 | 1.066-1.528 | 1.297 | +0.750 | 9 | 11.84 | 48.68 |
| 4 | 1.528-1.989 | 1.758 | 1.63 | 11 | 14.47 | 63.16 |
| 5 | 1.989-2.451 | 2.220 | 2.30 | 8 | 10.53 | 73.68 |
| 6 | 2.451-2.912 | 2.681 | 2.85 | 4 | 5.26 | 78.95 |
| 7 | 2.912-3.373 | 3.143 | 3.30 | 4 | 5.26 | 84.21 |
| 8 | 3.373-3.835 | 3.604 | 3.70 | 3 | 3.95 | 88.16 |
| 9 | 3.835-4.296 | 4.065 | 4.05 | 2 | 2.63 | 90.79 |
| 10 | 4.296-4.757 | 4.527 | 4.36 | 1 | 1.32 | 92.11 |
| 11 | 4.757-5.219 | 4.988 | 4.64 | -- | -- | 92.11 |
| 12 | 5.219-5.680 | 5.449 | 4.89 | -- | -- | 92.11 |
| 13 | 5.680-6.141 | 5.911 | 5.13 | 2 | 2.63 | 94.74 |
| 14 | 6.141-6.603 | 6.372 | 5.34 | 1 | 1.32 | 96.05 |
| 15 | 6.603-7.064 | 6.833 | 5.55 | 1 | 1.32 | 97.37 |
| 16 | 7.064-7.526 | 7.295 | 5.73 | -- | -- | 97.37 |
| 17 | 7.526-7.987 | 7.756 | 5.910 | -- | -- | 97.37 |
| 18 | 7.987-8.448 | 8.218 | 6.08 | -- | -- | 97.37 |
| 19 | 8.448-8.910 | 8.679 | 6.24 | 1 | 1.32 | 98.68 |
| 20 | 8.910-9.371 | 9.140 | 6.38 | 1 | 1.32 | 100 |

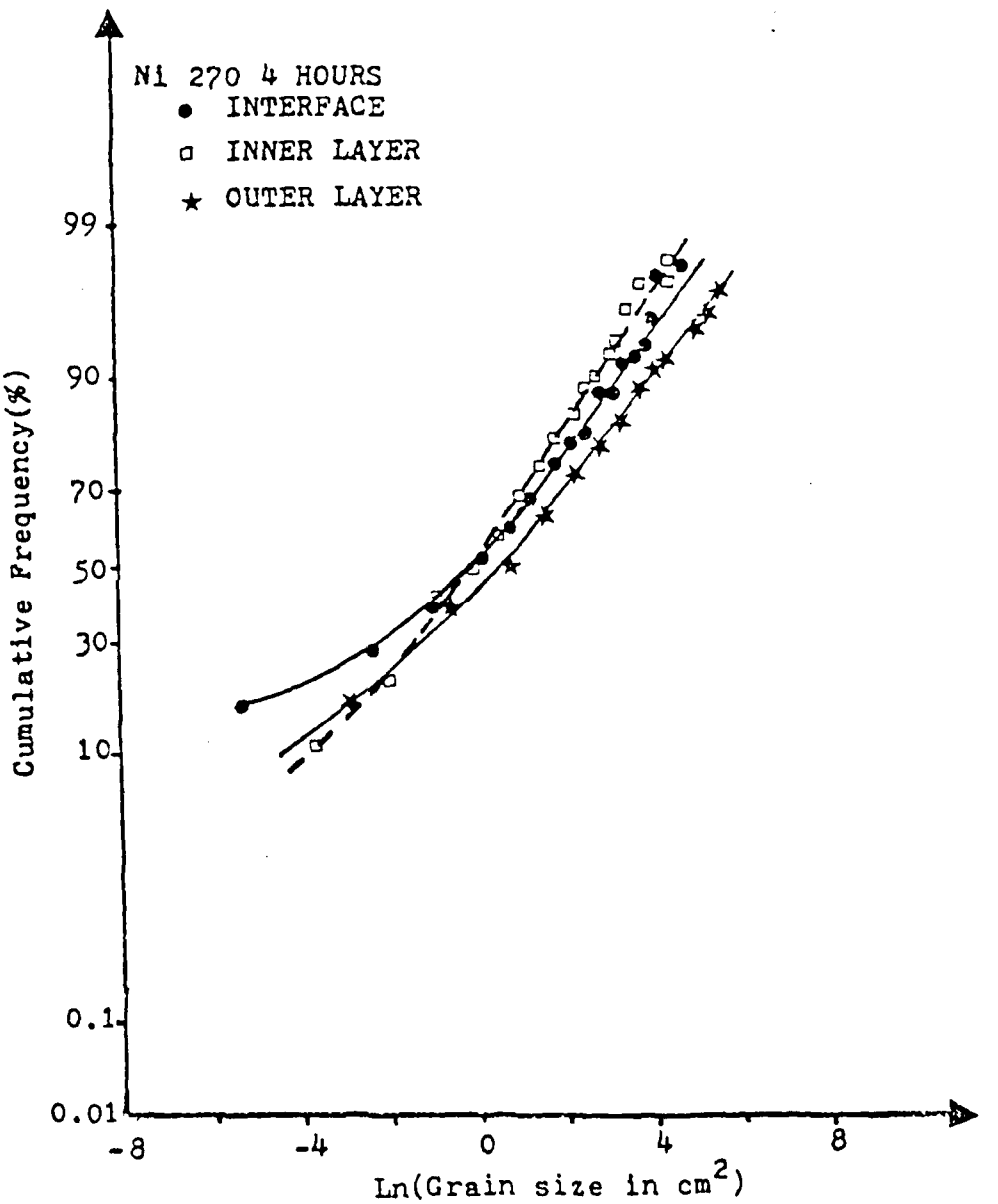


Figure 18. Grain area distribution of NiO within the scale of Ni 270 specimen.

Table XIII

Parameters of the Grain Area Distribution Within the Body of the Scale

| Oxidation Time in Hours | Location | Slope ($\ell n\ \sigma_A$) | Mean Grain Area in $cm^2$ at 3000X |
|---|---|---|---|
| | Interface | 1.138 | 1.446 |
| 4 | Inner Layer | 0.786 | 1.370 |
| | Outer Layer | 1.026 | 2.066 |

(a) Specimen oxidized for 49 hours, 1500X.

(b) Specimen oxidized for 49 hours, stereographic pair, 3000X.

Figure 19. SEM photomicrographs of exterior surface of NiO scale showing local clustering of small grains. It can be attributed to the inhomogeneous plastic deformation.

The grain area distribution study has lead to several conclusions which support the authors proposed mechanism for the oxidation of pure nickel. These are summarized as follows:

(1) The grain size distribution at the metaloxide interface in log-normal, except that there is an excess of the smallest grains. New grains being nucleated at the metal-oxide interface account for the excess.

(2) The number of excess small grains (newly nucleated ones) is directly proportional to the number of $NiO^3$-Ni quadruple points; therefore, new grains are nucleated at these points.

(3) The distribution of grain cross-sectional areas within the body of the scale is log-normal.

(4) The average grain size of the distribution either at the metal-oxide interface or within the body of the scale increases with time; the whole system undergoes normal grain growth during oxidation.

(5) The grain size distribution throughout the scale is uniform and homogeneous; the entire scale grows uniformly due to swelling.

## The Proposed Mechanism for the High-Temperature Oxidation of Nickel 270

Based upon the results obtained from the study of the oxidation of relatively pure nickel (Ni-270) by both an analysis of the kinetics of scale thickening and the microstructural evolution of the scale during the course of oxidation, and upon evidence obtained from the oxidation literature the authors have deduced a mechanism of oxidation which accounts for the deficiencies of the classical viewpoint of oxidation.

The following discussion presents the proposed mechanism and describes some noteworthy microstructural features related to the process of oxidation.

The authors propose that the high-temperature oxidation of nickel proceeds in three stages as described in the following paragraphs:

(1) Stage One: $O_2$ Absorption - - Oxygen Pressure Control

The onset of oxidation occurs by the fast chemisorption of oxygen which covers the nickel surface [92-93]. Nucleation of the first NiO islands occurs almost instantaneously along nickel grain boundaries [36, 95-96]. These islands spread to impingement with one another covering the entire surface with "pancake" grains which grow in thickness by the addition of oxygen at their external surfaces [92]. During this stage of growth, $Ni^{++}$ ions are available in excess so that all the oxygen reaching the surface is immediately converted to NiO. The rate of oxidation is controlled by the supply of oxygen and is therefore sensitive to the pressure of oxygen.

(2) Second Stage: $Ni^{++}$ Deficient - - Nickel Control

After the metal surface is covered with oxide islands grown to impringement, as the scale thickens, the rate of delivery of nickel ions through NiO to the external surface becomes insufficient to react with all of the available oxygen. Thus, $Ni^{++}$ delivery becomes rate controlling. There are at least three possible substages of this second stage of scale growth.

(a) While the scale is very thin, the rate of delivery of $Ni^{++}$ through the scale to the external surface is great enough, so that supply of $Ni^{++}$ is controlled by the rate of nickel solution

into NiO at the metal-oxide interface. This rate is dependent upon the orientation of the metal crystals at the metal oxide surface and obeys a logarithmic [17, 93, 104, 105] or quasi logarithmic law [2, 17, 18]. The duration of this substage is limited by the diffusion of $Ni^{++}$ through the NiO or until the scale is approximately 500° A thick.

(b) During the second substage, new NiO is formed at the external surface, but is controlled by the rate of $Ni^{++}$ delivery through the NiO lattice. The growth rate diminishes according to the parabolic rate law. Grains which earlier were broad and thin ("pancake") become columnar.

(c) As the grains of NiO become more columnar, the role of the oxide grain boundaries becomes important to the scale thickening process. Oxygen ions, diffusing inward along NiO grain boundaries meet nickel ions diffusing outward through the NiO grains to form new NiO upon the grain boundaries. Because new material is deposited along the columnar boundaries, the resulting "wedging effect" upon neighboring NiO grains produces lateral compressive stresses between the grains [30]. Expansion of the scale occurs locally at first, and the plastic response to such stresses is the extrusion of oxide upward in the regions of the columnar grain boundaries toward the external surface. Evidence of this extrusion can readily be observed at the external surface by scanning electron microscopy where extruded oxide forms ridges upon the external surface outlining the NiO grains along grain boundary intersections with the surface. A typical SEM photomicrograph, Figure 20, shows this feature on the external surface of a Ni-270 specimen oxidized

Figure 20. SEM photomicrograph of external surface of NiO scale upon Ni-270, oxidized for 1 hour at 800°C in pure oxygen at one atmospheric pressure. It shows ridges of the extruded NiO, 5000X.

for one hour at 800° C. As new oxide formation along NiO grain boundaries becomes more and more abundant, the parabolic law gives way to an accelerating rate of oxidation, because the average diffusion distance for the reacting species becomes one-half the attained scale thickness [56].

(3) Third Stage: Grain Boundary Sweeping - - Micro-Structure Control

The NiO extruding under the pressure of new oxide being formed at the NiO grain boundaries, increases the local curvature of the grain boundaries [121]. Increasing the grain boundary curvature causes the boundaries to migrate under the driving force of surface tension. The result is grain growth of the NiO. As the columnar grains grow longer, the degree of grain boundary distortion increases and grain boundary sweeping spreads across the volume of the grains.

When the columnar grains have attained a length to breadth ratio of about three, plastic deformation occurs throughout the entire volume of the scale. The ridges of extruded oxide upon the external surface become broader and less distinct, Figure 21 until a later time the grains take on a faceted appearance at the external surface due to dominance of surface tension over oxide extrusion [23], Figure 21(b). Sweeping grain boundaries supply oxygen throughout the volume of the scale meeting $Ni^{++}$ ions which have diffused into the NiO grains. New NiO is therefore formed everywhere within the volume of the scale and its growth is the result of general swelling.

AD-A090 235 FLORIDA UNIV GAINESVILLE DEPT OF MATERIALS SCIENCE --ETC F/G 11/6
ROLE OF MICROSTRUCTURE IN HIGH TEMPERATURE OXIDATION.(U)
MAY 80 F N RHINES, R G CONNELL, M S CHOI DAAG29-77-G-0056
UNCLASSIFIED ARO-13968.2-MS NL

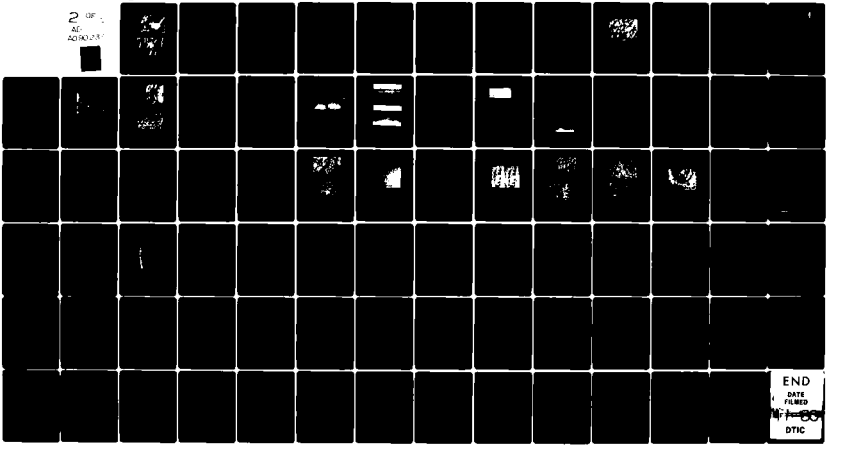

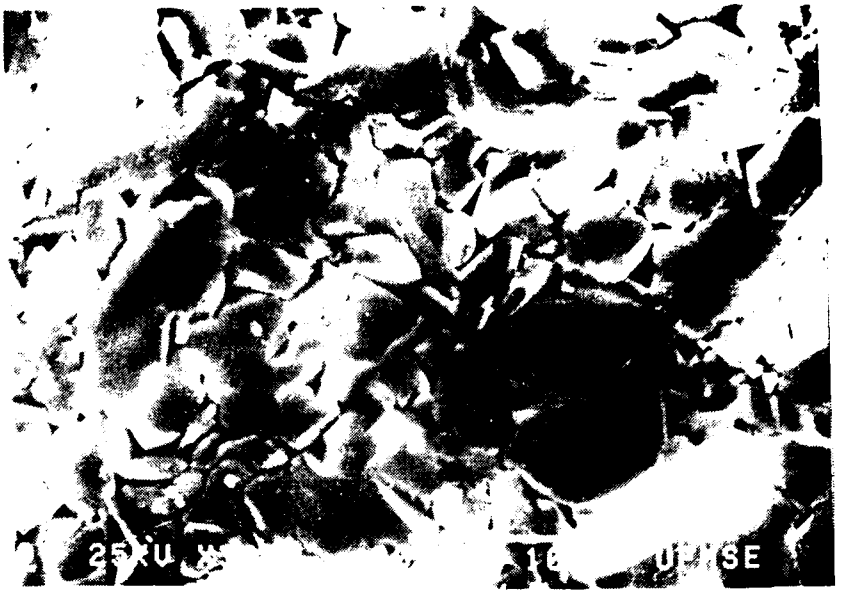

(a) Smooth and cusped NiO grains after intermediate oxidation times, specimen oxidized for 4 hours, 3000X.

(b) Faceted grains after long oxidation times, specimen oxidized for 81 hours, 3000X.

Figure 21. SEM photomicrographs of surface morphologies of NiO scales upon Ni-270, oxidized at 1000°C in pure oxygen of one atmospheric pressure.

As grain boundaries move, conventional grain growth of the columnar grains occurs resulting in an increase in the average lateral dimension of the grains. Such grain growth would be unlikely without distortion of the grain boundaries caused by plastic deformation of the NiO in response to stresses generated by new oxide formation along NiO grain boundaries, because of pinning of the relatively flat boundaries both by the metal-oxide interface and the external surface.

With grain growth in progress, the surface energy of the system continuously diminishes through the reduction of the total NiO grain boundary area. Lengthwise growth of the columnar grains continues as the scale thrusts outward and swells.

A geometric steady state now develops wherein the mean intercept grain size (breadth) of the columnar grains is always maintained at a constant ratio to the thickness of the columnar layer or to the total thickness of the scale, i.e., a ratio of 1/3 and 1/5, respectively. Should the lateral grain growth exceed the thickening to deviate from this ratio, the lateral span of plastic deformation would not cover the breadth of the grains and the rate of grain growth would diminish. Conversely, should the thickening get ahead of the breadth-wise increase in grain dimension the amount of plastic deformation would increase thus accelerating grain growth. It is in this way that grain growth and scale growth are interrelated during the oxidation process.

Figure 22 schematically shows the structural evolution of the NiO scale and the coordinated growth of both scale layers.

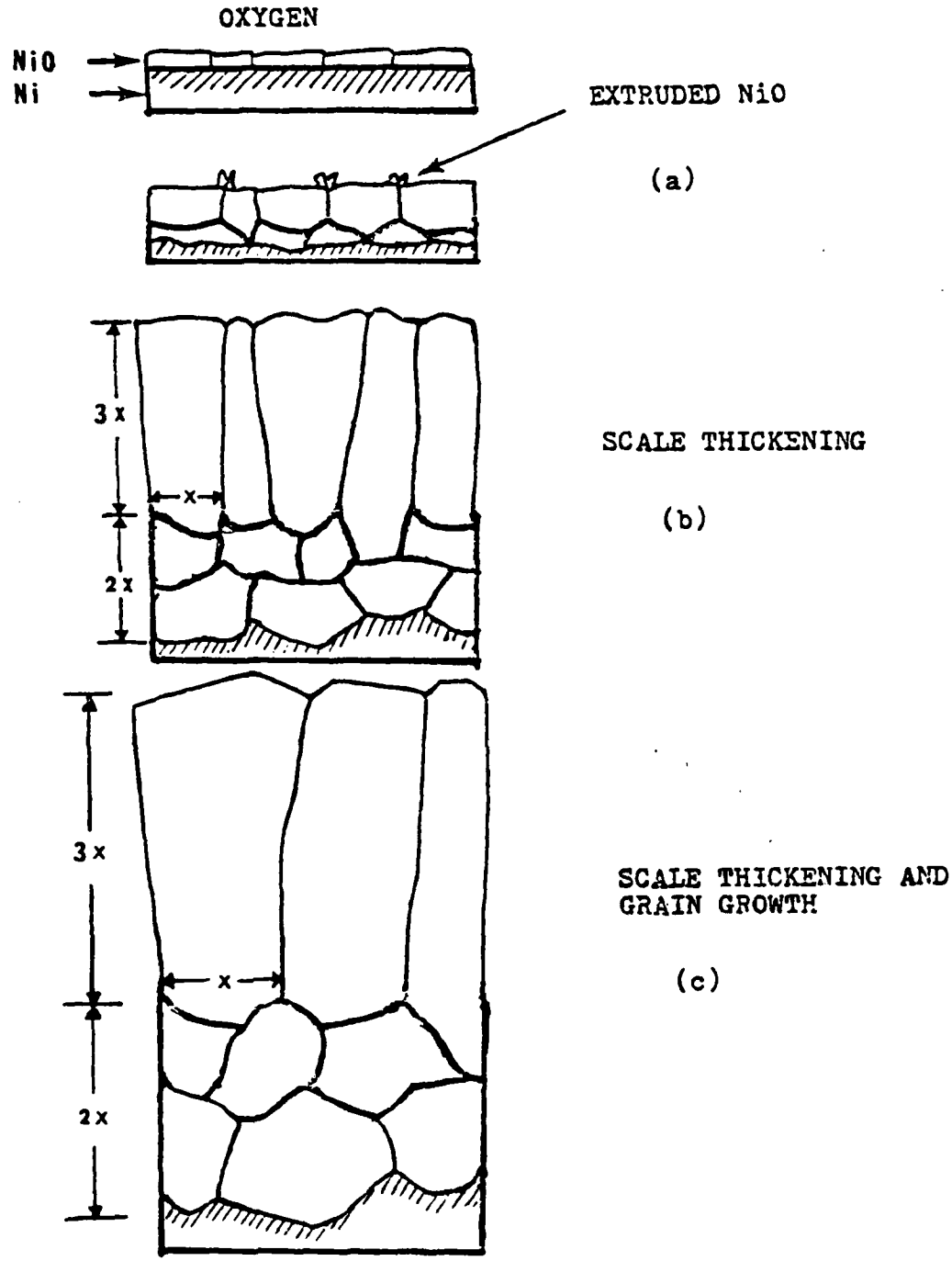


Figure 22. Schematic representation of microstructural change of NiO in thickness and grain size, showing the coordinated growth of both layers.

The combined processes are driven by the potential of the reaction whose equilibrium constant is $K = P(Ni^{++})\ P(O^{--}) / P(NiO)$. The value of K is in its turn dependent upon the diffusion rates of the reactants. The process which makes the reactants come together, however, is the grain growth which occurs by surface tension induced grain boundary motion. Grain growth diminishes in proportion to the cube root of time [122]; thus, it is the rate of grain growth which ultimately is rate controlling in scale thickening. New oxide forms uniformly throughout the volume of the scale, and the scale thickens by swelling rather than layer by layer accretion.

The original metal-gas interface can be observed in the scale separating the outer columnar-grained layer from the inner equiaxed-grained layer. By the time grain boundaries begin to sweep, the inner layer has already grown into the metal to a depth equal to about two times the mean grain boundary intercept grain size of the columnar (or equaxed) grains. Figure 23 shows graphically the several stages of NiO scale growth.

Nucleation of NiO Grains in the Inner Layer

That the two scale layers grow according to the same growth process, and that new NiO forms at like rates in both layers and is distributed uniformly throughout the scale all the way through the inner layer, are supported by the measurements of mean intercept grain size. These measurements show the grain size remains essentially uniform throughout the entire scale thickness. This kind of microstructural homogeneity can be explained only in a system wherein the growth proceeds by uniform swelling.

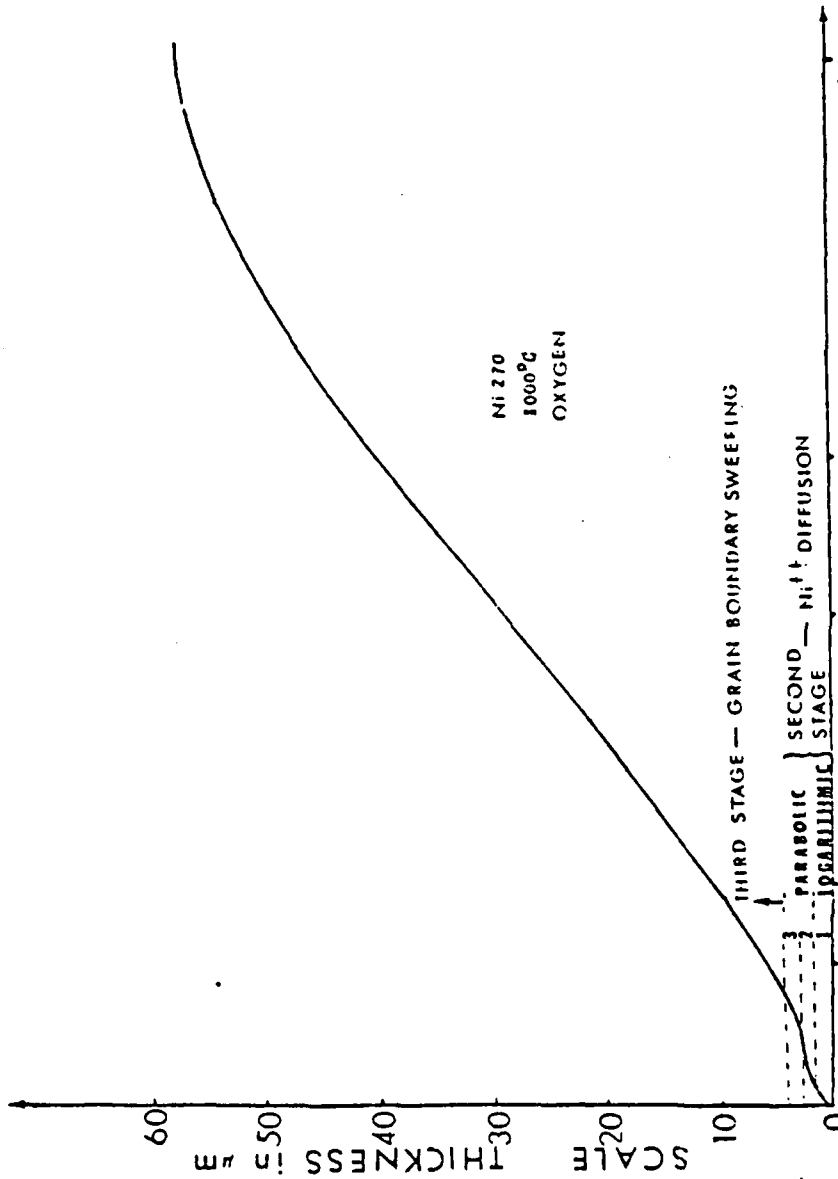


Figure 23. Schematic drawing of the proposed stage behavior in columnar layer formation of NiO upon Ni 270.

Any oxidation mechanism that is based upon the formation of new oxide upon a reaction front that advances parallel to the metal-oxide interface cannot result in new oxide distribution within the scale. For such a mechanism, the new oxide would form as a band parallel with the original metal surface. On the other hand, if new oxide is uniformly distributed in the scale, the reaction front must be effectively perpendicular to the metal-oxide interface, and it must sweep.

Consider now the grain morphology of the inner layer. If, from the outset, the grains of the inner layer merely had grown inward from the same nuclear NiO islands that gave birth to the columnar grains of the outer layer, they themselves would have also grown as columnar grains. The structure of the inner layer, however, is seen to be composed of separate equiaxed grains to the depth of about two grains. It is therefore necessary to conclude that some new NiO grains new nucleated in the inner layer. Because the individual grain size of the inner layer remains similar to that of the columnar layer, it is deduced that the rate of new grain nucleation is somehow related to the existing grain size. A unique situation must have existed in order to promote new grain nucleation beneath the original surface. This would have required a relatively high oxygen potential at the nickel surface.

While the original grains of the columnar layer are growing lengthwise, the grain boundary diffusion paths for oxygen ions to the metal surface would have been relatively short. Along the triple lines of the columnar boundary network, the oxygen potential would be expected to be particularly high. Upon the metal-oxide interface, the oxygen potential would have peak values at the intersections of NiO triple lines with the nickel surface. Such points would likely serve as potential nucleation

sites. The most direct evidence that these points serve as new grain nucleation sites was from microstructural observations that indicated the presence of very small NiO grains at $NiO^3$-Ni quadruple points of the metal oxide interface, Figures 11-14.

Only about one half of such quadruple points seem to have been active. Because the number of nodes in the two-dimensional view of the grain boundary network at the metal-oxide interface is twice the number of grain centers, it is to be concluded that the nucleation of new NiO grains at one half of the total number of quadruple points would produce the same mean intercept grain size as the columnar grains. This loosely accounts for the equality of the grain size in both layers as measured in taper section.

It may be presumed that the nucleation process would operate continuously during scale growth; however, since the number of quadruple points essential for the nucleation rapidly diminishes with time after the onset of grain boundary sweeping, the nucleation process practically stops after one or two successive operations. Moreover the oxygen diffusion path length - - grain boundary triple lines - - markedly increases with scale thickening thus diminishing the peaks in oxygen potential at the metal-oxide interface. Once the nucleated oxide grains have grown to the prevailing size of the columnar grains, the whole scale, inner layer included, begins to grow by the grain boundary sweeping mechanism. The path of microstructural change of the inner layer, in both scale thickness and grain size, is closely related to that of the outer layer.

Factors Which Determine the Morphology of the Metal-Oxide Interface and Control the Nucleation of New NiO Grains

Two factors are presumed to contribute to the advance of the Ni-NiO interface into the metal, namely: (1) Rate of solution of Ni into the NiO. (2) Formation of new oxide along the NiO grain boundaries. Because new oxides are generated principally along the grain boundaries, it creates a nickel consuming zone along the NiO grain boundaries, thus, accelerating the dissolution of $Ni^{++}$ into the oxide. The rate of Ni solution into NiO at the metal-oxide interface becomes an important factor in the control of the morphology of the metal-oxide interface.

This might be understood more easily by a closer look at the microstructure upon the metal-oxide interface. Photomicrograph of Figure 24(a) shows a SEM photomicrograph of the metal-oxide interface, similar to Figures 11-14, which were all obtained from the bromine treated scale. Figure 24(b) is a schematic representation section view of Figure 24(a), which shows the NiO grain boundary triple lines which meet nickel grains at the $NiO^{3}$-Ni quadruple points upon the metal surface. As seen in these figures, the diffusion distance of nickel ions from the metal toward the NiO grain boundaries where nickel ions are constantly consumed, varies from place to place over the metal oxide interface. This distance is relatively short near the NiO grain boundaries, because $Ni^{++}$ does not diffuse readily upon NiO grain boundaries. It is longer near the center of the NiO grains, Figure 24(b). This corresponds to a faster rate of $Ni^{++}$ take-up around the rim of each grain, slower solution rate at the center and edges. Therefore, shape of NiO grains will be dished in the middle, high around the rim, and sharply rounding off at the edges of grains.

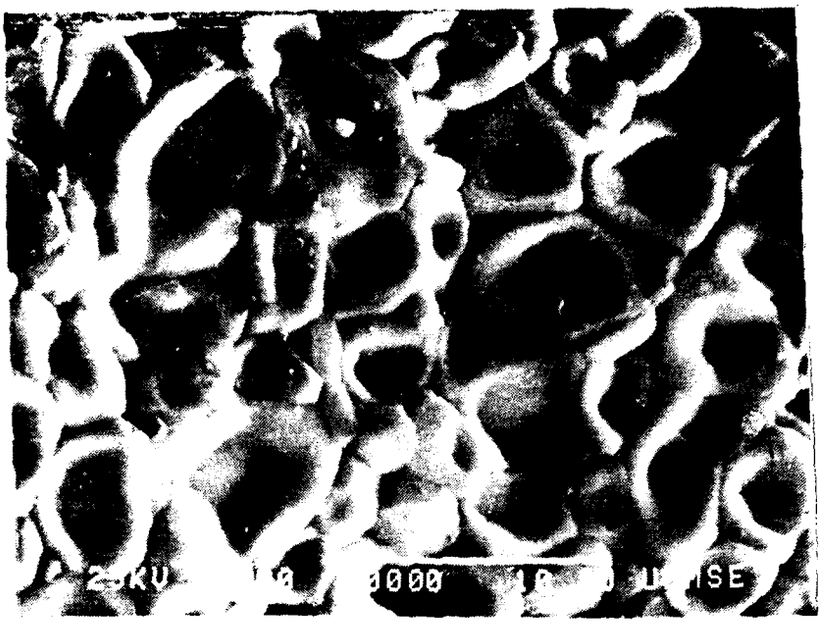

Figure 24. SEM photomicrograph of NiO grains at the metal-oxide interface of Ni-270 specimen, oxidized at 1000°C in pure oxygen of one atmospheric pressure.

Figure 24(a). Specimen oxidized for 4 hours, 3000X.

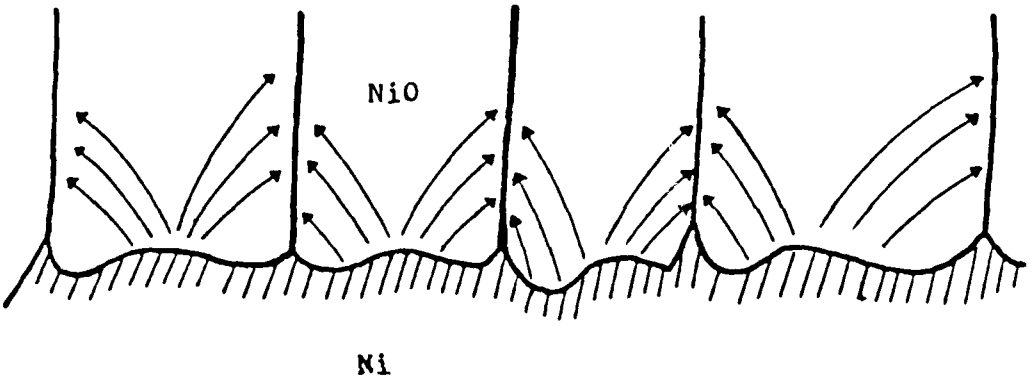


Figure 24(b). Schematic side view of (a), showing NiO grain boundary triple lines and $Ni^{++}$ diffusion path.

The variety in "dishedness" or the relative breadth of the thick region around the grain boundary compared to the shallow middle part may be related to the varying degree of grain boundary migration that is presently in progress. Another feature of Figure 24(a) is that the dishedness seldomly appears on very small grains. This might result for two reasons. First, the diffusion distance of nickel ions from the nickel surface to the grain boundary network is essentially uniform so that the nickel solution rate does not vary with position. Second, the size of the grains is relatively small compared to the velocity of the sweeping boundaries. In this case, the thick region near the rim of the grains is broadening so reapidly that the development of the shallow near the center of the grains is relatively slow.

Porosity

Microstructural evidence at the metal-oxide interface has clearly demonstrated that the NiO scale formed on flat Ni-270 specimens at 1000° C would not have any porosity as it grows, except for a few relatively small gas blown cavities, presumably associated with carbon in the nickel. Nevertheless, the majority of investigators of the microstructure of high temperature scales on pure metals have insisted upon the existence of varying kinds and numbers of pores in the scales. The small angle sections provide a superior opportunity to study the occurrence of such pores as may exist. Photomicrographs of Figures 25(a and b) show two small angle sections in the polished condition, corresponding to two times of oxidation. As seen in these pictures, there are many small, dark spots throughout each section, but they are most abundant within the inner layers, while the outer layers are relatively clean. Under deep focusing of the microscope, or at high magnification, the majority

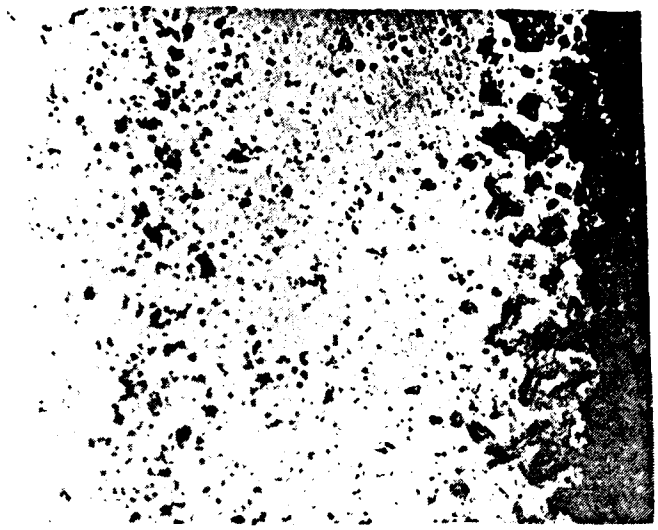

(a) Specimen oxidized for 4 hours, 250X.

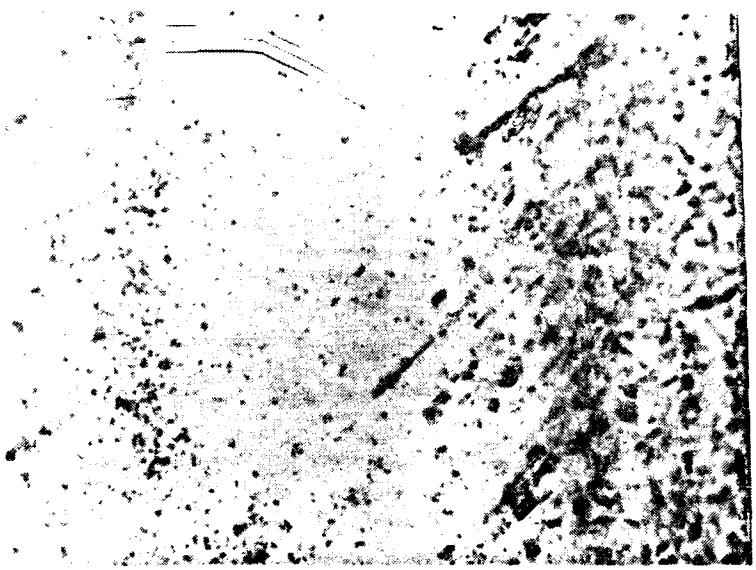

(b) Specimen oxidized for 36 hours, 200X.

Figure 25. Taper sections of NiO scale upon Ni-270, as polished.

of the dark features appear as pores. It has been concluded, however, that the major part of what are seen in Figure 25 are, in fact, metallographic artifact. Physical drop out of NiO grains during the metallographic polishing is difficult to avoid. Particles of foreign matter are most easily torn out.

The above conclusion seems to be inconsistent with the argument that the nickel atoms can not diffuse without a reverse flow of facancies that must be condensed as pores at the metal-oxide interface [18, 51]. It may be presumed that such a vacancy flux can be converted into dislocation loops and pass out of the system during the plastic deformation of the oxide scale.

There is, however, one kind of cavity that does appear occasionally in the sacle of Ni-270 and which is distinguished from the ordinary pores by the fact that it tends to be nested in a halo of finer grains, and is found only within the inner layer, photomicrograph of Figure 26. This is the origin of the local fluctuation in grain size distribution inside the scale, which was observed earlier in Figures 7(b)7(c). The microstructural evidence from the metal-oxide interface of bromine treated scale demonstrates that patches of finer grains are always being initiated upon the surfaces of pores that lie at the metal-oxide interface. Figures 27(a and b) are SEM photomicrographs showing such regions at the metal-oxide interface. In these figures, the edges of the pores are clearly seen and the fine grains are nested on the walls of the voids. Some of these grains are so fine that it can be concluded they must have been newly nucleated. Such pores become enveloped by the growing scale. They tend to spheroidize and eventually sinter shut.

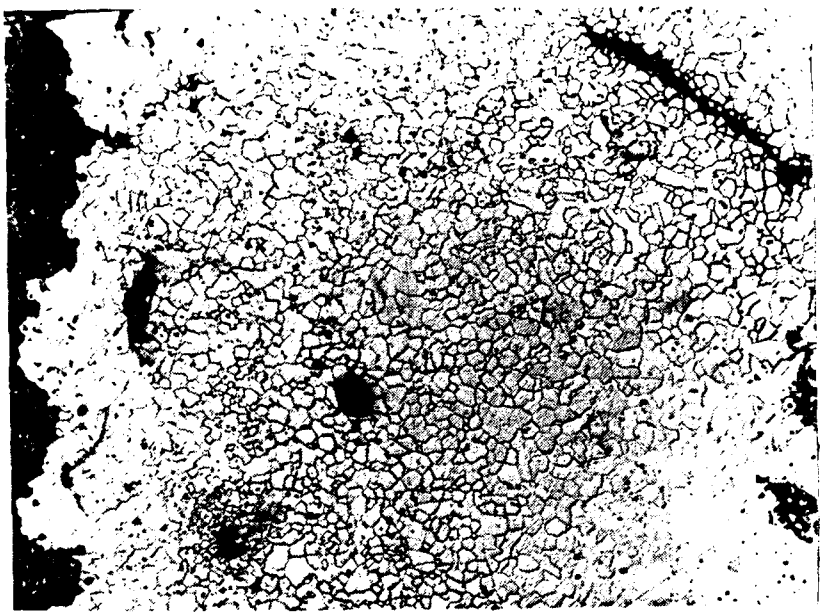

Figure 26. Two pores appearing in the inner layer scale of Ni-270, oxidized for 81 hours. Each pore is surrounded by a halo of finer grains. But, the one on the right side of the scale is not showing finer grains around it due to the etching effect. A micro-crack is also seen at the left edge, 200X.

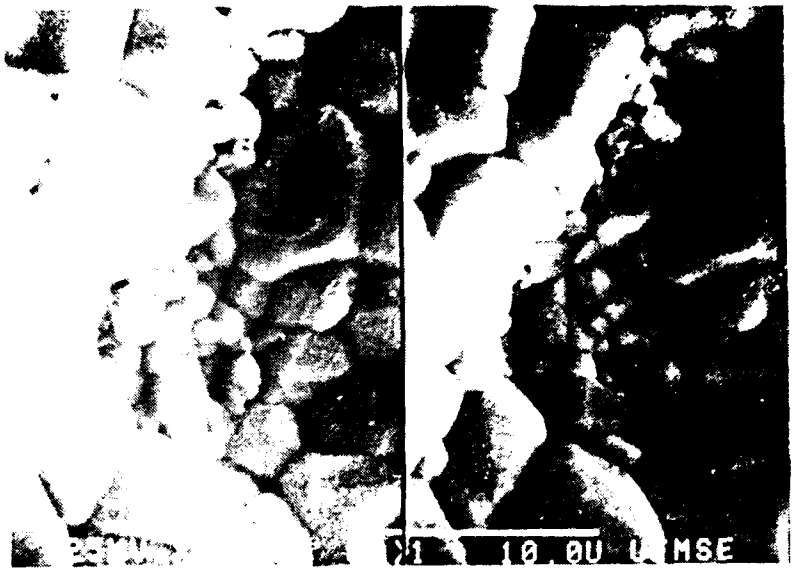

(a) Specimen oxidized for 64 hours, stereographic pair, 3000X.

(b) Specimen oxidized for 49 hours, 3000X.

Figure 27. SEM photomicrographs of voids nested by a halo of finer grains at the metal-oxide interface of Ni-270 specimens, oxidized at 1000°C in pure oxygen at one atmospheric pressure.

That these cavities are somehow associated with the presence of impurities in the metal can be deduced from the observation that they become more numerous in the scale upon less pure nickel. For reasons that will be cited in the discussion of Ni-200, it is believed that these pores are a direct result of the presence of a small concentration of carbon in the nickel. A reason why these pores are always associated with a halo of small grains will be proposed in connection with the identification of carbon as the active impurity.

Foreign Matter Contained in the Scale

Another feature that is best seen in taper sections is the distribution of the foreign matter in the scale. There are at least three possible sources of extraneous substances in the scale:

(i) The capture of inert matter that existed initially upon the metal surface.

(ii) Particles of inert matter that were originally contained within the metal and that were uncovered and enveloped by the oxide during oxidation.

(iii) Particles of oxides of less noble elements that had been in solution in the nickel and had formed a subscale (internal oxidation) just ahead of the oxidizing front, subsequently to become embedded in the scale as oxidation proceeds.

On the basis that the external columnar layer of the scale is formed by the outward diffusion of nickel ions from the metal surface, which have combined with oxygen ions that have diffused inward from the external surface, it would be expected that foreign matter could never enter this outer layer of the scale. Any such material should be contained within the inner layer, which is capable of undermining and

enveloping foreign particles when the inner layer developes inward from the original metal surface. The photomicrograph of Figure 28* reveals a representative distribution of foreign particles upon a polished small angle section. While observation of this figure verifies that the greater portion of the foreign matter exists confined within the inner layer, by no means all of it is so disposed. Some foreign particles are usually found in the columnar layer of the scale, Figure 28. They often appear in "streamers". These particles are believed to have been carried forward by the plastic flow of NiO when it is extruded from the inside of the scale toward the outer surface.

## Oxide Scales on Nickel 200

Parallel studies to those on the oxidation of high purity Ni-270 were made on comercial pruity nickel, Ni-200, whose nominal composition is 99.4% Ni including 1% cobalt in order to connect the differences in oxidation behavior with differences in the microstructural evolution of the oxide scale. The nominal major impurities in Ni-200 are 0.2% Mn, 0.10% C, 0.10% Cu, 0.15% Fe and 0.05% Si. Although the oxidation processes of the two grades of nickel might be similar, impurities in the Ni-200 appear to introduce a number of additional features into the microstructural evolution which account for its faster rate of scale thickening.

### Microstructures of NiO on Nickel 200

The photomicrographs of Figures 29(a and b) show the representative NiO microstructures of normal sections on Ni-200 specimens. The outer

---

*The distribution of what appears to be pores in this photomicrograph is believed to be associated with physical dropout of foreign particles and some surrounding NiO caused by mechanical polishing.

Figure 28. Distribution of foreign particles in the scale upon Ni-270, oxidized for 81 hours at 1000°C in pure oxygen of one atmospheric pressure, 100X.

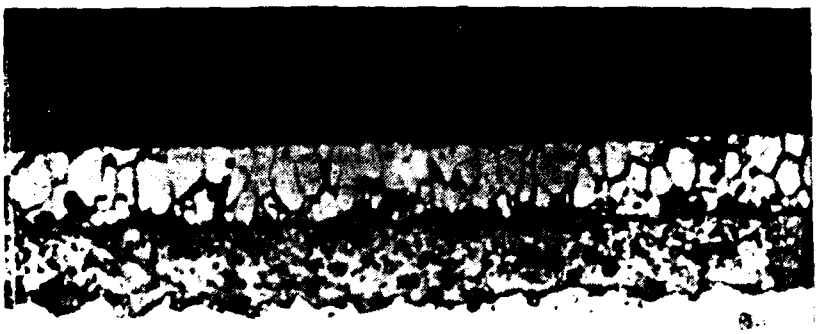

(a) Specimen oxidized for 4 hours, 1000X.

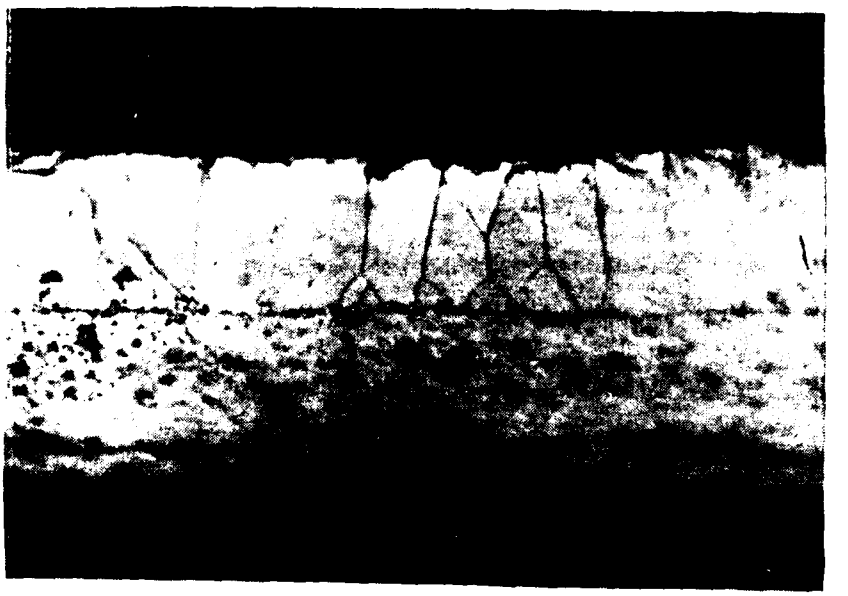

(b) Specimen oxidized for 81 hours, 600X.

Figure 29. Microstructure of NiO scale of Ni-200 normal sectioned specimens, oxidized at 100°C in pure oxygen of one atmospheric pressure, etched.

layer of the scale is columnar and closely resembles its Ni-270 counterpart, but the inner layer is porous and about equal to the thickness of the outer layer. These photomicrographs suggest that scale growth and grain growth of the outer layer are connected. Details of the inner layer are difficult to observe in normal section even after prolonged etching.

Internal Oxidation

A feature of the oxidation of Ni-200 which is significantly different from that of Ni-270 is the readily observable zone of subscale or internal oxidation. Because oxygen can reach the nickel surface during the course of oxidation by diffusing inward through the scale along NiO grain boundaries, its solution in the underlying metal can oxidize the more readily oxidizable impurities in the metal thus forming a zone within the metal of impurity oxide particles. As the metallic solute in the nickel is consumed, oxygen that is constantly supplied through the metal-oxide interface diffuses farther into the nickel producing an everthickening subscale layer. Subscales were found in all oxidized specimens of Ni-200, representative photomicrographic examples being shown in Figures 30(a and b). These photomicrographs show two important features related to the subscale, namely: (1) The thickness of the subscale zone is about twice as thick as that of the external NiO scale. (2) Subscales are heavy along nickel grain boundaries, and also are uniformly distributed throughout the nickel grains. This indicates that the segregation of dissolved oxidizable impurities along nickel grain boundaries is far from complete at 1000° C.

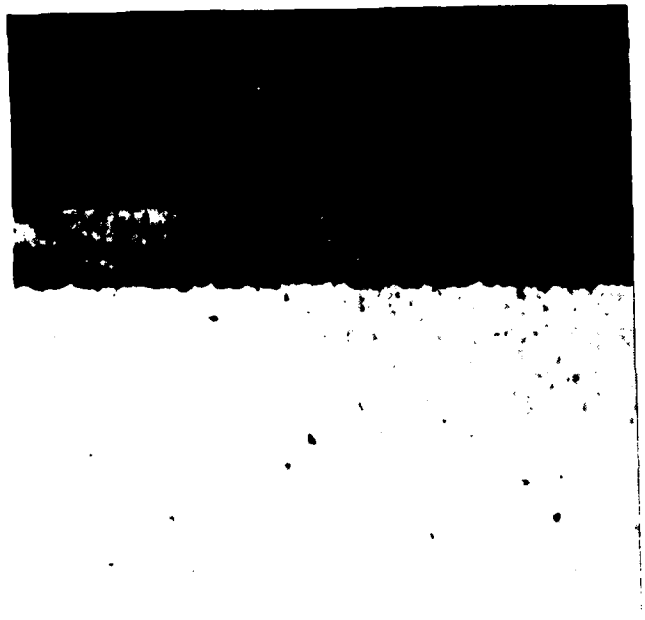


(a) Specimen oxidized for 4 hours, 600X.

Figure 30. Normal sections of Ni-200 specimens showing internal oxidation.

Figure 30(b). Specimen oxidized for 225 hours, 560X.

Kinetics of Scale Growth and Grain Growth of NiO Formed Upon Nickel 200

Quantitative metallographic measurements made on normal sections of Ni-200 scales are summarized in Table XIV. The mean values of the number of NiO grain boundary intercepts of the columnar grains along with 95% confidence intervals are recorded in column 2. Column 3 gives the corresponding mean grain intercept lengths and columns 4, 5, and 6 give values of columnar layer, inner layer and total scale thicknesses, respectively.

As is the case with NiO scales grown upon Ni-270, the columnarity of the columnar grains is always three, independent of the oxidation time (column 8). Although this geometric similarity exists for the columnar layers of the two grades of nickel, the inner to outer layer thickness ratios differ. This is shown in column 7 where the inner scale layer is about one half the total scale thickness. For Ni-270 scales the inner layer amounted to only about 40% of the total scale thickness.

An equation of the form $Y = AX^B + C$* was used to express the kinetics of Ni-200 scale growth. Total NiO thickness versus $(\text{time})^B$, where B is the time exponent is shown in Figure 31. It was found that the total oxide thickness is neither parabolic nor proportional to the cube root of time, but is linearly proportional to time to the 0.4 power. Figures 32 and 33 respectively, show that the columnar layer of Ni-200 scales thicken parabolically with time and the inner layer thickens according to the cube root of time.

---

*The precision of the time exponent B in this equation, based upon the correlation coefficient r, is not good enough to represent an exact value of B; therefore, the value of B is only an estimate.

Table XIV

Summary of the Experimental Results Made on Normal Sections of Ni 200 Specimens

| (1) Oxidation Time in Hours at 1000°C | (2) Mean Number of NiO Grain Boundary Intercepts at the Columnar Layer * | (3) Mean Grain Intercept Length of the Columnar Layer, ($\bar{\lambda}_{COL}$, μm) | (4) Columnar Layer Thickness, ($X_{COL}$, μm) | (5) Inner Layer Thickness, ($X_{INN}$, μm) | (6) Total NiO Thickness, ($X_{TOT}$, μm) | (7) $\frac{X_{TOT}}{X_{INN}}$ | (8) Columnarity $\frac{X_{COL}}{\bar{\lambda}_{COL}}$ |
|---|---|---|---|---|---|---|---|
| 1 | 82.5 ± 3.79 | 1.79 | 4.83 ± 0.26 | 3.52 | 8.35 ± 0.16 | 2.37 | 2.70 |
| 4 | 42.75 ± 1.02 | 3.45 | 9.75 ± 0.15 | 8.91 | 18.66 ± 0.19 | 2.09 | 2.83 |
| 16 | 25.62 ± 1.44 | 5.75 | 17.61 ± 0.31 | 17.95 | 35.67 ± 0.25 | 1.99 | 3.08 |
| 36 | 17.64 ± 0.60 | 8.36 | 23.36 ± 0.21 | 26.66 | 50.02 ± 0.56 | 2.14 | 2.81 |
| 64 | 14.74 ± 0.58 | 10.0 | 29.00 ± 0.42 | 39.24 | 68.26 ± 0.29 | 1.74 | 2.9 |
| 81 | 12.84 ± 0.61 | 11.49 | 35.15 ± 0.91 | 42.41 | 77.56 ± 0.84 | 1.83 | 3.06 |
| 225 | 8.88 ± 0.65 | 16.61 | 55.43 ± 0.61 | 58.97 | 114.4 ± 1.13 | 1.94 | 3.34 |
| Average | | | | | | 2.01 | 2.96 |

*The length of test line which was applied to the microscopic image of the scale was 147.5 μm.
$\bar{\lambda}$ values equal the reciprocal of the corresponding values of column 2 divided by 147.5 μm.

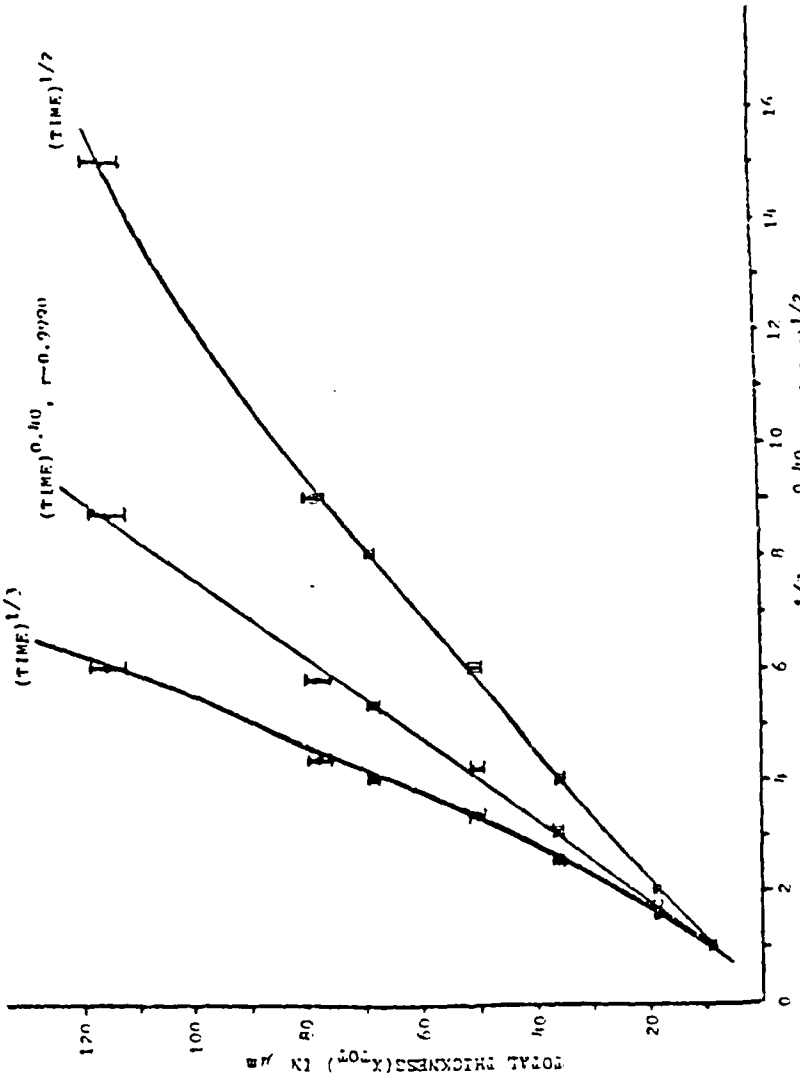


Figure 31. Kinetics of the total scale thickness for Ni 200 specimens, oxidized at 1000°C in pure oxygen of one atmospheric pressure.

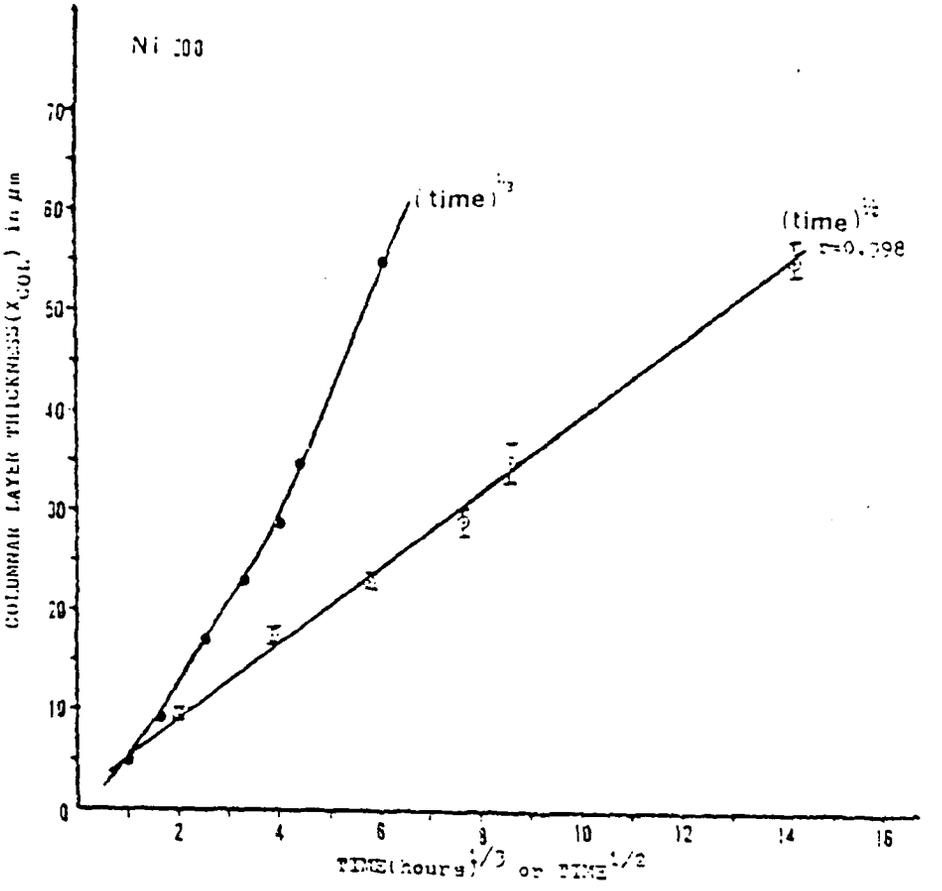


Figure 32. Kinetics of the columnar layer thickness for Ni 200 specimens, oxidized at 1000°C in pure oxygen of one atmospheric pressure.

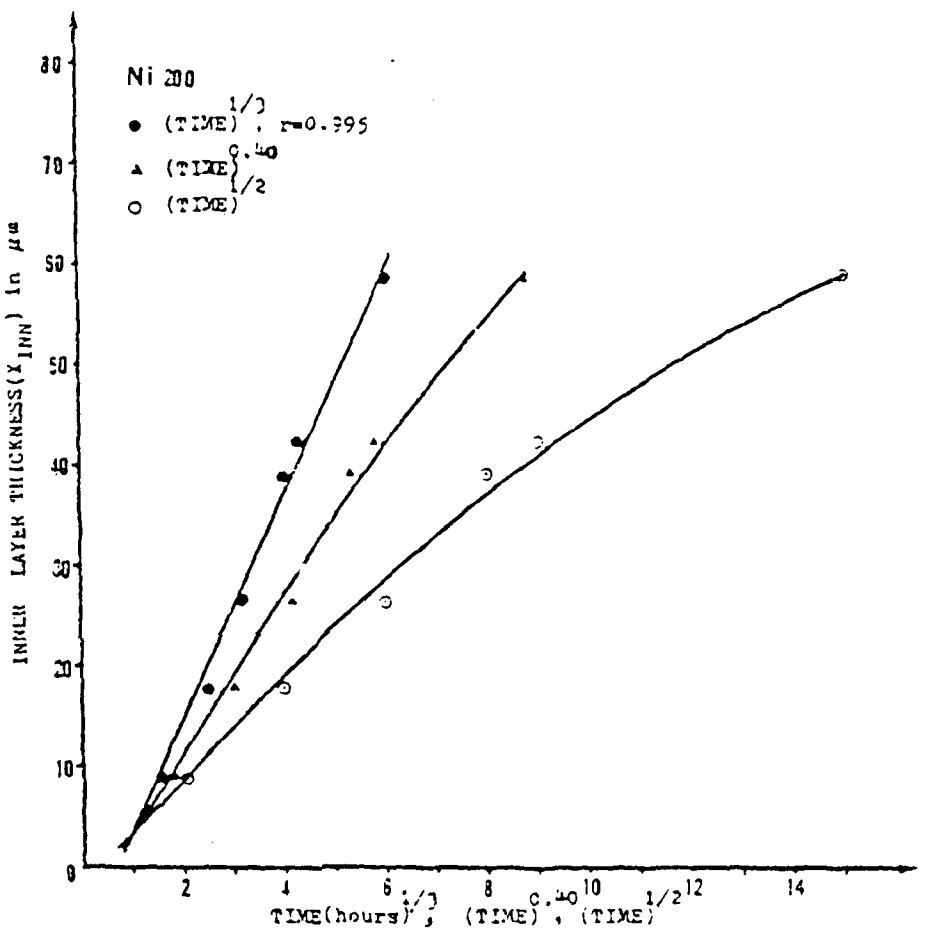


Figure 33. Kinetics of the inner layer thickness for Ni 200 specimens, oxidized at 1000°C in pure oxygen of one atmospheric pressure.

On the other hand, the mean grain size of the columnar layer, as measured by the mean grain intercept length ($\bar{\lambda}_{COL}$), is proportional to (time) $^{0.4}$, Figure 34. The graph of total scale thickness ($X_{TOT}$) versus the mean grain intercept ($\bar{\lambda}_{COL}$), Figure 35, confirms that scale thickening is proportional to grain growth as in the case of Ni-270. It is important to note that all of the best fit kinetic curves, whether scale thickness or grain size, do not extrapolate through the origin; therefore, indicating that grain growth controlled scale thickening is preceeded by a kinetically different early stage of oxidation.

Structural Evolution of the Inner Layer

The inner layers of Ni-200 scales contain a large amount of porosity and tend to spall freely; whereas, scales on higher purity metal, Ni-270, were nearly innocent of such porosity and adhered tightly to their metal substrates. The etching attack on the inner layer of Ni-200 scales was rather inhomogeneous causing the destruction of major portions of the inner layer before the grain boundaries could be revealed. Usually the grain size of the inner layer was so fine that it could not be resolved except at magnifications in excess of 1000. A few satisfactorily prepared taper sections proved useful in observing some of the details of the inner layer.

Details of the metal-oxide interface were studied from bromine-treated scales as well as from observations of taper sections. Several new distinctive features were observed in Ni-200 inner layers through both quantitative metallographic measurements and observations made at high magnifications using the SEM and conventional optical microscopy. These new features are described in the following sections.

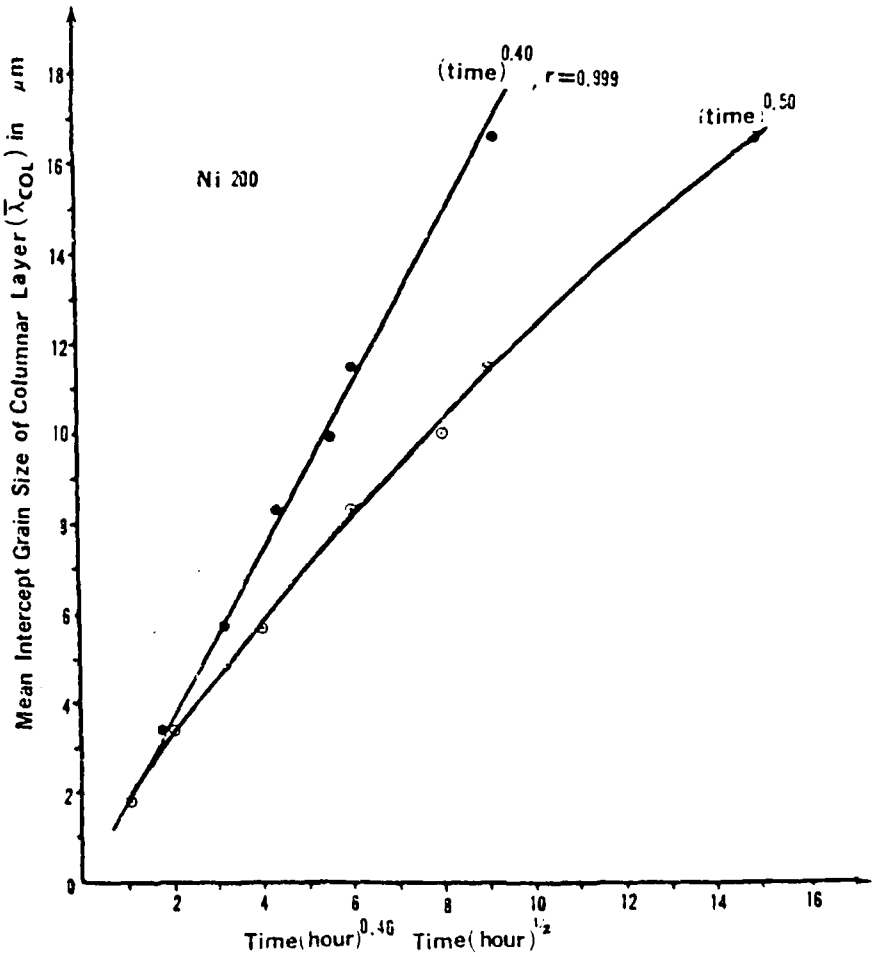


Figure 34. Grain growth of the columnar layer of NiO upon Ni 200, oxidized at 1000°C in pure oxygen of one atmospheric pressure.

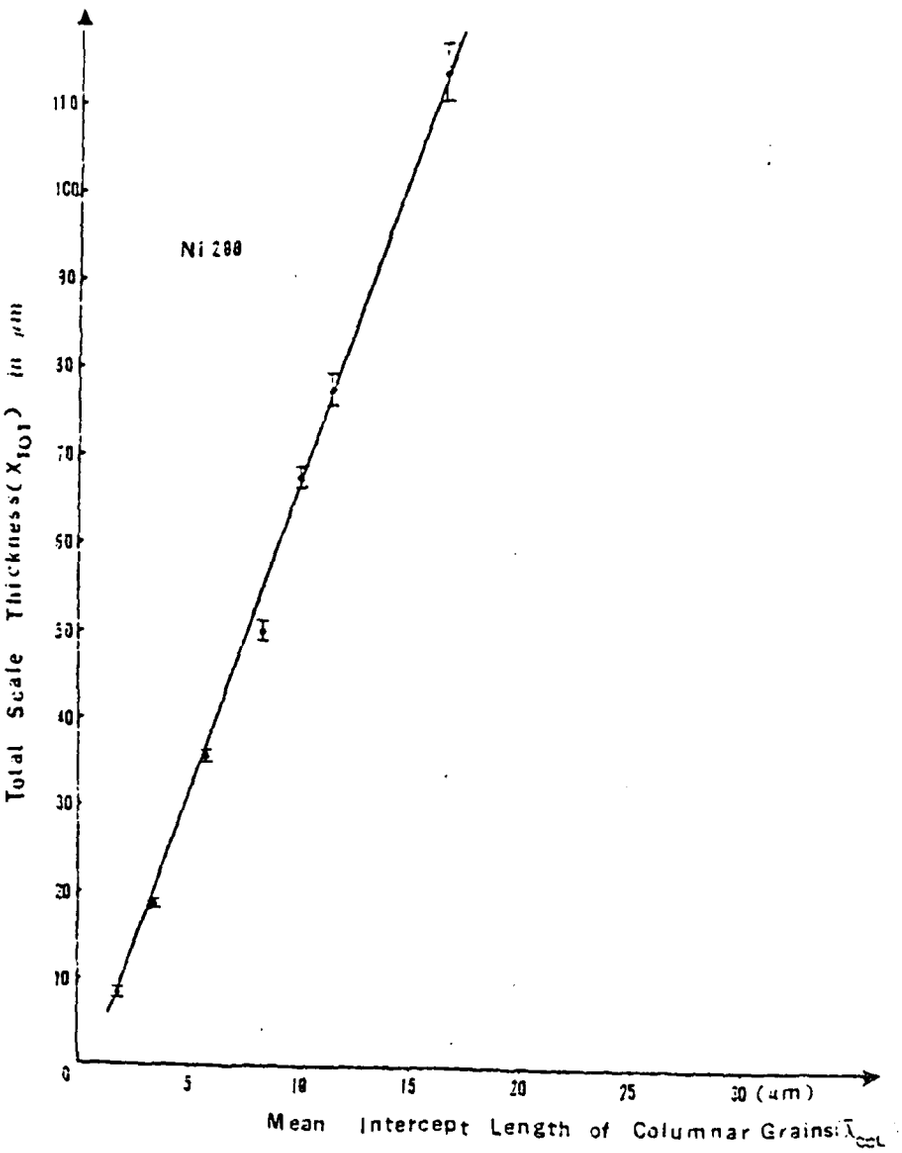


Figure 35. Relationship between scale growth and grain growth of Ni 200 specimens, oxidized at 1000°C in pure oxygen of one atmospheric pressure.

Microstructure of NiO Upon Nickel 200 at the Metal-Oxide Interface

SEM micrographs of Ni-200 scales taken of taper sections near the metal-oxide interface are shown in Figure 36(a and b) for scales produced by 9 and 81 hours of oxidation, respectively. The 9 hour specimen was moderately etched, and the 81 hour specimen was etched only slightly. A similar SEM micrograph is shown in Figure 37, for a specimen oxidized for 4 hours. This micrograph was taken using x-ray back scattering, where white, gray and black shades correspond to nickel, nickel oxide and porosity, respectively.

For Ni-200 scales the following observations can be made from these and other similar micrographs:

(1) The sizes of NiO grains near the metal-oxide interface are much smaller than those upon Ni-270 and remain essentially of the same size after all times of oxidation. The grain size near the metal-oxide interface in Figure 36(a and b) is less than 1.5 μm. Corresponding grain sizes near the metal-oxide interface on Ni-270 specimens range from 4.6 to 7.4 μm (Table IV). Thus, it appears that new grains are continually being nucleated at the metal-oxide interface during the course of oxidation.

(2) Unlike Ni-270, channels of pores are observed along the metal-oxide interface, Figure 36(b), and sometimes these pores extend into the metal, Figures 36 (a) and 37.

(3) Foreign particles of idiomorphis form, presumeably foreign oxide particles, exist upon the nickel surface, righthand side of Figure 36(a).

A photomicrograph of the metal-oxide interface (oxide side) taken from a bromine treated scale of a specimen oxidized for 4 hours is shown

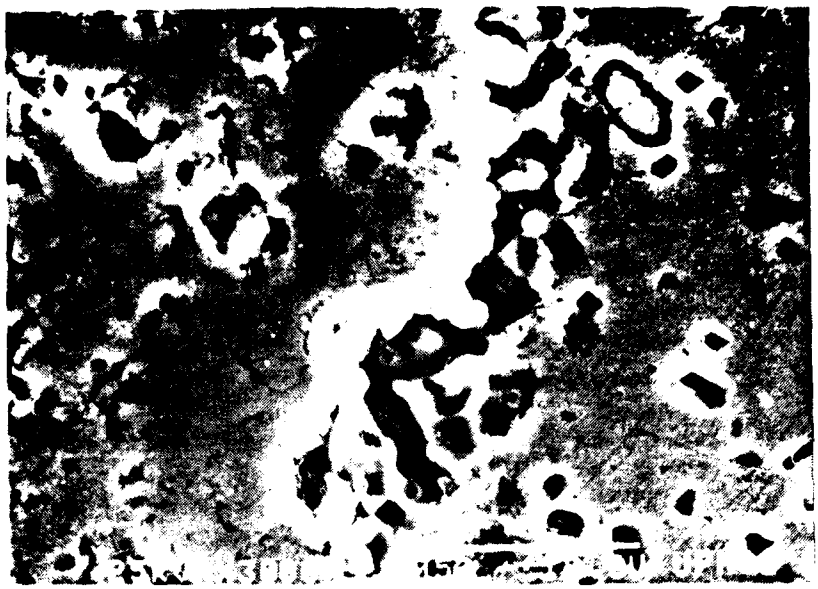

(a) Specimen oxidized for 9 hours, etched, 3000X.

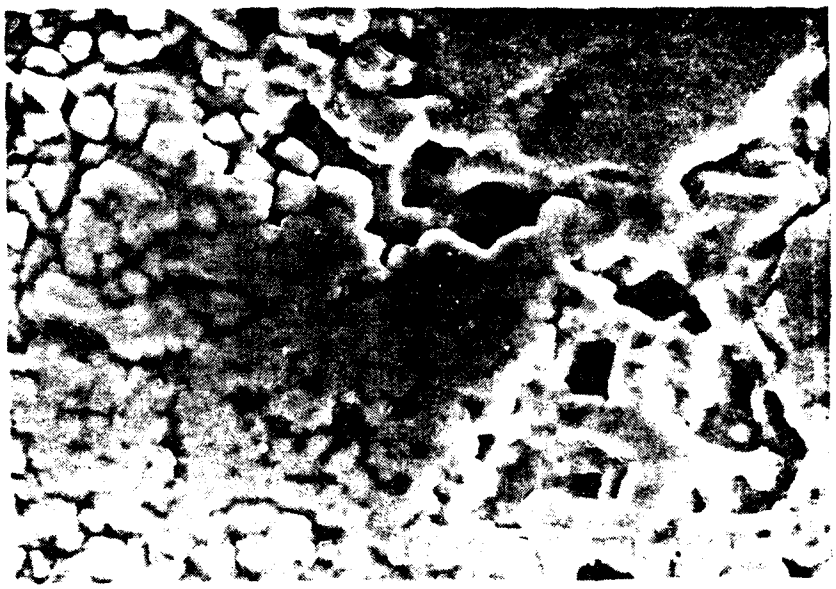

(b) Specimen oxidized for 81 hours, unetched, 3000X.

Figure 36. SEM photomicrographs of NiO scale at the metal-oxide interface, small angle sections of Ni-200 specimens, oxidized at 1000°C in pure oxygen of one atmospheric pressure.

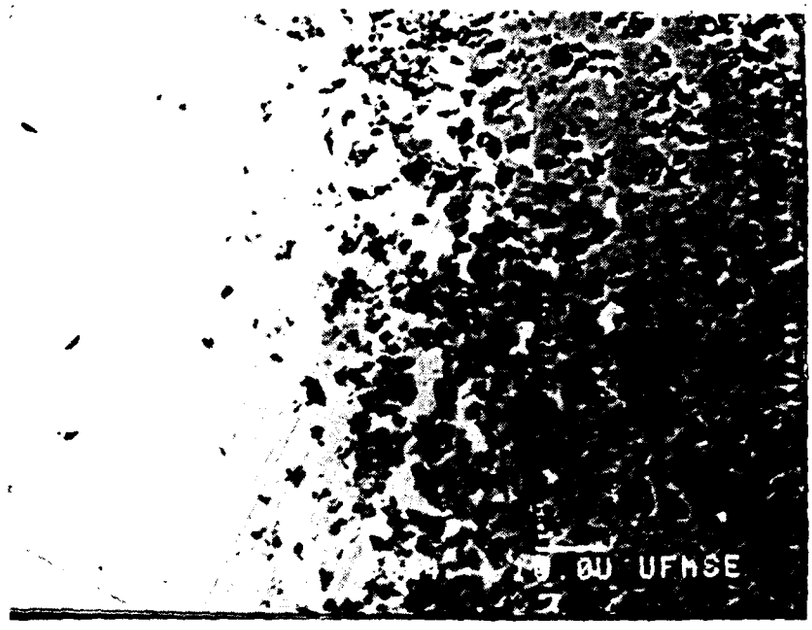


Figure 37. SEM photomicrograph of taper section of Ni-200 specimen at the metal-oxide interface, taken by x-ray back scattering, oxidized for 4 hours at 1000°C in pure oxygen of one atmospheric pressure, unetched, 1000X.

in Figure 38. Similar photomicrographs of Figures 39 (a and b) show the metal-oxide interface for a specimen oxidized 9 hours. Comparison of these micrographs with those of Figure 36 confirm that the NiO grain size at the metal-oxide interface is always very small and approximately of the same average size throughout the course of oxidation. The existence of pores is real. Note that most of the pores upon the metal-oxide interface are larger than the NiO grains. The pores apparently initiate at the metal-oxide interface and are usually lined with fine idiomorphic particles of NiO upon their interior walls, Figure 39. These idiomorphic particles lining the pore space walls are more clearly seen in taper section, Figure 40(a and b). When viewed in taper section slightly removed from the metal-oxide interface, the idiomorphic particles of NiO appear as a layer of fine grains surrounding each pore, Figure 41. This feature was also noted in the case of Ni-270, but its occurance was much rarer.

Variation of the NiO Grain Size in the Inner Layer of the Scale on Nickel 200

Quantitative measurements of grain size were made as a function of distance into the inner layer from the metal-oxide interface. This was accomplished by making lineal intercept measurements on taper sections at intervals between the metal-oxide interface and the inter layer boundary. Measurements made on scales grown at 1000° C could not be made due to spalling during etching of the scales, but one set of measurements was successfully made on a scale grown at 1200° C in 54 hours. Scales produced at 1200 C adhered more tightly to the metal, probably as a result of higher plasticity at the oxidizing temperature, and resisted spalling during etching.

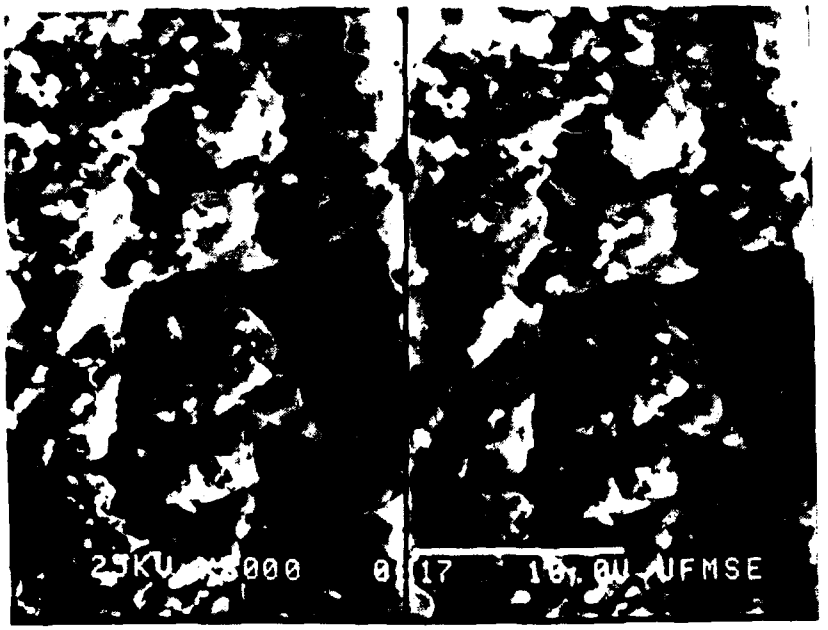


Figure 38. SEM stereographic pair of metal-oxide interface taken from the bromine treated scale upon Ni-200, oxidized for 4 hours at 1000°C in pure oxygen of one atmospheric pressure.

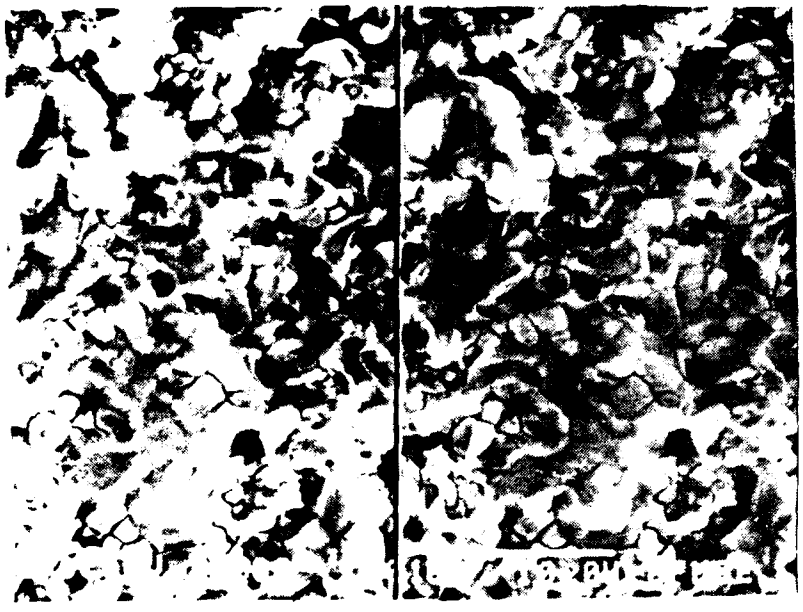

(a) Specimen oxidized for 9 hours, 3000X.

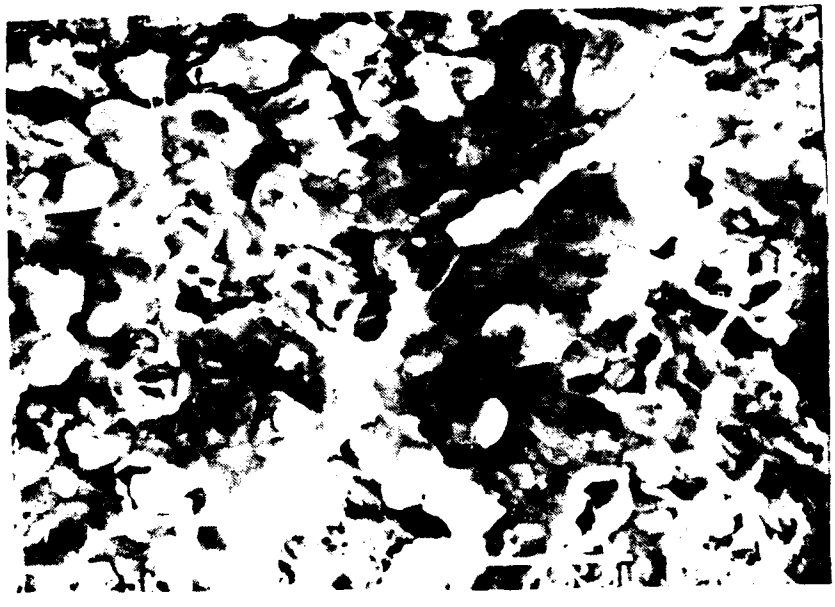

(b) Specimen oxidized for 9 hours, stereographic pair, 3000X.

Figure 39. SEM photomicrographs of metal-oxide interface taken from the bromine treated scale upon Ni-200, oxidized at 1000°C in pure oxygen of one atmospheric pressure.

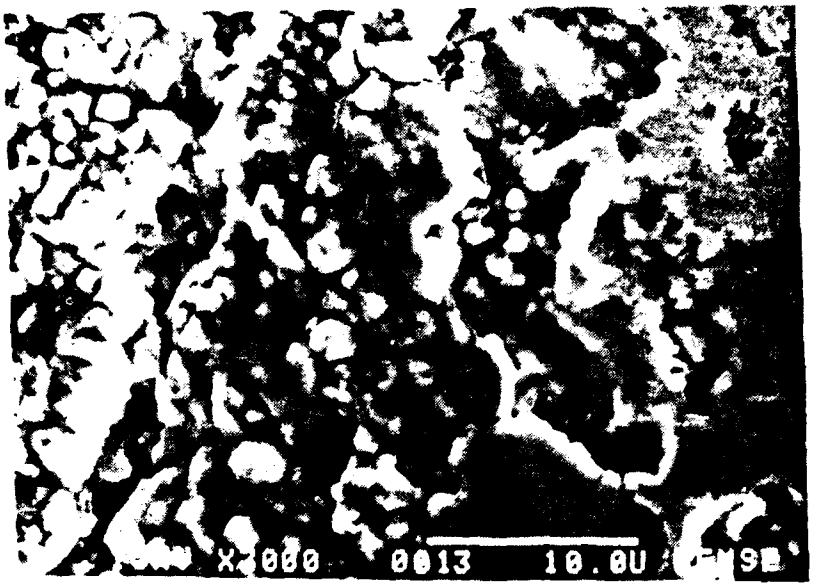


(a) Specimen oxidized for 4 hours, 10,000X.

(b) Specimen oxidized for 81 hours, 3000X.

Figure 40. SEM photomicrographs of taper sections near the metal-oxide interface of Ni-200 specimens, oxidized at 1000°C in pure oxygen of one atmospheric pressure. They show small idiomorphic particles lining the pores, unetched.

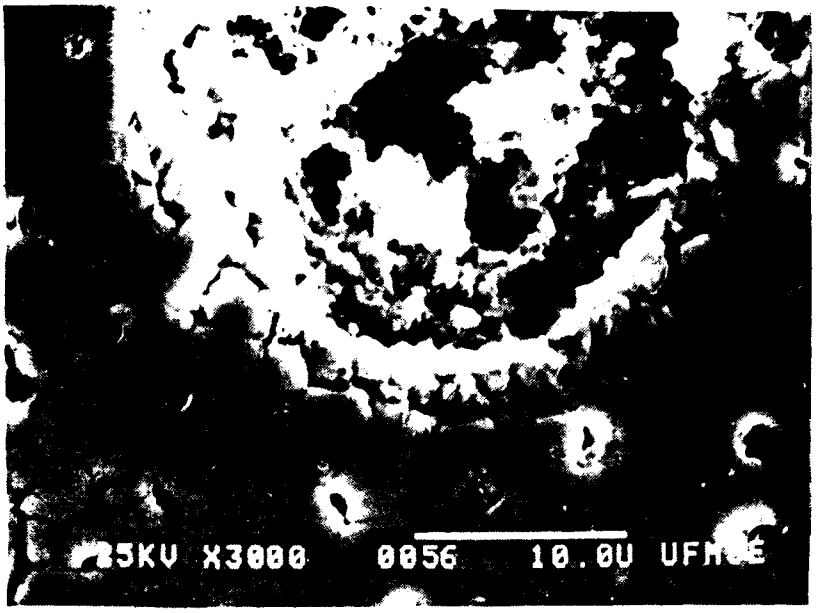


Figure 41. SEM photomicrograph of a round pore nested with a halo of fine grains in the inner layer of NiO scale upon Ni-200, oxidized for 4 hours at 1000°C in pure oxygen of one atmospheric pressure, etched, 3000X.

A composite photomicrograph is shown in Figure 42, of the taper section (sectioning angle 1° - 2°) that was used for these measurements. Each successive photomicrograph of the composite, starting at the metal-oxide interface was taken after successively increased etching times, thus revealing the grain structure of the entire inner layer. By the time that the etching was sufficiently long to reveal the grain boundaries at the outermost portion of the inner layer, the scale at the metal-oxide interface had become destroyed by over etching.

Counting measurements were made directly upon composite photomicrographs such as the one shown in Figure 42 using a test line of 5 cm in length. From the lineal intercept counts, values of $\bar{\lambda}$ eq, "mean intercept grain size", were obtained. These values are given in Table XV for 23 successive steps along with the mean number of grain boundary intercepts per unit length, $N_L$ ($cm^{-1}$), and their 95% confidence intervals. The values of $Ni = \frac{1}{\bar{\lambda}_{EQ}}$ are plotted versus distance from the metal-oxide interface in Figure 43. It can be concluded from these data that the grain size varies from very small near the metal-oxide interface to a size equivalent to that of the columnar layer. Along with previously stated observations it seems apparent that new grains are nucleated at the metal-oxide interface, and as the scale thickens, the grains throughout the inner layer experience grain growth.

The Occurance of Porosity in the Inner Layer of Nickel 200 Scales

The relatively large amount of porosity in Ni-200 scales compared to Ni-270 scales is easily observed in taper sections, and most of the porosity is confined to the inner layer, Figure 44. Using photomicrographs of taper sections, the volume fraction of pores was obtained by point counting with 4 x 4 or 6 x 6 square grids where the unit spacing

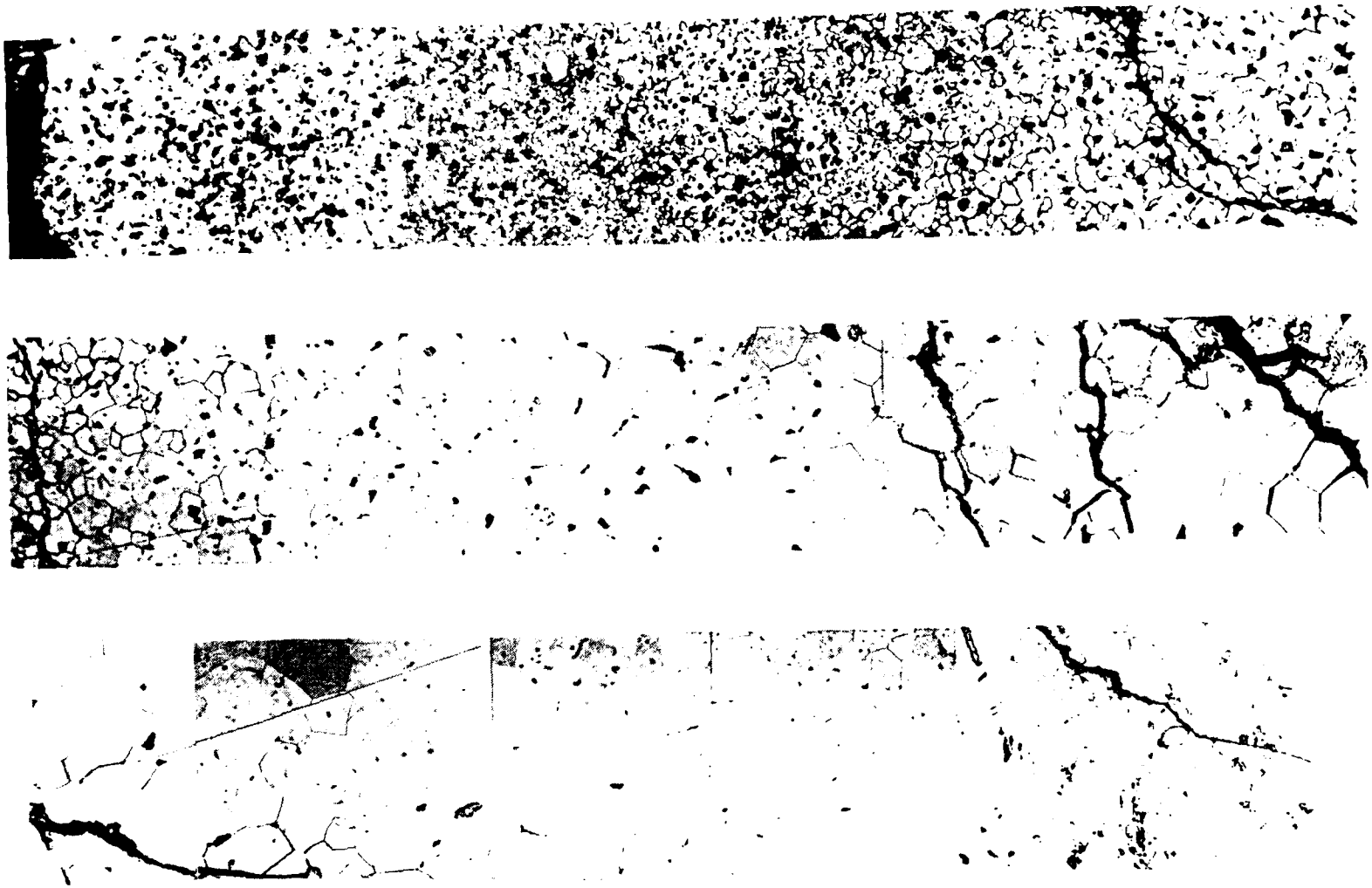

Figure 42. Composite photomicrograph of small angle section (sectioning angle, 1°-2°) showing whole layer of NiO upon Ni 200 oxidized at 1200°C for 54 hours, etched, 320X (actual magnfication is reduced into 1/2 for the reproduction). Notice the grain size change from the metal-oxide interface (left edge of the top figure) to the outer surface of NiO (right edge of the bottom figure).

Table XV

Values of the Mean NiO Grain Boundary Intercept Counts and the NiO Grain Sizes Within the NiO Scale Upon Ni 200

| Distance from the Metal-Oxide Interface, 1 unit = 159.38 μm | Mean Number of NiO Grain Boundary Intercepts per Unit Length, $\bar{N}_L$ ($cm^{-1}$) or 1/2 $S_V$ ($cm^2/cm^3$) | NiO Grain Size, $\bar{\lambda}_{EQ}$ (μm) |
|---|---|---|
| 1.5-3 | 1395.2 ± 39.41 | 7.17 |
| 3-4 | 1440 ± 33.52 | 6.94 |
| 4-5 | 1293 ± 61.80 | 7.73 |
| 5-6 | 1178 ± 6578 | 8.49 |
| 6-7 | 1109 ± 58.15 | 9.02 |
| 7-8 | 1361 ± 49.88 | 11.48 |
| 8-9 | 760 ± 26.96 | 13.16 |
| 9-10 | 662.86 ± 55.04 | 15.09 |
| 10-11 | 575 ± 33.45 | 17.39 |
| 11-12 | 476.95 ± 25.01 | 20.97 |
| 12-13 | 382.46 ± 22.63 | 26.15 |
| 13-14 | 325 ± 26.71 | 30.77 |
| 14-15 | 313 ± 13.03 | 31.95 |
| 15-16 | 267-73 ± 12-19 | 37.35 |
| 16-17 | 269.63 ± 15.13 | 37.08 |
| 17-18 | 255 ± 15.13 | 39.2 |
| 18-19 | 259.73 ± 13.74 | 38.5 |
| 19-20 | 233.98 ± 17.02 | 42.7 |
| 20-21 | 233.6 ± 21.58 | 42.80 |
| 21-22 | 235.1 ± 15.62 | 42.51 |
| 22-23 | 228.82 ± 15.26 | 43.7 |
| 23-24 | 231.88 ± 16.15 | 43.15 |
| 24-25 | 237.58 ± 19.87 | 43.12 |

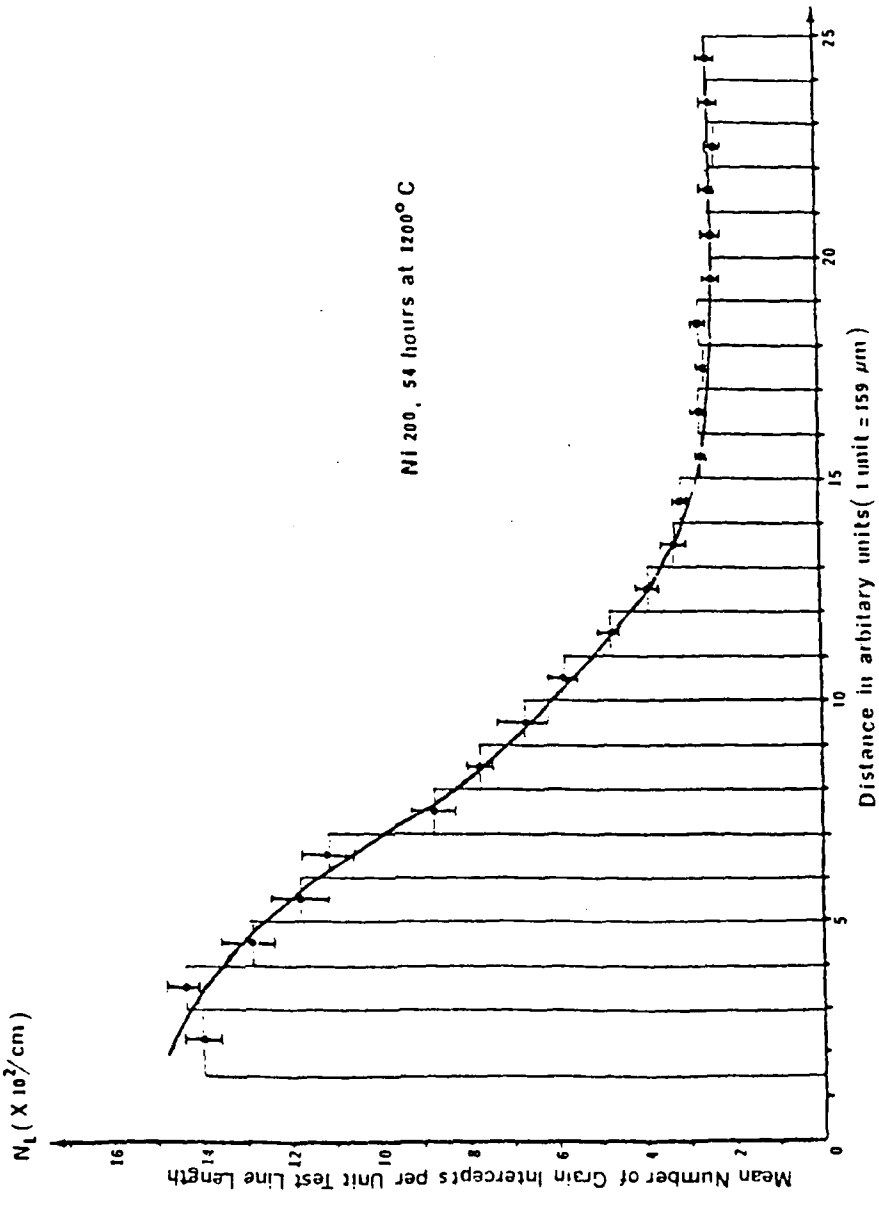


Figure 43. Change of the NiO grain size in terms of $\bar{N}_L$, from the metal-oxide interface (left) to the outer surface (right) of the NiO scale upon Ni 200.

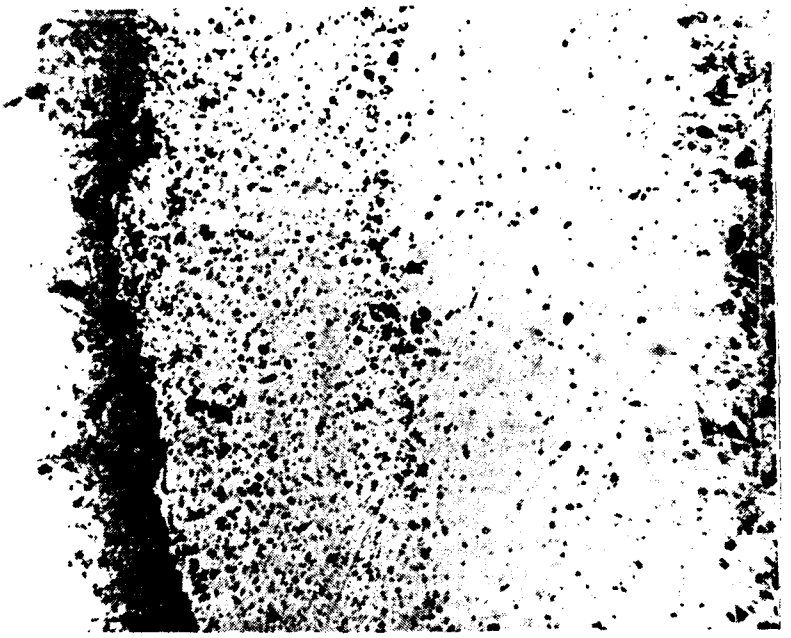

Figure 44. Taper section view of NiO upon Ni-200, oxidized for 16 hours at 1000°C in pure oxygen of one atmospheric pressure, unetched, 200X. Porosities are confined mostly within the inner layer.

was 1 cm at 320x. The results of the point counts, from the same specimen upon which the grain size of the inner layer was measured, are recorded in Table XVI along with corresponding 95% confidence intervals. The graph of Figure 45 shows the volume fraction of porosity plotted as a function of distance from the metaloxide interface.

Because of the presence of metallographic artifacts, the experimentally determined values for the volume fraction of porosity are expected to exceed the real values; however, the contribution of these artifacts to the porosity is presumed to be uniform throughout the inner layer. Thus, the general trend shown by the measurements would not be altered. That the volume fraction of porosity is the greatest near the metal-oxide interface and diminishes as the distance into the scale increases, suggests that the pores originate at the metal-oxide interface and gradually spheoridize and eventually sinter shut as the scale thickens, Figure 41.

Foreign Particles in the NiO Scale Upon Nickel 200

The distribution of foreign matter the Ni-200 oxide scales was investigated, again using taper sections. The photomicrograph of Figure 46 (Ni-200 specimen oxidized at 1000° C for 4 hours) shows rather more particles of foreign matter in the outer layer than equivalently oxidized scales on Ni-270. No conclusions could be made for the inner layer due to the presence of porosity.

Particles of foreign matter in the outer layer, when viewed in normal section appear as "streamers" extending upward into the scale from the inner layer. These particles are presumed to have been carried upward into the outer layer from the inner layer during plastic extrusion.

Table XVI

Volume Fraction of Pores as a Function of the Distance from the Metal-Oxide Interface to the Outer Surface of the NiO Scale Upon Ni 200

| Total Number of Grid Points | Distance from the Interface 1 unit = 159.38 μm | Mean Number of the Grid Points Intersecting with Pores | Porosity (%) |
|---|---|---|---|
| 36 | 1.5-3 | 12.68 ± 0.98 | 35.2 |
| 36 | 3-4 | 9.0 ± 1.20 | 25.0 |
| 36 | 4-5 | 6.56 ± 0.98 | 18.2 |
| 36 | 5-6 | 7.70 ± 1.70 | 21.4 |
| 36 | 6-7 | 5.58 ± 2.02 | 15.50 |
| 36 | 7-8 | 3.86 ± 0.89 | 10.72 |
| 25 | 8-9 | 1.22 ± 0.60 | 4.88 |
| 25 | 9-10 | 1.19 ± 0.59 | 4.76 |
| 25 | 10-11 | 0.778 ± 0.25 | 3.11 |
| 25 | 11-12 | 0.721 ± 0.20 | 2.92 |
| 25 | 12-13 | 0.333 ± 0.24 | 1.33 |
| 25 | 13-14 | 0.229 ± 0.33 | 0.91 |
| 25 | 14-15 | 0.344 ± 0.29 | 1.38 |
| 25 | 15-16 | 0.277 ± 0.26 | 0.91 |
| 16 | 16-17 | -- | -- |
| 16 | 17-18 | -- | -- |
| 16 | 18-19 | -- | -- |
| 16 | 19-20 | -- | less than 1% |
| 16 | 20-21 | -- | -- |
| 16 | 21-22 | -- | -- |
| 16 | 22-23 | -- | -- |
| 16 | 23-24 | -- | -- |
| 16 | 24-25 | -- | -- |
| 16 | 25-26 | -- | -- |

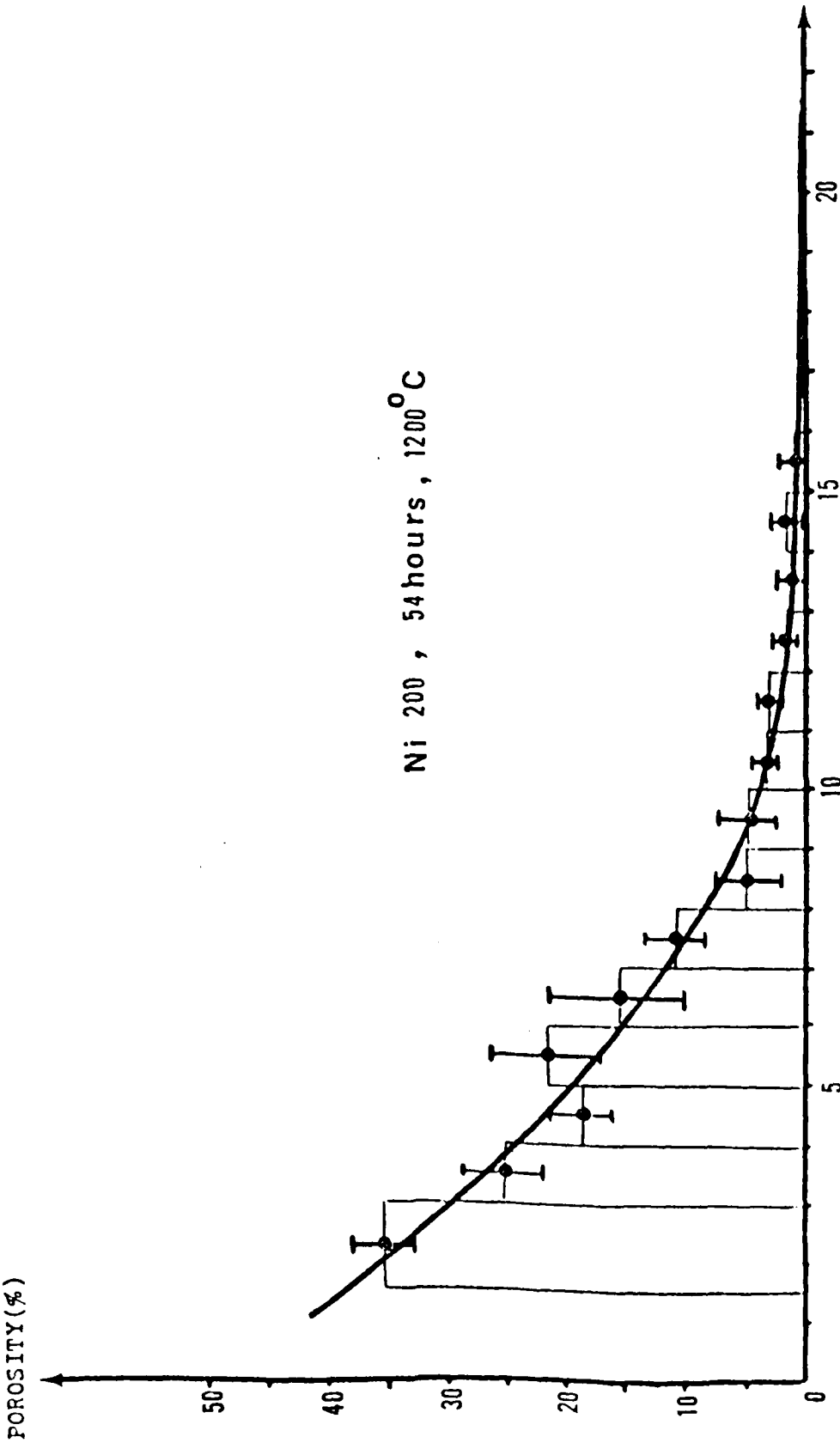


Figure 45. Change of porosity (%) from the metal-oxide interface to the outer surface of the NiO scale upon Ni 200.

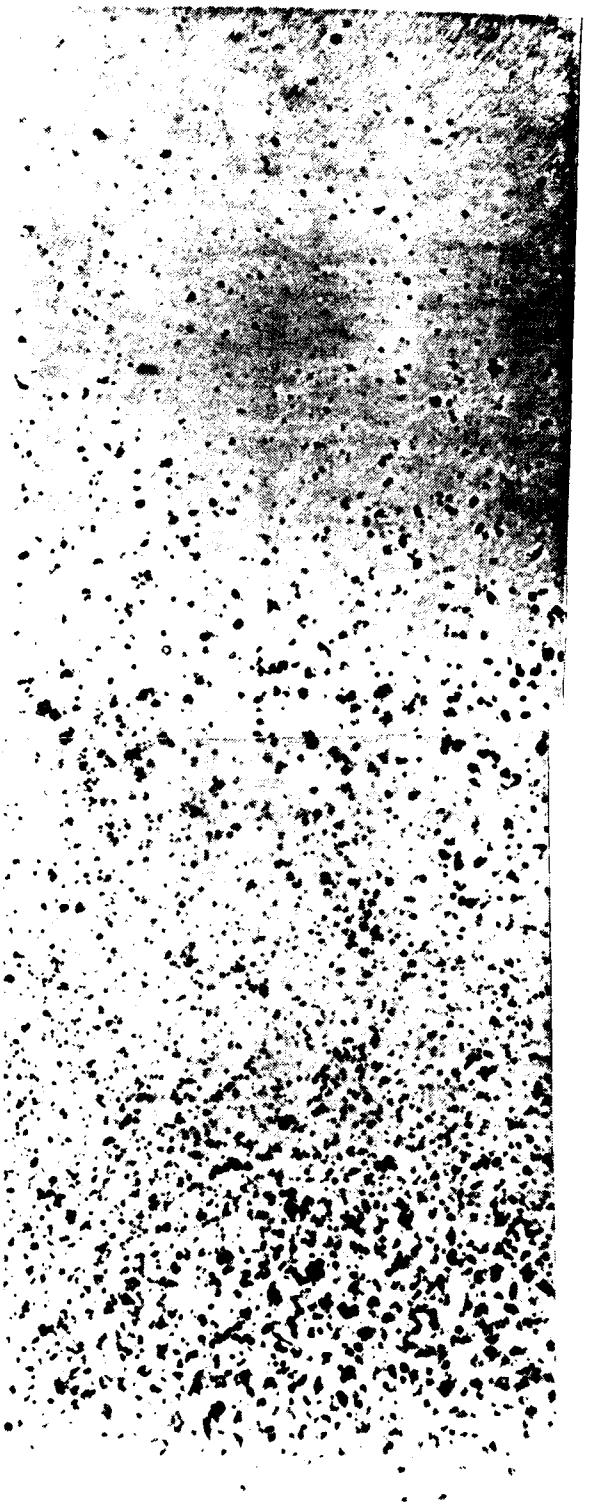

Figure 46. Taper section of the NiO scale upon Ni-200 showing approximate distribution of foreign particles. Specimen oxidized for 4 hours at 1000°C in pure oxygen of one atmospheric pressure, as polished, 400X.

## DICUSSION OF THE EXPERIMENTAL RESULTS OF THE NICKEL 200 SPECIMENS

### Comparison of NiO Scale and Grain Growth Between Nickel 270 and Nickel 200 Specimens

In order to deduce the oxidation mechanism of Ni-200 and connect it to that of pure nickel, it is very useful to compare the kinetics of the microstructural changes of Ni 200 scales to those of Ni-270. Table XVII contains the assembled data on NiO scale and grain growth to facilitate a quantitative comparison between Ni-270 and Ni-200.

The graphs of Figures 47(a through c) show changes in the microstructures (thicknesses of scale layers and mean grain intercept lengths) with time for both grades of nickel. Referring to these, it can be said that the path of microstructural change is essentially identical for the pure and the less pure nickel except for the difference in their magnitude. Some other important results can be derived from Table XVII:

(1) Ni-200 oxidizes faster than does Ni-270 so that, for any given time of oxidation, the Ni-200 scale is always thicker than that grown upon Ni-270. (Table XVII, rows 7 and 8) The same is true for both the inner and outer layer of the scale (Table XVII, rows 1, 2, 4, and 5).

(2) The mean intercept grain size of the columnar layer formed upon Ni-200 is always greater than that upon Ni-270 (Table XVII, rows 10 and 11).

(3) From (1) and (2), it is presumed that for both grades of nickel, at least in the columnar layer, scale thickening and

Table XVII

Comparison of the Thicknesses of Scales and Mean Intercept Lengths for Ni 270 and Ni 200

(unit in μm)

| Row Number | Time (hours) | 4 | 16 | 36 | 64 | 81 | 225 | Average |
|---|---|---|---|---|---|---|---|---|
| 1 | $X_{COL}$ (270) | 6.56 | 12.34 | 18.70 | 23.0 | 23.90 | 33.48 | |
| 2 | $X_{COL}$ (200) | 9.75 | 17.72 | 23.36 | 29.0 | 35.15 | 55.43 | |
| 3 | $\frac{X_{COL}\ (200)}{X_{COL}\ (270)}$ | 1.49 | 1.44 | 1.25 | 1.26 | 1.47 | 1.66 | 1.43 |
| 4 | $X_{INN}$ (270) | 4.06 | 8.20 | 10.48 | 16.69 | 17.30 | 24.25 | |
| 5 | $X_{INN}$ (200) | 8.91 | 17.95 | 26.66 | 39.24 | 42.41 | 58.97 | |
| 6 | $\frac{X_{INN}\ (200)}{X_{INN}\ (270)}$ | 2.19 | 2.19 | 2.54 | 2.35 | 2.45 | 2.43 | 2.36 |
| 7 | $X_{TOT}$ (270) | 10.62 | 20.54 | 29.18 | 39.69 | 41.21 | 57.73 | |
| 8 | $X_{TOT}$ (200) | 18.86 | 35.67 | 50.02 | 68.26 | 77.56 | 114.4 | |
| 9 | $\frac{X_{TOT}\ (200)}{X_{TOT}\ (270)}$ | 1.78 | 1.74 | 1.71 | 1.72 | 1.88 | 1.98 | 1.80 |
| 10 | $\bar{\lambda}_{COL}$ (270) | 2.19 | 4.11 | 6.23 | 7.66 | 7.97 | 11.55 | |
| 11 | $\bar{\lambda}_{COL}$ (200) | 3.45 | 5.75 | 8.31 | 10.0 | 11.49 | 16.61 | |
| 12 | $\frac{\bar{\lambda}_{COL}\ (200)}{\bar{\lambda}_{COL}\ (270)}$ | 1.58 | 1.40 | 1.33 | 1.30 | 1.44 | 1.44 | 1.42 |

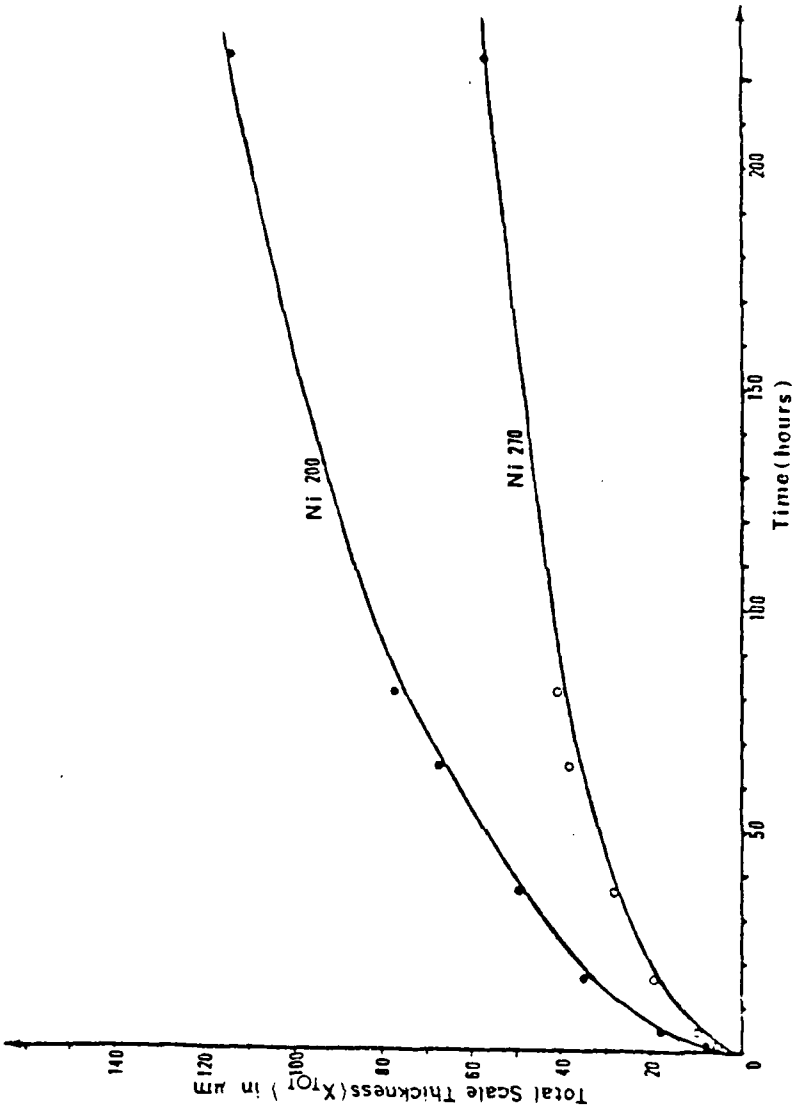


Figure 47 Path of microstructural change with time of the NiO scales upon Ni 270 and Ni 200, oxidized at 1000°C in pure oxygen of one atmospheric pressure.

Figure 47(a). Total thickness ($X_{TOT}$) versus oxidation time.

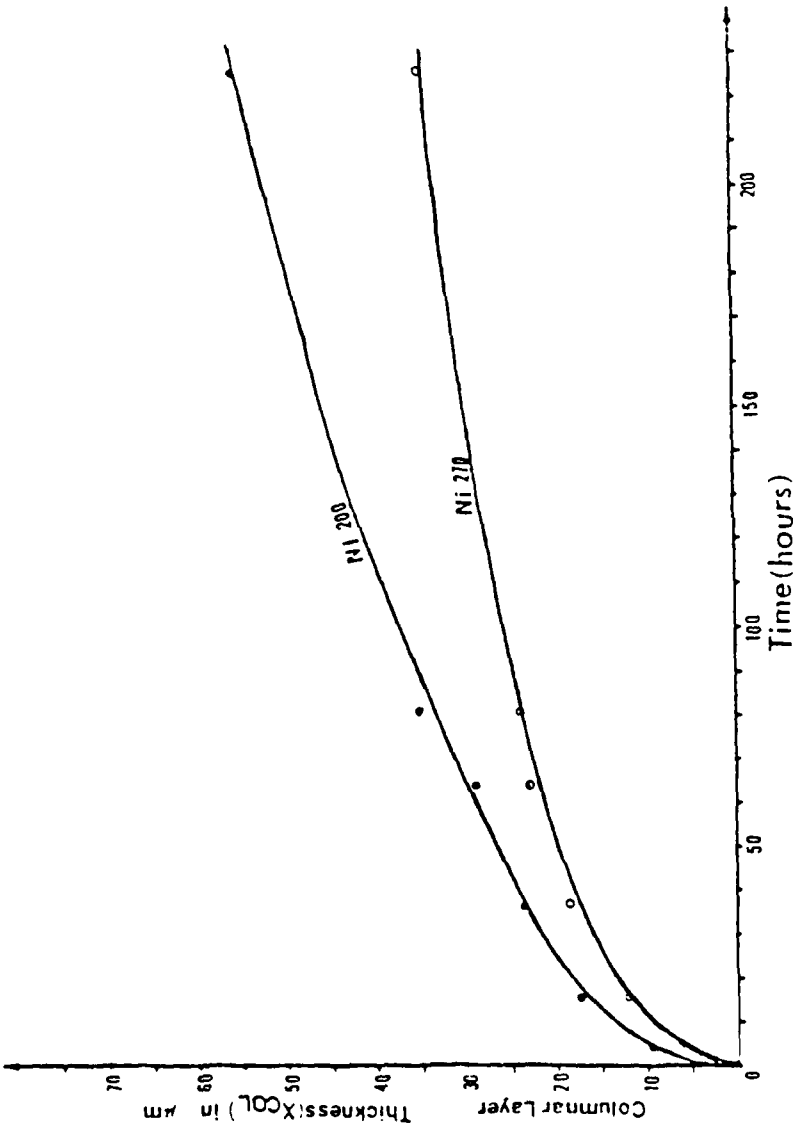


Figure 47(b). Columnar layer thickness ($X_{COL}$) versus oxidation time.

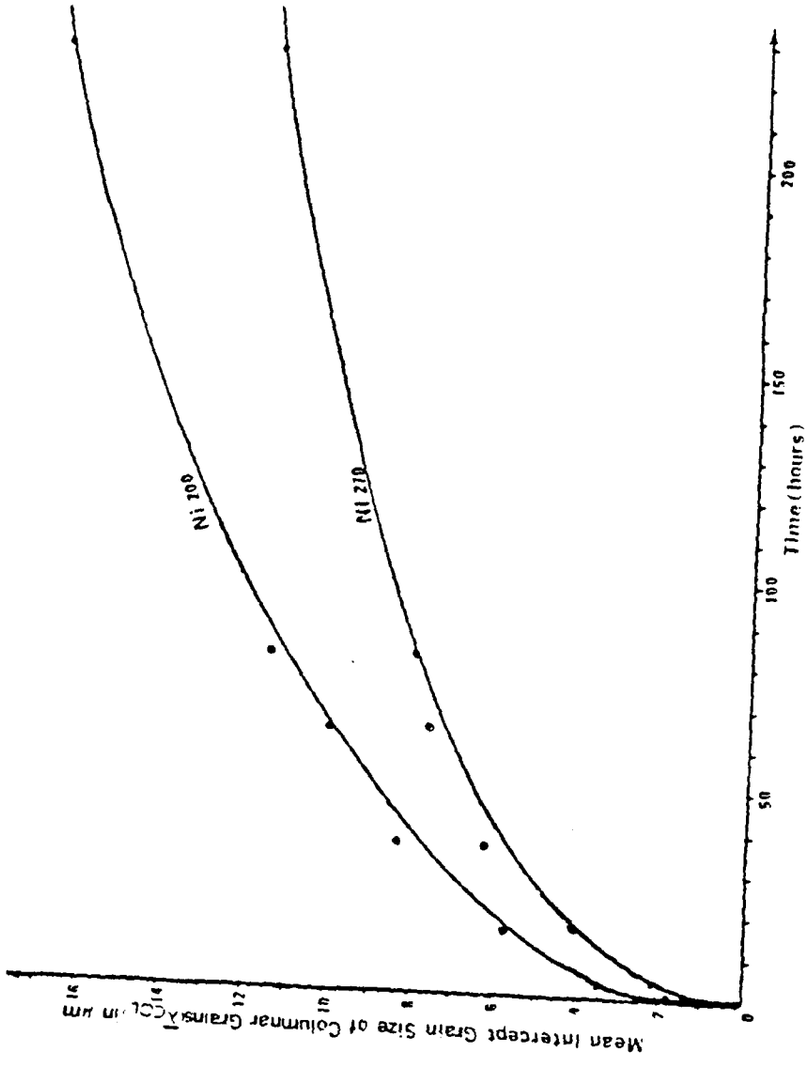


Figure 47(c). Mean intercept length of columnar grains ($\bar{\lambda}_{COL}$) versus oxidation time.

grain growth go hand-in-hand,* Figure 48(a and b). This presumption is supported by the observation that the columnarity of the outer scale layer is about three and is independent of oxidation time for both Ni-200 and Ni-270.

(4) From the existence of the quantitative relationship between scale growth and grain growth for the columnar layer scales upon Ni-200, and the microstructural similarity of the outer scale layers between two grades of nickel, it can be said that the formation of the NiO columnar layer upon Ni-200 is controlled by grain boundary sweeping mechanism.

The greater rate of thickening of Ni-200 over Ni-270 scales is dependent upon its greater rate of grain growth. The rate of grain growth is dependent upon the amount of new oxide formed within the thickness of the scale, and in its turn, upon the rate of transport of the reactants into the scale. Because it is believed that the oxygen in the grain boundaries is in excess, the supply of nickel should be rate limiting. Therefore, it is apparent that more nickel should come up through the thicker, porous, inner layer of the Ni-200 scales than would be delivered through the thinner, relatively sound inner layer of Ni-270 scales.

The main features of the Ni-200 scales which could possibly account for a faster rate of transport of reactants through the scale are, porosity within the inner layer and finer grain sizes within the inner layer of Ni-200 scale.

---

*Grain growth results from the plastic deformation. And the evidence of plastic extrusion was easily observed in the outer layer scales upon both grades of nickel where Ni-200 scales, Figure 45, show many more foreign particles than that upon Ni-270, Figure 24.

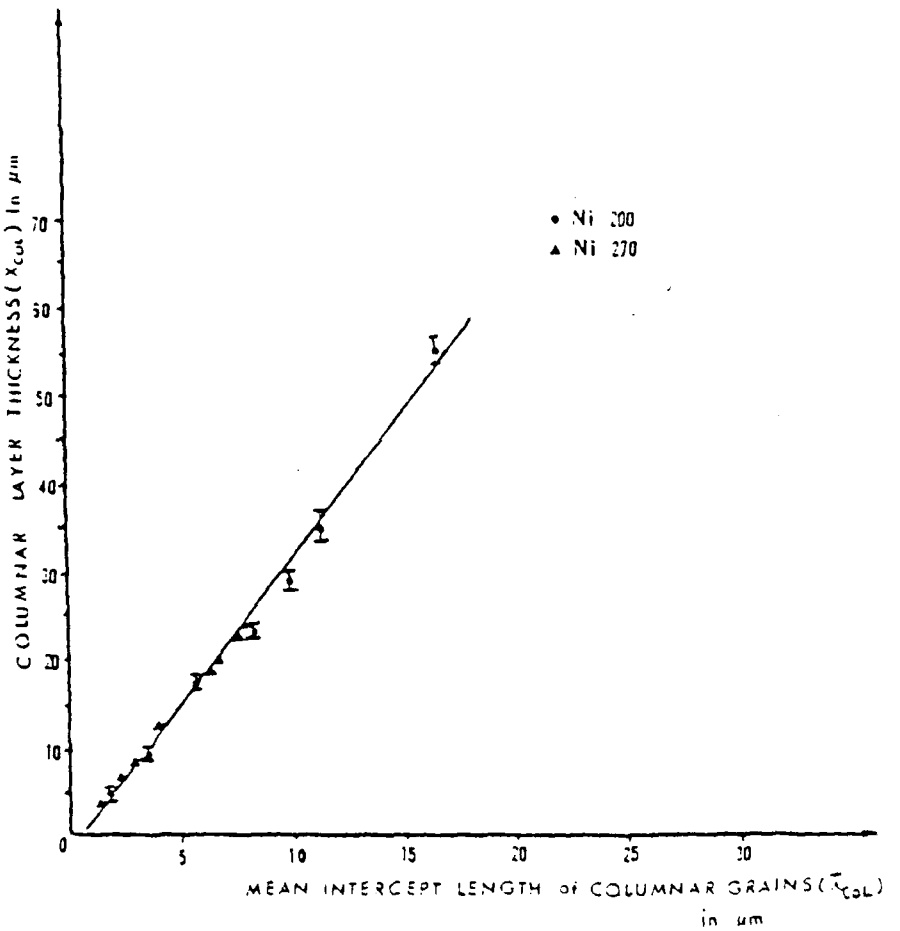


Figure 48. Interrelationships between the scale growth and grain growth of the NiO scale upon Ni 270 and Ni 200.

Figure 48(a). Columnar layer thickness ($X_{COL}$) versus mean intercept length of the columnar grains ($\bar{\lambda}_{COL}$).

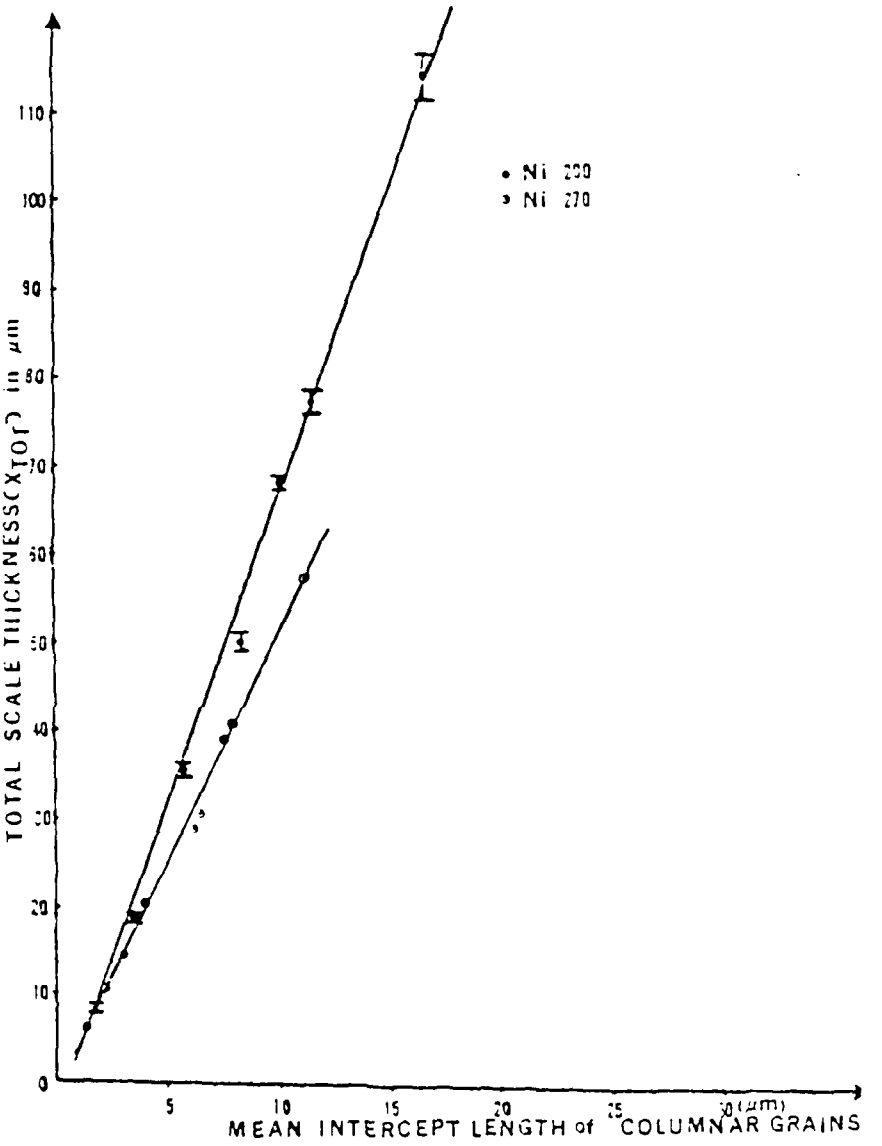


Figure 48(b). Total thickness ($X_{TOT}$) versus mean intercept length of the columnar grains ($\bar{\lambda}_{COL}$).

Role of the Vapor Phase in Scale Growth Upon Nickel 200

The seemingly small difference in purity of Ni-200 as compared with Ni-270 was found to be associated with the following gross differences in oxidation behavior of the inner layer:

(1) A faster scale thickening, Table XVII.

(2) A relative thickening of the inner layer with respect to the outer layer, i.e., about 40% of the total thickness is composed of the inner layer for Ni-270, Table V, whereas that value becomes 50% for Ni-200, Table XIV.

(3) Near the metal surface, the grain size of NiO is very fine and the size gradually increases until it becomes equal to the transverse mean intercept length of the columnar grains at the boundary between the inner and outer layers of the scale, Figure 43.

(4) The grain size at the metal-oxide interface always stays about the same, independent of oxidation time, Figure 36.

(5) The presence of pores appearing in the metal, Figure 37, close to the metal-oxide interface, Figures 38-39, and extend to, but not beyond, the boundary between the inner and outer layers of the scale, Figure 45. The size and volume fraction of pores tend to be largest next to the metal and to become smaller toward the outer boundary of the inner layer, Figure 45.

(6) The presence of fine idiomorphic NiO grains lying on the inside of pores, Figure 40(b). These grains are suggestive of the clusters of crystals that are formed when a solid phase condenses as sublimate particles from a vapor.

(7) The presence of an increased number of particles of foreign oxides in the inner layer and extending into the outer layer, Figure 46.

All but the last one of these differences can be attributed by the presence of carbon, if it is supposed that carbon can react with oxygen to form a subscale of pores containing $Ni(CO)_4$ and/or CO in mixture. This occurrence becomes more probable through the common experience that carbon bearing nickel tends to develop porosity when it is heat treated in hydrogen. In this case, it has been supposed that the porosity is created by the presipitation of methane, $CH_4$. At elevated temperature, nickel carbonyl, $Ni(CO)_4$, is gaseous. At ordinary pressure, $Ni(CO)_4$ decomposes to form CO and Ni, but in the high pressure of confinement of a nickel matrix, the undecomposed form of this gas might be stable to a certain degree.

The formation of the inner layer upon Ni-200 follows essentially the same oxidation sequences as that upon Ni-270. By the time NiO islands grow to form the columnar layer upon the original metal surface, the inner layer begins to grow by nucleating new NiO grains upon the $NiO^3$-Ni quadruple points of the metal-oxide interface. Simultaneously, the subscale composed of foreign oxides and also voids containing the gas phase is eroded into the growing oxide scale. Thus, pores become surrounded by NiO. The NiO matrix as a p-type semiconductor carries a gradient of nickel ion concentration across the scale. With this condition, the vapor content of the pore is exposed to a diminishing nickel concentration from its inward end to its outward end. In the same pore, therefore, it is possible for the $Ni(CO)_4$ content of the gas to be higher at the inward end of the pore than at its outward end. This

concentration gradient provides for nickel transport through the vapor phase, either by gaseous diffusion, convection, or both. In any case, this mechanism may provide for more rapid nickel transport than is expected by solid state diffusion through the bulk of the NiO. This would account, not only for a more rapid thickening of the inner layer, but also a higher concentration of nickel at the boundary between the two layers where $Ni^{++}$ ions are fed into the outer layer. This accounts for an increase in the rate of thickening of the outer layer scale.

When the $Ni(CO)_4$ decomposes, either of two results is possible; namely: (1) $Ni^{++}$ and 4 CO could be produced. The $Ni^{++}$ might then dissolve in NiO matrix. The CO would diffuse back to the base of pore for further reaction with nickel. (2) The decomposition occurring in the presence of excess oxygen could form NiO directly, releasing carbon to react with oxygen as additional CO which again would return for more nickel. It is presumed that this would be the predominant case at the intersections of NiO grain boundary triple lines with the pore, where the oxygen content is maximized.

Each of these processes would produce a different physical result and both results seem to be occurring. The first case leads to an accelerated transport of nickel and more rapid scale growth, as has been observed. The second case would provide for the growth of NiO sublimate particles at the outward ends of the pores. The sublimated NiO grains, being nucleated at the $NiO^3$-pore quadruple points, provide for the fine grains that are seen adjacent to the metal-oxide interface, Figures 38-39. They also provide for the halos of fine grains surrounding pores, Figure 41, as was observed in the case of Ni-270, Figure 27.

Some verification of the above supposition can be obtained by looking at the total structure of the scale upon Ni-200 seen as a typical ternary diffusion layer structure. A hypothetical 1000° C isotherm of the phase diagram of the ternary system Ni-C-O is given in Figure 49. As seen in this figure, the layers in succession are,

(1) Nickel metal, either with or without free carbon.

(2) An interface between this two-phase layer and another two-phase layer composed of nickel and vapor, giving three phases of nickel, carbon, and vapor.

(3) Two-phase nickel plus vapor layer.

(4) Another three phase equilibrium of nickel, NiO, and vapor.

(5) A two phase layer of NiO plus vapor.

(6) Finally the outer surface where oxygen is rich.

In a ternary diffusion system, the composition path normally is as remote as possible from the fastest diffusion species [131]. In this case, the interstitial carbon may be expected to be faster moving than either oxygen or nickel; therefore, the composition path is drawn nearly parallel to the NiO side of the phase diagram in Figure 49.

In Figure 49 the composition path of oxide scales upon Ni-270 is represented by the Ni:O binary side of the ternary isotherm. Referring to this figure, the layers in succession are

(1) Nickel metal.

(2) Two phase nickel plus nickel oxide.

(3) One phase of NiO.

(4) A two phase layer of NiO plus oxygen.

(5) Outer surface where oxygen is rich.

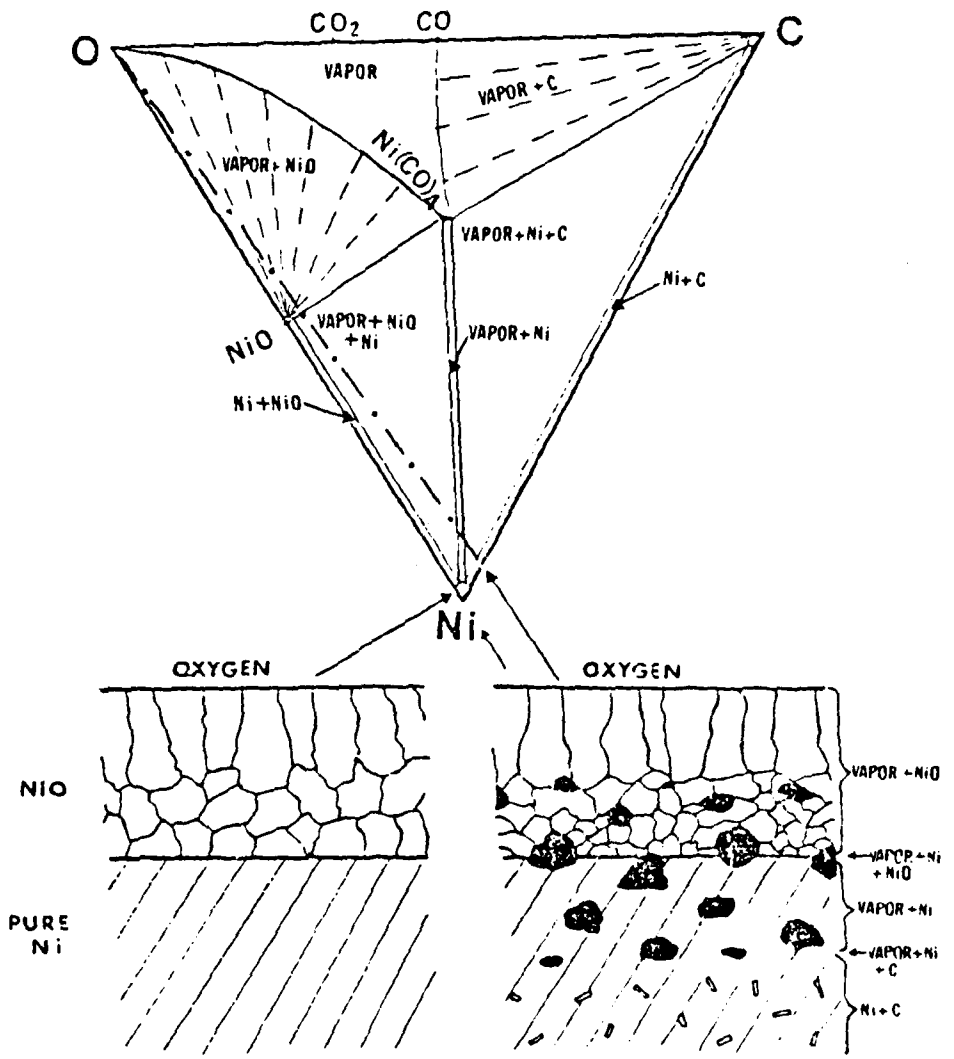


Figure 49. 1000°C isotherm of Ni-C-O ternary phase diagram.

As discussed above, the presence of pores introduce some faster ways for the outward transport of nickel. This does not change the basic grain boundary sweeping model of the growth of the inner layer which is still similar to that of the columnar layer. The inner layer displays simultaneous grain growth and scale thickening, Figure 43, suggesting that the two processes are closely linked. It should be noted, however, that the grain size at the metal-oxide interface is always the same, because new grains are continually being formed there, whereas nucleation in Ni-270 is of minor import. The gradual shrinkage of the pores as they retreat from the metal-oxide interface toward the outer surface, also implies plastic deformation in the inner layer [133]. Also, as the volume of pores decreases with oxide thickness, the supply of newly nucleated grains associated with $Ni(CO)_4$ decomposition should diminish toward the outside. Since grain growth is in progress, the above result can bring about the grain size gradient observed within the inner layer, Figure 43.

The deduction that the sublimate grains of NiO form because of the availability of oxygen near the metal-oxide interface, together with the evidence of the envelopment of inert particles across the metal-oxide interface, suggests that oxygen is present in sufficient amount to react with any available nickel throughout the scale. Under this curcumstance, the ultimate rate control of the scale growth should reside in the rate of transport ions as shown by the comparison between Ni-270 and Ni-200. This is now seen to be a highly complex process. In the case of impure nickel, it involves both solid state diffusion and gaseous diffusion upon ill defined paths.

Finally, it is to be noted that the well-known tendency of Ni-200 scales to spall freely can be mostly ascribed to the formation of a porous layer of NiO along the metal-oxide interface, together with the stresses that result from the swelling of the scale.

Effect of Grain Size in the Inner Scale Layer Upon the Oxidation Rate of Nickel 200

One of the factors which result in faster thickening of Ni-200 scales compared to that of Ni-270 is the difference in their inner layer grain size. There are two major effects of the fine grain size upon the oxidation rate, namely:

(1) Smaller grain size of the inner layer scale implies that there is greater amount of reaction front, i.e., grain boundary surface area, and hence, enhanced rates of plastic deformation and attendant grain boundary sweeping.

(2) Due to the smaller grain size, the probability of new grain nucleation of metal-oxide interface becomes higher, because new grains nucleate at the $NiO^3$-Ni quadruple points.

The Oxidation of High-Purity Copper

Paralleling the work on Ni-270 and -200, a secondary investigation on the oxidation of high-purity copper was undertaken to study scale thickening through a coordinated evaluation of the scale microstructure. The copper was oxidized at 800° C in air, so that the $C^{u20}$ scale would predominate. The following sections of this part of the report deal separately with the investigation of copper oxidation.

Object of the Investigation

For Ni-270 and -200 it had been established that scale growth and the microstructural evolution of the scale (grain growth) were inter-

related, and upon the evidence gained from the microstructure, the authors proposed a mechanism for oxidation in which the rate of grain boundary sweeping controlled the rate of scale thickening. To begin to test the application of this mechanism to the oxidation of other metals, the study of the oxidation of copper was undertaken.

Scope of the Study

The original plan of the study was to investigate the oxidation of copper in a temperature range wherein only one oxide ($Cu_2O$) predominated and to expand the study to a wide variety of dilute alloys of copper to study the effects of impurities upon both the microstructural evolution of the scale and the kinetics of scale thickening. This plan proved to be too ambitious when the experimental difficulties of scale spalling and metallographic preparation were encountered. Therefore, only a brief study was made of the high-purity copper to establish the interrelation between scale growth and grain growth of the scale.

The Oxidation of Copper

High-purity copper (99.999% Cu) in the form of 1/2" diameter rod was sliced into wafers varying in nominal thickness from 0.060" to 0.100" to provide oxidation coupons. These wafers were prepared for oxidation according to the same procedure as were used for the nickel specimens. The specimens were oxidized in air in a small preheated heat-treating furnace operated at 800° C. To prevent excessive contamination of the scales grown on the specimens, they were placed on edge on a heavily oxidized copper hearth in the furnace. Spalling of the scales during a normal cool down to room temperature from 800° C rendered the specimens useless for study of the oxide scale. It was necessary to slowly cool the specimens by turning off the power to the

furnace and allowing the specimens to cool to room temperature in the furnace. The cool down period was of the order of 16 hours. Admittedly, the specimens continued to oxidize as they cooled, but each specimen received the same treatment. As discussed in a later section, it is believed that the effect of the slow cool upon the relative oxidation of the specimens does not play a major role in the outcome of this study.

Metallographic Preparation

The oxidized discs were mounted on edge in Buehler Epoxide mounting material for metallographic preparation, so that sections normal to the metal-oxide interface could be viewed. Thermosetting mounting materials proved to be unsatisfactory because they were too brittle or because pressures developed in the mounting press damaged the oxide scales. About one-half of each disc was ground away in sectioning the specimens. Conventional metallographic polishing down to 6μ diamond was used to render the scales suitable for etching. Further polishing with finer abrasives resulted in the "pulling out" of pieces of the scale. The as-polished scales were etched by immersion in a solution containing 50% concentrated nitric acid, 25% glacial acetic acid, and 20% orthophosphoric acid; all percentages being by volume. Etching times were of the order of three seconds. Due to the rapid attack of the etchant upon the scale, it was difficult to control the degree of attack necessary to reveal the grain boundaries of the scale. Microstructures with sufficient contrast for photomicrography were difficult to produce; however, reliable quantitative microscopy was possible.

Microstructure of the Scale

The scale produced on the copper was predominately $Cu_2O$; however, a thin external layer of CuO was observed. This CuO layer could just be

resolved at a magnification of 1000x. For the most part, the $Cu_2O$ consisted of columnar grains. Careful examination showed that the scale apparently consists of two layers of about equal thickness, both made up of columnar grains. The boundary separating the two layers is not clearly defined as in the case of Ni-270. At all times of oxidation, the columnar grains of the two layers were of the same average size.

The scales formed on the copper were free of both porosity and foreign oxide particles, as might be expected in view of the high pruity of the copper. Etching of the scale produced some artifacts which were determined to be the result of portions of grains dropping out of the scale. Grain drop out is no doubt the combined result etching attack and cracking of the scale, the cracks having been introduced during the mechanical grinding and polishing of the scale.

Lineal intercept measurements were made with the test line parallel to the metal-oxide interface in order to determine the average breadth dimensions of the columnar grains. Scale thicknesses were also measured. The procedures followed for these measurements were the same as those utilized in the research on nickel. Table XVIII gives both scale thickness measurements (x) and mean grain intercepts ($\bar{\lambda}$) with tolerance intervals at a confidence level of 95%.

Scale Growth Kinetics

Scale thickness (X) is plotted versus time (t) in Figure 50. By using linear regression and seeking a maximum in the correlation coefficient, the best fit of the scale thickness-time data was obtained for an equation of the form:

$$x = At^B + C,$$

where x is scale thickness (millimeters, t is time (hours) and A, B and

TABLE XVIII

SCALE THICKNESS AND MEAN GRAIN BOUNDARY INTERCEPT LENGTH DATA FOR HIGH-PURITY COPPER SPECIMENS OXIDIZED IN AIR AT 800°C

| TIME (Hrs.) $t$ | SCALE THICKNESS (mm) $x$ | MEAN GRAIN BOUNDARY INTERCEPT LENGTH ($\times 10^{-2}$ mm) $\bar{\lambda}$ |
|---|---|---|
| 3 | 0.123 | 2.4 ± 0.2 |
| 5 | 0.169 | 2.7 ± 0.3 |
| 7 | 0.189 | 3.6 ± 0.4 |
| 9 | 0.226 | 4.0 ± 0.3 |
| 13.5 | 0.241 | 3.1 ± 0.2 |
| 15 | 0.256 | 3.0 ± 0.2 |
| 17 | 0.282 | 3.5 ± 0.2 |
| 19 | 0.305 | 3.6 ± 0.3 |
| 21.5 | 0.320 | 3.9 ± 0.2 |
| 26 | 0.364 | 4.6 ± 0.3 |
| 29.5 | 0.310 | 4.9 ± 0.4 |
| 32 | 0.363 | 4.5 ± 0.2 |
| 35 | 0.409 | 5.0 ± 0.4 |

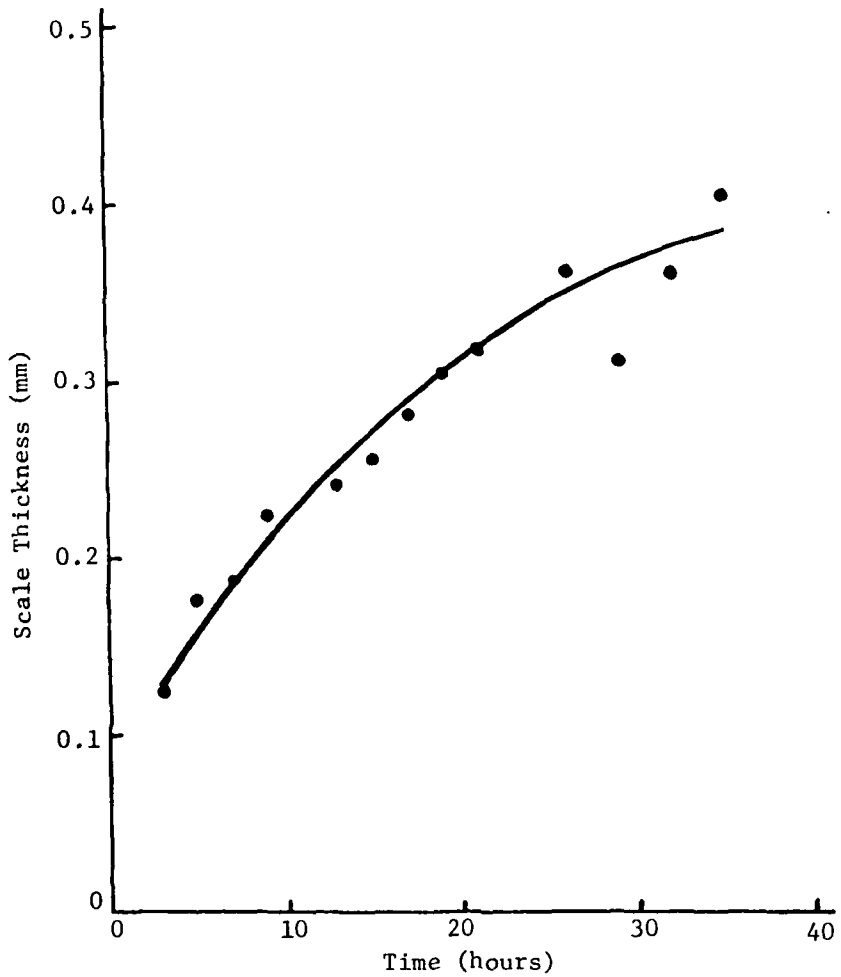


Figure 50. Scale thickness versus time for $Cu_2O$ scales grown upon high-purity copper in air at 800°C.

C are constants. The values of the constants and correlation coefficient are as follows: A = 0.1017, B = 0.395, C = 0.029 and r = 0.9835. It is important to note that since the value of C is negative, the curve crosses the time axis at a positive value of time. This observation suggests that there exists early stages of oxidation which behave kinetically different from that which prevails over the range of oxidation time studied.

Scale Thickening and Grain Growth

In Figure 51, the mean grain intercept ($\bar{\lambda}$) as measured parallel to the metal-oxide interface at a position about midway through the scale thickness is plotted versus the scale thickness (X). As the scale thickens, so does the mean breadth dimension of the columnar grains. The relationship between the two is reasonably linear. Scatter in the data is attributed to the fact that the thirteen specimens were oxidized in three batches, and it is speculated that oxidation during the slow cooling after the predetermined oxidation period was not uniform among the three batches.

As indicated by the data, there seems to be little doubt that scale thickening is related to grain growth of the scale.

Nucleation of New Oxide Grains

As with the growth of NiO on high-purity nickel, (64) there seems to be little evidence of new grain nucleation during the growth of $Cu_2O$ on copper. Both scales are composed of predominately columnar grains. That both the inner and outer layers of $Cu_2O$ scales are columnar and that the grains in both layers have approximately the same breadth dimensions, suggests that the inner layer represents the nucleation of new grains only to form the inner layer. It is presumed that new grains

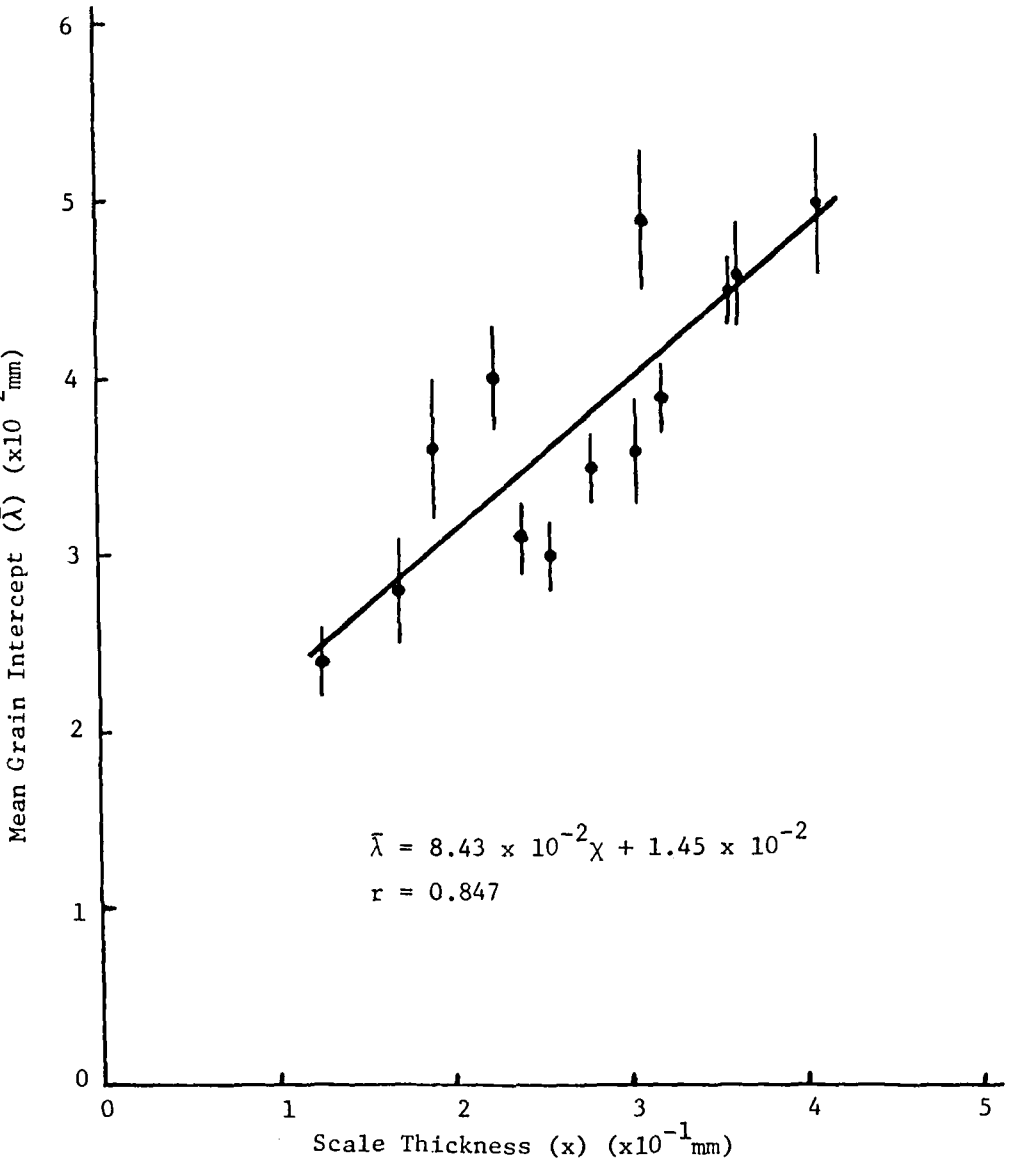


Figure 51. Mean grain intercept versus scale thickness for $Cu_2O$ scales grown upon high-purity copper in air at 800°C.

nucleate at the intersections of $Cu_2O$ triple lines with the metal-oxide interface. Once the new grains of the inner layer are nucleated, they merely grow lengthwise in proportion to their lateral growth which is growth by grain boundary sweeping.

## CONCLUSIONS

A. Nickel 270

1. The NiO scale formed upon a flat specimen at 1000° C is composed of two layers. The outer layer consists of columnar grains, and the inner layer is made up of three dimensionally equiaxed grains.
2. The mean intercept size of grains, measured parallel with the metal-oxide interface, is essentially identical throughout the whole NiO scale layer. On the basis that scale growth is related to grain growth, this means that the scale is growing by a homogeneous swelling that is uniform throughout the scale.
3. The ratio of the outer layer thickness to the mean intercept grain size of the columnar layer (columnarity) is always maintained at three during oxidation. The thickness of the inner layer and the whole layer is about two times and five times as thick as the mean intercept grain size, respectively.
4. Oxidation is presumed to proceed in three stages:
   (1) A fast chemisorption of oxygen followed by the almost instantaneous formation of islands of NiO and their spreading upon the entire original surface to form a polycrystalline surface film. At this stage, nickel ions are available in

excess so that the rate of oxidation is controlled by the supply of oxygen and is pressure sensitive.

(2) As these oxide islands thicken to form columnar grains, the rate of delivery of nickel ions to the external surface becomes the controlling factor. There are three substages:

(a) The thickness of the scale is so thin that the supply of nickel is controlled by the rate of nickel dissolution into NiO at the metal-oxide interface. A logarithmic law results.

(b) Diffusion controlled growth of columnar grains results in a parabolic law.

(c) The onset of the NiO grain boundary sweeping, results in a cubic law. During this stage the structure of the inner layer is under development through the nucleation of new NiO grains at the NiO3-Ni quadruple points upon the metal-oxide interface. The nucleation process is repeated continuously but its frequency is so rapidly diminishing that it nearly stops after about two layers of grains are nucleated.

(3) A general swelling of the whole scale including the inner layer, regulated by the grain boundary sweeping-cube root time law. In this stage, the mean intercept grain size of the columnar grains is already established to be at a constant ratio of 1/3 and 1/2 to the thickness of the columnar layer and equiaxed layer, respectively.

5. Foreign matter is enveloped by the inner layer of the growing scale. Growth by the swelling of the scale maintains their

relative positions within the inner layer. Some particles are occasionally swept up into the outer layer by the plastic extrusion of the NiO that occurs in oxidation.

6. The NiO formed upon pure nickel is essentially porefree except for few gas blown micropores. Occasionally, macropores develop at the metal-oxide interface. Such voids eventually spheroidize and shrink as the scale thickens. Each pore is surrounded by a halo of fine grains, the generation of which is associated with the existence of carbon in the metal.
7. The NiO grain size distributuion at the metal-oxide interface is log-normal, except that grains of the smallest size are appearing in excess. This is because new small grains are being nucleated at the metal-oxide interface.
8. The number of newly nucleated grains is directly proportional to the total number of the $NiO^3$-Ni quadruple points at the metal-oxide interface.
9. The distribution of grain size within the body of the NiO scale is also log-normal over the whole range of grain sizes.
10. The relative width of the log-normal distribution does not change during the oxidation, either upon the metal-oxide interface or within the body of the scale.

B. Nickel 200

1. The whole scale is composed of an outer columnar layer plus an inner porous and equiaxed layer, whose relative thickness is about the same.

2. The columnar layer and the inner layer grow much faster than those upon Ni-270.
3. There is quantitative correlation between scale growth and grain growth for the scale as a whole.
4. There exists internal oxidation. And the scale contains more foreign particles than does that on Ni-270.
5. The grain size of the inner layer is changing with distance from the metal-oxide interface and gradually increases to the transverse intercept length of the columnar grains at the interboundary between the two layers.
6. The grain size at the metal-oxide interface is always the same, independent of oxidation time.
7. Numerous pores exist near the metal-oxide interface and extend to, but not beyond, the boundary between the inner and outer layers of the scale. The size and volume fraction of pores tend to be largest next to the metal and become smaller toward the outer layer. The pores are usually nested with halos of fine idiomorphic NiO grains around the, which was also observed in the case of Ni-270.
8. The increased rate of oxidation (point 2) and the grains size refinement and the pores within the inner layer (points 5, 6, and 7) can be ascribed to the presence of carbon in the metal, which forms pores presumably containing $Ni(CO)_4$ and/or CO in mixture: Nickel carbonyl is postulated to provide faster ways of nickel transport, other than solid state diffusion, which increases the oxidation rate. The fine idiomorphic NiO grains around the pores are seen as sublimate particles from the gas

phase. These are the cause of the refinement of the grain size.

9. The path of microstructural change for scale growth and grain growth in the columnar layer is identical to those of Ni-270.

10. The mechanism of formation of the inner layer is also basically the same as that of Ni-270. It forms by nucleating new grains at the metal-oxide interface and grows by swelling mechanism. The only difference is that new tiny NiO grains are constantly added around the pores to reduce the average grain size.

C. High-Purity Copper

1. The $Cu_2O$ scales formed upon flat specimens of high purity copper oxidized in air at 800° C appear to be composed of two layers, both of the layers containing columnar grains. Each layer is about one-half the scale thickness.

2. Scale thickening kinetics are sub-parabolic ($t^{0.395}$) within the accuracy of the experiment.

3. Scale thickening and grain growth are related, i.e. the mean grain intercept is proportional to scale thickness.

4. The breadth (or mean grain intercept parallel to the metal-oxide interface) of the columnar grains is about the same throughout the scale thickness.

5. Scale growth is homogeneous throughout the scale thickness.

6. $Cu_2O$ scales are free of impurity oxide particles and porosity.

## REFERENCES


1. F. N. Rhines and R. G. Connell, Jr., J. Electrochem. Soc., 124, 1122 (1977).
2. G. Tammann, Z. Anorg, Chemie, 111, 78 (1920.
3. N. B. Pilling and R. E. Bedworth, J. Inst. Metals, 29, 529 (1923).
4. C. Wagner, Z. Phys. Chem., B21, 25 (1933).
5. J. A. Sartell and C. H. Li, J. Inst. Metals, 90[3], 92 (1961-62).
6. E. A. Gulbransen and K. F. Andrew, J. Electrochem. Soc., 101, 128 (1954).
7. G. Valensi, Compt. Rend., 201, 523 (1935).
8. H. Pfeiffer and K. Hauffe, Z. Metallkd., 43, 364 (1952).
9. J. A. Sartell, R. J. Stokes, S. H. Bendel, T. L. Johnson, and C. H. Li, Trans. AIME, 215, 420 (1959).
10. J. C. Bokros and W. R. Wallace, Corrosion, 16, 117 (1960).
11. L. Berry and J. Paidassi, Compt. Rend., 255, 2253 (1962).
12. F. S. Petit and E. J. Felton, J. Electrochem. Soc., 111, 135 (1964).
13. J. D. Christian and W. P. Gilbreath, Oxidation of Metals, 9, 1 (1975).
14. G. C. Wood, I. G. Wright, and J. M. Ferguson, Corrosion Science, 5, 645 (1965).
15. D. L. Douglass, Materials, 1 (1971).
16. Kazuo Fueki and J. Bruce Wagner, Jr., J. Electrochem. Soc., 112, 384 (1965).
17. M. G. Graham and M. Cohen, J. Electrochem. Soc., 119, 879 (1972).
18. G. B. Gibbs and R. Hales, Corrosion Science, 17, 487 (1977).
19. W. J. Tomlinson and J. E. Lutkin, Metall, Trans., 7A, 1469 (1976).
20. B. Lustman, Metal Progress, 850 (1946).
21. A. G. Evans, D. Rajdev, and D. L. Douglass, 4, 151 (1972). 22. H. John Healey, Jr., Ph.D. Thesis, University of Florida (1978).

23. F. N. Rhines and R. G. Connell, Jr., Stress Effects and the Oxidation of Metals, Ed. by J. V. Cathcart, 1974 Fall Meeting TMS-AIME, p. 94.

24. M. J. Graham, D. Caplan, and M. Cohen, J. Electrochem. Soc., Solid State Science and Technology, 119(9), 1265 (1972).

25. L. Czerski and F. Franik, Arch. Gornictwa i Hutnictwn, 3(1), 43 (1955).

26. H. Rickert, Z. Physikal Chem., 23, 355 (1960).

27. I. Ischner and H. Pfeiffer, Natur Wissenschaften, 40, 605 (1953).

28. L. Czerski, S. Mrowec, and T. W. Werber, Arch. Hutnicktwn, 3, 25 (1958).

29. V. I. Arkharvo, S. I. Ivanovskaya, and A. S. Krivonosova, Physics Metals Meta-lography, 22, 75 (1966).

30. F. N. Rhines and J. S. Wolf, Metall, Trans., 1, 1707 (1970)

31. T. Ueno, Trans. Jap. Inst. Metals, 15, 167 (1974).

32. U. R. Evans, Symp. on Internal Stresses in Metals and Alloys, p. 291, London, 1947.

33. P. D. Dankov and P. V. Churaev, Dokl. Akad, Nauk, SSSR, 73, 1221 (1950).

34. F. Morin, G. Beranger, and P. Lacombe, Oxidation of Metals, 4, 51 (1972).

35. Carl E. Lowell, S. J. Grisaffe, and D. L. Deadmore, Oxidation of Metals, 4, 91 (1972).

36. H. M. Flower and B. A. Wilcox, Corrosion Science, 17, 253 (1977).

37. R. Herchl, N. N. Khoi, T. Homma, and W. W. Smeltzer, Oxidation of Metals, 4, 35 (1972).

38. W. E. Campbell and U. B. Thomas, Trans. Electrochem. Soc., 91, 623 (1947).

39. M. M. Ryabkina and I. L. Rogelberg, Zashch. Met., 13(1), 100 (1977).

40. J. C. Rocaries and M. Rigaud, Scripta Met., 5, 59 (1971).

41. G. P. Sabol and S. B. Dalgaard, J. Electrochem. Soc., 122, 316 (1975).

42. T. Ueno, Japanese J. Appl. Physics, 13(5), 773 (1974).

43. A. Dravnieks and H. J. McDonald, J. Electrochem. Soc., 94, 139 (1948).

44. S. Mrowec, Corrosion Science, 7, 563 (1967).

45. B. M. Vasyutinsky and G. N. Kartmajov, Physics Metals Metallography, 15, 120 (1963).

46. G. C. Wood and I. G. Wright, Corrosion Science, 5, 841 (1965).

47. L. A. Menzie and P. Aldred, Corrosion Science, 8, 525 (1968).

48. J. Paidassi and L. Berry, Metaux-Corrosion-Inds., 44, 129 (1969).

49. O. A. Pashkova, H. P. Zhuk, B. K. Opara, and N. I. Burtseva, Zashita Metallov, 6, 591 (1970).

50. A. Preece and G. Lucas, J. Inst. Metals, 81, 219 (1952).

51. R. Hales and A. C. Hill, Corrosion Science, 12, 843 (1972).

52. F. H. Stott, I. G. Wright, T. Hodgkiess, and G. C. Wood, Oxidation of Metals, 11, 141 (1977).

53. F. N. Rhines, J. Inst. Metals, p. 246 (1940).

54. L. B. Pfeil, J. Iron and Steel Inst., 119, 501 (1929).

55. J. M. Perrow, W. W. Smeltzer, and R. K. Ham, Acta Met., 15, 577 (1967).

56. R. T. Phelps, E. A. Gulbransen, and J. W. Hickman, Ind. Eng. Chem. Analyt. Edn., 18, 391 (1946).

57. D. Caplan, M. J. Graham, and M. Cohen, J. of Electrochem. Soc., 119, 1205 (1972).

58. J. S. Choi and W. J. Moore, J. Phys. Chem., 66, 1308 (1962).

59. M. T. Shim and W. J. Moore, J. Chem. Phys., 26, 802 (1952).

60. A. Atkinson and R. I. Taylore, J. Materials Sci., 13, 427 (1978).

61. R. Lindner and A. Akerstrom, Discuss. Faraday Soc., 23, 133 (1957).

62. M. O'Keeffe and W. J. Moore, J. Phys. Chem., 65, 1438 (1961).

63. D. G. Barnes and J. M. Calvert et al., Phil Mag., 28(6), 1303 (1973).

64. J. A. Holbrook, Control of Environmental Surface Reactions, Diffusion Transport, Final Report NSF Grant GH-34550, 47 (1973).

65. D. G. Lees and J. M. Calvert, Corrosion Science, 16, 767 (1976).

66. M. Kuise, Angew, Elektrochemie, 9, 318 (1971).

67. Y. Oshi and W. D. Kingery, J. Chem. Phys., 33, 480 (1960).

68. F. J. Wilkins and E. K. Rideal, Proc. Roy. Soc., A, 128 (1930).

69. H. Hashimoto and M. Hama, J. Appl. Phys., 43, 4828 (1972).

70. D. Caplan and G. I. Sproule, Oxidation of Metals, 9, 459 (1975).

71. R. F. Tylecote, J. Iron Steel Inst., 196, 135 (1960).

72. D. Bruce and P. Hancock, J. Inst. Metals, 97, 140 (1969).

73. D. Bruce and P. Hancock, J. Inst. Metals, 97, 148 (1969).

74. A. Menzies and K. N. Strafford, J. Materials Sci., 2, 358 (1967).

75. M. W. Vernon and F. J. Spooner, J. Materials Sci., 4, 112 (1969).

76. J. Paidassi, Third Colloque de Metallurgie sur la Corrosion, sac lay, p. 171 (1959).

77. W. J. Moore, J. Chem. Phys., 21, 1117 (1953).

78. J. Stringer, J. Less-Common Metals, 16, 55 (1968).

79. E. J. Denisenko and V. V. Skorokhod, Poroshkovaya Met., 4, 83 (1972).

80. A. Norin, Oxidation of Metals, 9, 259 (1975).

81. J. V. Cathcart and G. F. Petersen, Stress Effects and the Oxidation of Metals, Ed. by J. V. Cathcart, 1974, Fall Meeting TMS-AIME, p. 114.

82. L. J. Weiriclc and W. L. Larsen, J. Electrochem. Soc., 119, 465 (1972).

83. R. E. Pawel, J. V. Cathcart, and J. J. Campbell, J. Electrochem. Soc., 110, 551 (1963).

84. T. Homma, S. Issiki, Acta Met., 12, 1092 (1964).

85. W. K. Appleby and R. F. Tylecote, Corrosion Science, 10, 325 (1970).

86. R. Hales, Corrosion Science, 12, 555 (1972).

87. J. V. Cathcart, G. F. Petersen, and C. J. Sparks, Jr., J. Electrochem. Soc., 116, 664 (1969).

88. J. E. Antill and J. B. Warburton, J. Electrochem. Soc., 114, 1215 (1967).

89. M. S. Seltzer, A. H. Caluer, and B. A. Wilcox, [Proc. of Symp.] Stress Effects and the Oxidation of Metals, Detroit, 1974, 1975, 134-154.

90. J. V. Cathcart, R. E. Pawel, and G. F. Petersen, High Temperature Oxidation of Uranium Alloys, Intern, Corrosion Conference, Tokyo, June, 1972.

91. J. Maldy, Commissariat a l'Energie Atomique 7th Colloque de Metallurgie, Saclay, p. 71 (1963).

92. P. M. Holloway and J. B. Hudson, Surface Sci., 43, 123 (1974).

93. D. F. Mitchell, P. B. Sewell, and M. Cohen, Surf, Sci., Dec. 1, 69, 210 (1977).

94. F. Robin, Bull, de la Societe de Encouragement, CXVIV, 204 (1912).

95. U. M. Martins, Canadien J. Phys., 33, 466 (1955).

96. G. C. Wood and B. Chattopadhyay, Corrosion Science, 10, 471 (1970).

97. J. M. Perrow, W. W. Smeltzer, and J. D. Embury, Acta Met., 16, 1209 (1968).

98. J. B. Newkirk and W. G. Martin, Trans. Met. Soc. AIME, 212, 398 (1958).

99. C. A. Papageorgopoulous and J. M. Chen, Solid State Commun., 13, 1455 (1 Nove., 1973).

100. M. G. Graham, G. I. Sproule, D. Caplan, and M. Cohen, J. Electrochem. Soc., 119, 883 (1972).

101. K. M. Carlsen, Acta Met., 5, 58 (1957).

102. M. J. Graham, R. J. Hussey, and M. Cohen, J. Electrochem. Soc., 120, 1523 (1973).

103. E. A. Gulbransen, Corrosion, 12, 61 (1956).

104. K. Hauffe, L. Petre, and R. Schmidt, J. Electrochem. Soc., 115, 456 (1968).

105. J. M. Ritchie, Phil. Mag., 19, 421 (1969).

106. Uhlig, J. Pickelt, and J. Macnairn, Acta Met., 7, 111 (1959).

107. E. A. Gulbransen and K. F. Andrew, J. Electrochem. Soc., 104, 334, 451 (1957).

108. G. Tammann and K. Bochow, Z. Anorg, Chemie, 169, 42 (1928).

109. F. H. Stott, J. E. Forrest, and G. C. Wood, Oxidation of Metals, 11, 109 (1977).

110. V. O. Nwoko and L. L. Shreir, Practical Metallic Composites, Mar., F21-F25 (1974).

111. K. Hauffe and H. Pfeiffer, Wiss. Z. Universitat Greifswald, Jahrgang I. Mathematisch-Naturwissen-Shaftliche Reihe, Nr. (1951/52).

112. C. Wagner and K. E. Zimens, Acta Chem. Scand., 1, 539 (1947).

113. K. Hauffe and Ch. Gensch, Z. Phys. Chem., 195, 116 (1950).

114. G. B. Gibbs, Phil. Mag., 18(156), 1175 (1968).

115. N. Birks and H. Rickert, J. Inst. Metals, 91, 308 (1963).

116. R. J. Hussey, P. E. Beaubien, and D. Caplan, Metallography, 6, 27 (1973).

117. T. Walec and E. Szczawinska, Rev. int. Htes Temp. et Refract., t. 14, 117 (1977).

118. J. Romanski, Corrosion Science, 8, 89 (1968).

119. S. Mrowec, Zeit. Physikal Chem. [Frankfort], 29, 47 (1961).

120. U. R. Evans, J. Chem. Soc., 1024 (1927).

121. F. N. Rhines, Met. Trans., 1, 1105 (1970).

122. R. N. Rhines, K. R. Craig, and R. T. DeHoff, Metall. Trans., 5, 413 (1974).

123. R. T. DeHoff and F. N. Rhines, Quantitative Microscopy, McGraw-Hill, New York (1968).

124. H. B. Aaron, R. D. Smith, and E. E. Underwood, Proc. First Int. Cong. for Stereology, Vienna (1963).

125. P. A. Beck, Phil. Mag. Suppl., 3, 245 (1954).

126. W. M. Williams and C. S. Smith, Trans. AIME, 194, 755 (1952).

127. K. Okazaki and H. Conrad, Trans. Jpa. Inst. Metals, 13, 198 (1972).

128. B. R. Patterson, Ph.D. Dissertation, University of Florida (1978).

129. P. Feltham, Acta Meta., 1, 97 (1957).

130. I. Hayashi and H. Sakata, The 18th Japan Congress on Materials Research--Metallic Materials, 1 (1975).

131. J. B. Clark and F. N. Rhines, Trans. ASM, 51, 199 (1959).

132. F. N. Rhines, Proceedings 1958, 3d Plansee-Seminar, June 22-26, Reutte/Tyrol, Austria.

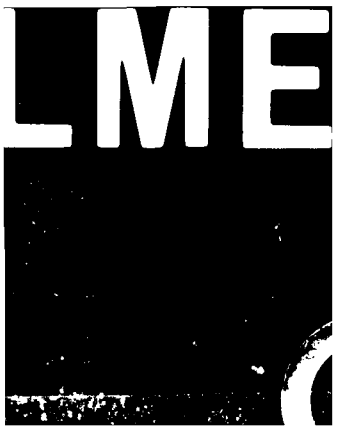
LME